Western Graduate&PostdoctoralStudies

Western University
Scholarship@Western

Electronic Thesis and Dissertation Repository

8-16-2024 2:00 PM

3D-printable Open Source Hardware Developed For Sustainable Technology

Dawei Liu, *Western University*

Supervisor: Pearce, Joshua M., *The University of Western Ontario*

A thesis submitted in partial fulfillment of the requirements for the Master of Engineering Science degree in Electrical and Computer Engineering

© Dawei Liu 2024

Follow this and additional works at: https://ir.lib.uwo.ca/etd

Part of the Electro-Mechanical Systems Commons, Equipment and Supplies Commons, Manufacturing Commons, Polymer and Organic Materials Commons, and the VLSI and Circuits, Embedded and Hardware Systems Commons

This work is licensed under a Creative Commons Attribution 4.0 License.

Recommended Citation

Liu, Dawei, "3D-printable Open Source Hardware Developed For Sustainable Technology" (2024). *Electronic Thesis and Dissertation Repository*. 10387.
https://ir.lib.uwo.ca/etd/10387

This Dissertation/Thesis is brought to you for free and open access by Scholarship@Western. It has been accepted for inclusion in Electronic Thesis and Dissertation Repository by an authorized administrator of Scholarship@Western. For more information, please contact wlswadmin@uwo.ca.

Abstract

As open-source technology and additive manufacturing evolve, their advantages become increasingly evident, offering solutions to global challenges. This thesis presents the development of two open-source 3D-printable hardware tools to accelerate this trend: a melt flow index (MFI) tool and tourniquet tester. The MFI tool is introduced as a low-cost method for measuring the MFI of thermal-sensitive material, particularly assessing their suitability for recycling thermoplastics for 3D printing. The tourniquet tester provides a low-cost instrument for measuring the pressure of tourniquets to assess efficacy. This device offers a cost-effective solution to ensure the safety and functionality of these critical emergency tools including those 3-D printed from recycled materials. By making these designs open-source and reducing production costs, this initiative aims to lower the barriers to use recycled plastics in 3-D printing of high-value medical and scientific devices. Together, these devices support the creation of effective emergency medical tools in resource-limited settings.

Keywords

Open hardware; Pressure sensor; Sensors; Tourniquet; Material extrusion; Material properties; Melt flow index; Polymers; Recycling

Summary for Lay Audience

As open-source technology and additive manufacturing develop, their benefits are increasingly realized, broadening the impact of such innovations. This paper presents the development of two open-source hardware tools: a melt flow indexer and a tourniquet tester both of which are 3D-printable. The purpose of these tools is to provide affordable and accessible solutions for two distinct but important applications.

The melt flow indexer allows users to measure how certain materials flow when melted. This is particularly important for verifying whether a material is suitable for 3D printing. By providing a low-cost method to test these materials, the tool helps reduce the overall expenses associated with plastic recycling. This encourages more people to recycle plastics and use them for 3D printing.

The tourniquet tester is designed to fill a crucial need by offering a low-cost way for individuals to test the effectiveness of tourniquets, which are vital in emergency situations to stop bleeding. This is especially useful for those who use or produce tourniquets made at home or through 3D printing, ensuring these homemade medical devices work correctly when they are needed the most.

By making the designs of these tools open-source, the paper aims to make it easier for people around the world to build and use these testers. This approach not only lowers costs but also promotes more widespread adoption and customization according to individual needs.

These two tools together have the potential to make a significant impact, particularly in areas where access to medical supplies and recycling infrastructure is limited. They enable communities to create their own emergency supplies and recycle materials locally, aligning with broader efforts to enhance sustainability and healthcare accessibility.

Co-Authorship Statement

This thesis is comprised of two articles:

1. Dawei Liu, Aditi Basdeo, Catalina Suescun Gonzalez, Alessia Romani, Hakim Boudaoud, Cécile Nouvel, Fabio A. Cruz Sanchez and Joshua M. Pearce. Low-cost Open-Source Melt Flow Index System for Distributed Recycling and Additive Manufacturing. (to be published).

Author Contributions: Conceptualization, H.B. and J.M.P..; methodology, D.L., A.B., C.S.G.; software, D.L.; validation, D.L., A.B., C.S.G., A.R.; formal analysis, D.L., A.B., C.S.G., A.R., H.B, C.N., F.A.C.S. and J.M.P.; investigation, D.L., A.B., C.S.G., A.R.; resources, H.B, C.N., F.A.C.S. and J.M.P.; data curation, D.L.; writing—original draft preparation, D.L., A.B., C.S.G., A.R., and J.M.P. ; writing—review and editing, D.L., A.B., C.S.G., A.R., H.B, C.N., F.A.C.S. and J.M.P.; visualization, D.L., .; supervision, H.B, C.N., F.A.C.S. and J.M.P.; project administration, J.M.P.; funding acquisition, H.B, C.N., F.A.C.S. and J.M.P.. All authors have read and agreed to the published version of the manuscript.

2. **Liu, D.,** Kulkarni, A., Jaqua, V.F., Cole, C.A. and Pearce, J.M., 2023. Distributed manufacturing of an open-source tourniquet testing system. *HardwareX*, *15*, p.e00442. https://doi.org/10.1016/j.ohx.2023.e00442

Published under CC-by

Dawei Liu developed the design, performed all experiments and was the first and primary author. Other authors helped with experiments, development of the design, and writing.

Acknowledgments

The author would like to thank colleagues and friends who contributed to this study.

Special thanks to Dr. Joshua Pearce, who gave his guidance to the author during the research.

Thanks also to Dr. Alessia Romani, Dr. Apoorv Kulkarni, and Catalina Suescun Gonzalez for their significant contributions and assistance to this study.

Thanks to all the colleagues of the FAST lab.

Table of Contents

Abstract ii

Summary for Lay Audience iii

Co-Authorship Statement iv

Acknowledgments v

Table of Contents vi

List of Tables viii

List of Figures ix

List of Appendices xii

Chapter 1 1

1 Introduction and background 1

Chapter 2 4

2 Low-cost Open-Source Melt Flow Index System for Distributed Recycling and Additive Manufacturing 4

2.1 Introduction 4

2.2 Materials and Methods 8

2.2.1 Mechanical system 9

2.2.2 Electronics 13

2.2.3 Testing and Validation 14

2.3 Results 16

2.4 Discussion 21

2.5 Conclusions 24

Chapter 3 26

3 Distributed Manufacturing of Tourniquet Testing System for Open-Source Tourniquets 26

3.1 Hardware in context 26

3.2 Hardware Description 31
3.3 Operation instructions 32
3.3.1 Calibration of the force measurement. 33
3.3.2 Calibrate the pressure parameter. 34
3.4 Validation 40
3.5 Limitations and future works 41
Chapter 4 43
4 Conclusions 43
References or Bibliography 45
Appendices 61
Curriculum Vitae 111

List of Tables

Table 1: MFI test parameters and results (mean values and standard deviations) of virgin PLA (vPLA), rPET90/rHDPE10, rPET90/rHDPE10/SEBS10, and recycled PETG (rPETG) obtained with the commercial and OS MFI devices. 17

Table 2. Commercial tourniquet test systems 29

Table 3. Calibration data 38

Table 4. BOM of the make parts and files for the OS MFI device (hardware). 61

Table 5. BOM of electronic components. 69

Table 6. BOM of mechanical components. 71

Table 7. Tourniquet tester design files. 101

Table 8. Bill of materials. 105

Table 9. 3-D printing parameters 106

Table 10. Wire connections. 107

List of Figures

Figure 1: Overall hardware structure of the OS MFI device. 12

Figure 2: Electronic schematic of the OS MFI device..... 14

Figure 3 Virgin PLA measurement results. 19

Figure 4. Virgin PLA MFI values changing through different pre-heating times from the tests with the OS MFI device. 20

Figure 5. MFI measurement results of virgin PLA (vPLA), recycled PETG (rPETG), rPET90/rHDPE10, and rPET90/rHDPE10/SEBS10 obtained with the commercial equipment (left side bars) and OS MFI devices (right side bars). 21

Figure 6. Calibration process with no platform. 34

Figure 7. Calibration against the blood pressure cuff 36

Figure 8. Experiment data of the force measured as a function of the pressure in the various angles of rotation..... 36

Figure 9. Cuff position at (a) 0°,(b) 45° and (c)90° 37

Figure 10. Measurement process (a) Plug in the power cord (b) Insert Tournbutton-M (c) Wrap the tourniquet to the tester (d) Turn the tourniquet windlass. 40

Figure 11. Validation tests, BL cuff vs tourniquet tester readings (p=5). 41

Figure 12 Part 1: Stand. 63

Figure 13. Linear support..... 64

Figure 14. Motor mount. 64

Figure 15. Flange support. 65

Figure 16. Loadcell fit (left), Shaft loadcell coupler (right). 65

Figure 17. Cutter connector (left), blade fix (right). 66

Figure 18. Extra frame (left), extra frame b (right)..... 66

Figure 19. Foot support (left), Housing (right). 67

Figure 20. Insulation housing 67

Figure 21. Cap band. 68

Figure 22. Piston guide (left), piston tip guide (right). 68

Figure 23. Scale housing (left), scale plate (right). 69

Figure 24. Frame 74

Figure 25. Piston tip. 75

Figure 26. Coupler connection. 76

Figure 27. Piston assembling step. 76

Figure 28. Heating pipe 77

Figure 29. Cap assembly. 78

Figure 30. Assembling steps in step 3. 78

Figure 31. Scale assembly 79

Figure 32. Overall structure 81

Figure 33. Operation instruction step 4 83

Figure 34. Operation instruction step 5 83

Figure 35. Operation instruction step 6 (left), step 7 (right). 83

Figure 36. 3-D printed Amplifier. 102

Figure 37. 3-D printed Cap 102

Figure 38. 3-D printed Flat 103

Figure 39. 3-D printed thigh inside cylinder..... 103

Figure 40. 3-D printed Tournbutton-M..... 104

Figure 41. Tournbutton-T 104

Figure 42. Wire connections. 107

Figure 43. Assembly steps of physical components. (a) Put the flat part into the groove, (b) Insert the load cell, (c) Fix the load cell, (d) Fix the flat, (e) Fix the amplifier, (f) Fix the Arduino U no board, (g) Fix the LCD on the cap, and (h) Insert the TPU button..... 109

Figure 44. Optional calibration platform shown empty on left and calibrating the tester on the right. 110

List of Appendices

Appendix A: List of OS MFI parts. 61

Appendix B: OS MFI build instructions. 72

Appendix C: OS tourniquet testing system build instructions. 101

Chapter 1

1 Introduction and background

The term open-source comes from open source software originally, initially manifesting as spontaneous acts of source code sharing by software developers. Over time, these activities evolved into more formalized behaviors, eventually leading to the formation of widely recognized open-source communities. Within the framework of open-source technology, including software and hardware, technical information is fully disclosed, allowing individuals and organizations worldwide to freely access, utilize and modify these technologies. Typically, the disclosed materials include all necessary information to ensure that external users can accurately replicate or improve the disclosed technologies.

Concurrently, additive manufacturing technologies, particularly desktop-level fused filament fabrication (FFF) or commonly known as 3D printing, have rapidly advanced. 3D printing technology relies on 3D printers; for instance, in FFF technology, the printer's extruder converts thermoplastic filaments from a solid to a molten state and extrudes it layer by layer, ultimately forming a pre-designed three-dimensional object on the print bed. 3D printing exhibits unique advantages in producing customized products.

The integration of open-source technology with 3D printing not only reduces manufacturing difficulties but also enables the easy fabrication of various components needed for open-source projects through 3D printers. As more 3D printing technologies are made open-source, the barriers to related technologies are further lowered, making manufacturing and technological development more convenient and cost-effective. The promotion of open-source culture ensures that all stakeholders have the opportunity to participate in the development and iteration of open-source technologies, significantly accelerating technological advancement and dissemination.

Due to the many advantages of open-source technology and 3D printing, such as low cost, high customization, rapid development, and distributed production, these technologies have rapidly evolved globally, and the related concepts have become deeply ingrained in the public consciousness. Based on their unique features and benefits, open-

source technology and 3D printing are particularly well-suited to address issues of sustainable development and resource scarcity. For instance, in scenarios requiring the development of specific hardware, leveraging customization benefits, or needing to reduce costs and increase availability, open-source and 3D printing offer effective solutions. Consequently, this study has developed corresponding open-source hardware to provide a low-cost, effective, and sustainable solution strategy for addressing specific problems.

In regions with scarce resources, however, the raw materials for 3D printing can also be challenging to obtain. With the advancement of 3D printing technology, various potential materials for 3D printing have been developed, including some made from recycled plastics. Moreover, machines capable of printing directly from waste parts have also been developed. The recycling of plastics allows for the resourceful reuse of materials, enabling lower-cost 3D printing even in resource-poor areas. During the recycling process, the melt flow index (MFI) method can be employed to identify materials suitable for 3D printing. Measuring the MFI reveals the melt flow characteristics of the material, particularly its suitability for 3D printing. Compared to a rheometer, MFI testing is simpler and less costly, yet equally effective in distinguishing material. However, commercial MFI testers are expensive and difficult to acquire in areas with limited resources or under special circumstances.

To address such challenges, an open-source MFI testing system is introduced in Chapter 2. The open-source MFI system reduces manufacturing costs and is easier to operate compared to some commercial MFIs. The open-source MFI can facilitate plastic recycling, providing a practical tool for enhancing material reuse in 3D printing projects and applications.

For example, in practical applications, such as emergency medical response, tourniquets are commonly used emergency medical devices that effectively stop bleeding and significantly reduce deaths due to hemorrhage. In regions with scarce resources or severe conflict, however, tourniquets are often difficult to obtain due to disrupted supply chains, etc. Addressing this issue, a medical team from Canada developed a tourniquet that can

be produced using 3D printing technology. This tourniquet, designed with open-source plans and distributable production methods, not only simplifies manufacturing but also increases the accessibility of tourniquets in these regions.

Despite these advancements, the safety and practicality of these open-source 3D-printable tourniquets have been questioned during their dissemination, leading to a demand for devices capable of testing their efficacy. Given the absence of a recognized standard tester for tourniquets and ongoing discussions about production standards, evaluating the functionality of tourniquets, especially those produced via distributed manufacturing and 3D printing, presents a challenge. An open-source tourniquet testing system is developed in Chapter 3 to address this gap. The device is not only simple to manufacture but also reliable in testing, ensuring the effectiveness of tourniquets in critical situations.

Finally in Chapter 4, this research is discussed in the context of developing open-source hardware as a low-cost, feasible, and effective approach to assist regions with limited resources. By producing tourniquet testers and employing the MFI to identify recyclable materials, this study hopes to leverage the recycling of plastic resources to further reduce production costs. Consequently, this facilitates the manufacturing or acquisition of tourniquets, ultimately aiming to decrease the mortality rate associated with blood loss. This approach not only addresses critical medical needs but also promotes sustainable practices in material use. Future work is summarized.

Chapter 2

2 Low-cost Open-Source Melt Flow Index System for Distributed Recycling and Additive Manufacturing

The increasing adoption of distributed recycling additive manufacturing (DRAM) has facilitated the revalorization of materials derived from waste streams for additive manufacturing. Recycled materials often suffer from impurities and the mixing of different polymers, which can degrade their properties over multiple cycles. This degradation, particularly in rheological properties, limits their applicability in 3D printing. Consequently, there is a critical need for a tool that enables rap-id assessment of the flowability of these recycled materials. This study presents the design, development, and manufacturing of an open-source melt flow index (MFI) apparatus. The proposed MFI tool offers a user-friendly and cost-effective solution for evaluating the flow properties of materials from waste streams, thereby enhancing their viability for additive manufacturing applications.

2.1 Introduction

Due to a wide range of beneficial properties, synthetic polymers generally derived from fossil fuels are in widespread use, as over 390 million metric tons of plastic are produced globally [1]. One property, which has turned out to be something of a curse, is that plastics have great durability and are resistant to degradation, enabling them to persist as environmental pollutants for hundreds of years [2]. When not properly disposed, plastics can cause environmental pollution [3], harming wildlife and ecosystems, [4] as well as humans [5], [6]. Therefore, it is important to manage the waste plastic in a proper way. Obviously, recycling is a great way to minimize the harm caused by wasted plastic, and it can also benefit both the environment and humanity [7]. Unfortunately, only 9% of plastic has been recycled [8]. Of the rest, half is landfilled, 22% is mismanaged, and 19% is burned or incinerated [8]. Of the unrecycled plastics, thermoplastics present a substantial opportunity to profitably utilize available materials, reduce pollution, and redirect waste from landfills. A new approach to developing a circular economy for plastics is being developed in the additive manufacturing industry (AM). It has been

shown to be profitable [9], [10] using the process of distributed recycling for additive manufacturing (DRAM) [11], [12]. In this model, prosumers (a portmanteau of producing consumers) have a direct economic benefit by offsetting purchase of plastic products by recycling their waste into custom open-source products [10]. This model is in contrast to traditional centralized recycling models for plastic, which provide no incentive to consumers because of the low value of low density of collecting and transporting post-consumer plastic waste [12]. DRAM plastic converted to AM feedstock will increase in value between 4x and 20x as the value of bulk commercial plastic pellets ($1-5/kg) or commercial filament (~$20/kg). With DRAM, greenhouse gas (GHG) emissions from the embodied energy of transportation are minimized for AM materials [13], [14]. This result is possible in the most extreme case of consumers manufacturing their own products from their own waste in their own homes [15], [16]. Further reductions in GHG emissions are possible when DRAM uses renewable energy like solar photovoltaic technology [17], [18]. Community-level DRAM using a recycling network is also feasible [19], [20] and still more efficient than centralized recycling [21]. Overall, DRAM models challenge global value chains already under assault with distributed manufacturing [22].

In order to facilitate DRAM, open source (OS) waste plastic extruders called recyclebots [23], [24] have been developed to provide filament feedstock for Fused Filament Fabrication (FFF) processes. Recycled waste plastic filaments can be used in any low-cost self-replicating rapid prototype (RepRap)-class [25], [26], [27] 3D printer. A wide range of recycled plastic has already been shown to be DRAM compatible:

- polylactic acid (PLA) [28], [29], [30],
- acrylonitrile butadiene styrene (ABS) [10], [31],
- high-density polyethylene (HDPE) [23], [32], [33],
- polyethylene terephthalate (PET) [34], [35],
- linear low-density polyethylene (LLDPE) and low-density polyethylene (LDPE) [36], [37],
- polypropylene (PP) and polystyrene (PS) [33],
- elastomers [38],
- carbon-reinforced plastic composites [39],

- waste wood fiber reinforced plastics [35], [40]
- fiber-filled composites [41], [42].

Furthermore, the filament-making step can be avoided by 3D printing directly from shredded waste in Fused Particle Fabrication (FPF)/ Fused Granular Fabrication (FGF) systems [43], [44]. Using direct screw-assisted extruders, either single- or twin-screw systems, further expands the range of available DRAM materials [12], [45], including polymer blends and multi-material recycling thermoplastics [46], [47], multiple-recycled flake feedstocks [43], [48], and bio-based thermoplastics or composites[49], [50], [51]. Moreover, it improves the economics of DRAM [47], [47], [51], [52], reducing the cost of producing the material and environmental pollution [54].

There are, however, challenges remaining in DRAM, especially focusing on materials. For example, different types of polymers need different recycling processes, making sorting necessary [55]. Other limitations include impurities found in waste, as well as contamination by mixing with incompatible polymers. These impurities affect overall processability, such as flowability and printability, and diminish technical properties, e.g., mechanical and rheological properties. At the same time, incompatibilities increase material heterogeneity, making it difficult to accurately predict changes in properties. For unknown plastics of different types, there is a need for rapid characterization methods to identify the potential processability of the material to be used in DRAM, reducing the impacts and scraps due to initial tuning of the 3D printing setup. One proposed method is the melt flow index (MFI) measurement, which is a good reference for the melt flow behavior of a thermoplastic material, hence its flowability during the 3D printing process[56], [57]. MFI, or melt flow rate (MFR), measures the ability of the molten polymer mass to flow through an orifice or die below a heated barrel under a given loading pressure and temperature for a given amount of time [58], usually measured in g/10min. MFI is a feature related to the material's molecular weight [59], which means it can provide information about the material's viscosity and flowability, allowing a better understanding of its potential behavior in the 3D printer [55]. In general, the higher is the MFI, the lower are the viscosity and molecular weight of the tested material, increasing the flow per unit time. This value can be used to determine other properties, e.g., melt

volume rate (MVR) and intrinsic viscosity, giving further insight into the rheological behavior of the material[60]. MFI also helps set an initial melt temperature without the need for more complex characterization methods, such as differential scanning calorimetry (DSC). Although other thermal properties also affect printability in FFF/FGF, e.g., crystallinity index[61], the immediacy of MFI measurements and the availability of standardized methods make it an accessible and reliable way to assess the printability of thermoplastics[62]. For DRAM operationalized at the community scale, MFI represents a potential means to quickly screen potential AM feedstock materials [56], [63], as the material characteristics could be changed after one or multiple recycling processes due to thermomechanical degradation of thermoplastics during the recycling and extrusion steps [43], [64]. For example, the MFI of ABS will increase after recycling due to degradation, leading to a decrease in its viscosity [65], and hence, in its flowability. Thus, new 3D printing temperatures or speeds may be applied. In addition, MFI is not only used to assess the behavior of pure thermoplastic materials; it also provides a quick evaluation of the flowability and printability of materials that contain additives, such as compatibilizers [66], chain extenders [67], [68], fillers [69], and bio-sourced components [70], [71], further expanding its use.

To rapidly assess the printability of recycled materials, MFI presents a viable and rapid alternative to complex and longer rheological [72], [73]. Unfortunately, proprietary MFI systems are still expensive, ~ CAD$4,700 from Amazon [74] and ~CAD$2,000 from AliExpress [75]. This fact limits accessibility to resource-constrained settings for which DRAM is perhaps the most promising because prosumers could trade their labor for high-value products for themselves or to sell. Furthermore, exploiting rapid characterization tools for DRAM could improve the overall quality of the 3D printed products produced by the prosumers, hence increasing the adoption of this technology and its reliability for new product applications, e.g., reducing failures and material scraps from parameter tuning.

To address this issue, this article introduces a low-cost open-source Melt Flow Index er. First, the basic functioning of an MFI is outlined. The operation and design of each of the major subassemblies of the OS MFI device are then detailed. The complete bill of

materials (BOM) and assembly instructions are provided in Appendix A and B. Next, the OS MFI device is validated against a gold-standard commercial MFI and then used for the MFI assessment of some common waste plastics for DRAM: virgin PLA pellets, shredded recycled PETG flakes, and recycled HDPE/ PET pellet blends. The results are compared and discussed in the context of DRAM.

2.2 Materials and Methods

An MFI device is a measuring tool, which can measure the MFR of a thermal-sensitive polymer material. An MFI device normally comprises load weights, a piston, a heated barrel with a die, a cutter system, and a scale. Usually, the procedure of measuring MFR acts by these steps: first, heat up the barrel to the desired temperature; second, add the polymer sample into the heated barrel and wait for a certain time until the sample melts, i.e., preheat time; third, put the weight on the top of the piston then after a certain period of time, measure the mass of the extrudate forced to pass through the die. Before and after the tests, the barrel and die should be cleaned to ensure no contamination and repeatability of the tests, which usually follow ASTM or ISO standards to define timings, temperatures, and dimensions of the main MFI components [60]. Among the common commercialized MFI systems, some of them are cumbersome to operate and are not automated. For example, the MFI products from MRCLAB need operators to put the weight on the top of the instrument and count down the time [76]. Normally the operator needs to collect the samples and weigh them afterward, such as for many melt flow indexers on AliExpress [75]. To address this issue, the open-source MFI designed in this article was developed to be mostly automated. In the proposed design, the open source MFI can apply loads automatically via the DC motor, cut the extruded material, and weigh it automatically.

To fulfill the functionality of the MFI, the system here described relies on mechanics, electronics, and free and OS software, all of which are available on the Open Source Framework [77]. The BOM for the make, mechanical, and electronical parts are included in Appendix A. The mechanical components are composed of aluminum extrusion profiles, 3D printed parts, and fasteners. The overall structure is a vertical frame that holds a cylinder, which works as the heated barrel to melt the sample materials. In the

electronic part, the instrument is controlled by a Teensy 4.0 board [78], and temperature control, motor, and digital scale systems are integrated into one control system. The whole process will be controlled by the code upload to the teensy board to make it easy to operate and automatic. The cutter on the MFI device can cut the extrusions at set intervals to automatize the extrudate collection from the die, and the digital scale can weigh them and record data. Finally, the device designs are meant to be open source, hence digitally replicable and low cost. All the buy components used for the hardware design are readily available on the market. Custom parts are designed to be quickly produced with low-cost desktop-size FFF 3D printers and commercial filament feedstock, i.e., PETG and polycarbonate (PC). The structure of the frame is designed to optimize material usage, hence, to be produced with less material and require a limited amount of buy components. Far less machining is needed than conventional MFIs, further reducing costs.

2.2.1 Mechanical system

The framework consists of two 20x20 mm aluminum profiles, 75 mm and 30 mm respectively, and some 3D printed parts. This framework connects the different subassemblies together and keeps the whole structure steady. Compared to commercial MFI products, this design uses a stepper motor as the weight on the top of the piston. With the linear rail, the shaft of the motor can move up and down on the same track, which helps decrease the vibration on the motor rod. The piston is made of a piston head and a piston rod, and the piston head has a multi-layered structure, which consists of two nuts, one O-ring, and one washer. The O-ring keeps the piston head from leaking. The piston rod is a threaded steel rod, it allows the piston head to screw on it. There is a button shape load cell between the motor shaft and piston rod, which can measure the pressure so that there is a feedback loop for the motor to keep the same pressure. The barrel for heating up samples is a 304 stainless steel pipe, which can be found easily on the market. A copper cap with a hole is then added to the barrel to act as the die. A PC insulation housing with heat insulation cotton material covers the whole heated barrel to ensure heat stability. Below it, there is a servo motor equipped with a blade that acts as

the cutter for the material samples to be weighted. The overall design of the mechanical system of the MFI device is shown in Figure 1, and the BOM is visible in Appendix A.

As an open-source system, this design aims to lower the barriers to use, achieve low costs, and ensure ease of manufacturing. Therefore, when selecting components, the author has opted for products that are readily available on the market. Compared to conventional products, this design uses a stepper motor as the pressure source. The advantage of this approach is that it eliminates the need for the operator to manually add weights during measurement and allows automatic application of pressure when the preheating ends. Additionally, the absence of weights enhances portability.

The design incorporates a linear rail to provide a platform for the part that locks the motor rod and assists the piston in descending in the correct position, thereby reducing the impact of friction between the piston head and the inner wall of the heating barrel.

For the heating barrel, the author chose a commonly available steel pipe on the market, with a size of 1/2 inch to closely approximate standard designs. A typical metal cap with a drilled hole was used as the die. Compared to fully machined commercial products, this design allows for the low-cost production of the heating barrel, with the only machining step being the drilling of the hole in the cap, significantly reducing manufacturing complexity and cost.

To complement the heating barrel, the piston head uses an O-ring design. This design is compatible with the untreated inner wall of the heating barrel, allowing the piston head to provide pressure while also preventing leakage. Compared to commercial products that require high-precision machining, this approach reduces manufacturing difficulty and cost.

The digital scale casing is not connected to the main structure to avoid potential vibrations affecting the scale's measurements.

The design features an open and modular frame structure. During frame manufacturing, many 3D-printed parts were used. These parts are designed with both strength and material efficiency, making them easy to print and assemble. For example, the extra

frame is composed of two parts, top and bottom, allowing this large component to be successfully printed on most desktop-class 3D printers. The connection between the upper and lower parts uses a mortise and tenon joint with an interference fit, eliminating the need for fasteners. Due to the customizable nature of 3D printing, functional parts can also be added to the design. For instance, the flange support is combined with a piston guide, and the funnel-shaped piston guide part prevents material splashing when adding materials. This part can be customized, allowing users to add new components to expand functionality.

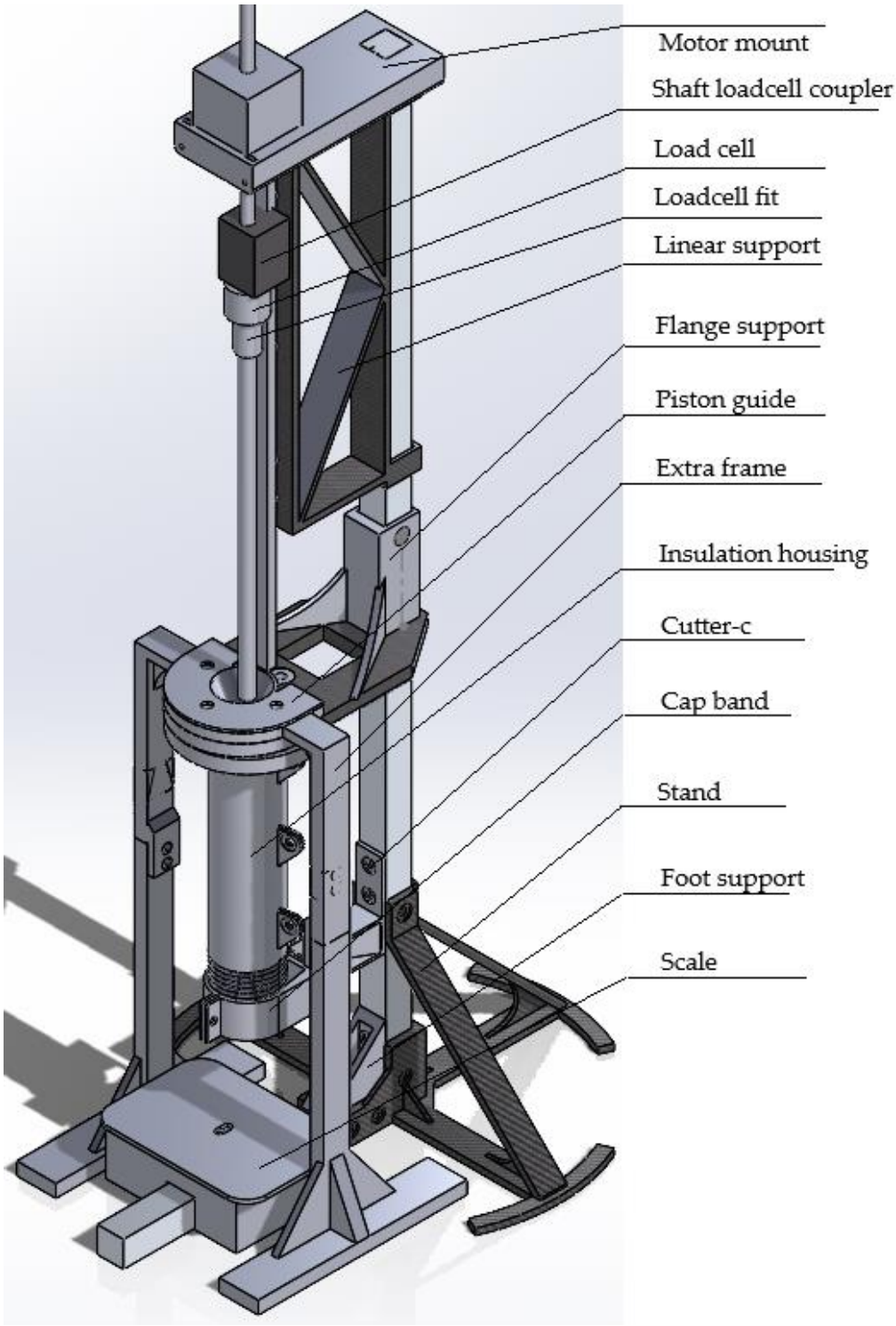

Figure 1: Overall hardware structure of the OS MFI device.

2.2.2 Electronics

The system is controlled by a Teensy 4.0 board, which is reasonably priced, compact, and has enough pins, making it suitable for integrating multiple subsystems. It supports the use of the Arduino IDE, reducing the barrier to use. To enhance circuit stability and reduce the difficulty of circuit connections, a dedicated PCB was designed. The control system, as shown in Figure 2, can be divided into three main parts, which are the heating system, digital scale and the motor force control system. As mentioned above, there is a feedback loop for the motor. When the force does not reach the desired value, the threaded rod will go down, letting the piston press on the samples. When the force reaches the desired value, the motor will stop and remain the force. Due to the need to address heat loss and the requirement for a removable cap, two distinct heating elements are necessary. A nichrome wire is used on the heat barrel, while a band heater is employed on the cap. This arrangement ensures efficient heat management and flexibility in the assembly and maintenance of the device. This approach complements the shape of the pipe, allowing the nichrome wire to heat the pipe over a large area, ensuring as even a temperature distribution as possible across the entire pipe. The addition of the band heater ensures that the temperature at the cap is maintained. The entire heating area is wrapped with insulation to assist in stabilizing temperature control. Also, as a heating element nichrome wire is highly cost-efficient. The temperature sensor chosen is a K-type thermocouple wire, selected for its affordability, wide temperature measurement range, and compact size, making it easy to install. PID control is applied to the heating control system. All the terms in the PID control system need to be adjusted according to different situations. For example, if the overshot is too high, then it can be improved by reducing the portion term. The simplicity and quick response of PID control contribute to the rapid operation of the entire integrated system while also lowering the barrier to use. The digital scale is based on cantilever beam shaped loadcell and HX711 amplifier. This system is notably cost-effective; however, the drifting issue of the load cell has been a persistent criticism. To mitigate this effect, one can employ strategies such as averaging multiple samples or implementing a compensation curve. In this design, a mechanism that samples at regular intervals allows for the scale to be tared before the cutter does sampling operation, effectively eliminating the impact of drifting. This method ensures

greater accuracy and reliability in measurements, enhancing the overall performance of the system. This system itself runs automatically, but all the input parameters like time, temperature and pressure need to be input manually in the firmware. There are two modes in the code, which are auto mode and manual mode. Manual mode is meant for adjusting the position of the piston head, and cleaning procedure after measuring process.

The cutter's blade is driven by a servo motor, which is more cost-effective and takes up less space compared to commercial products.

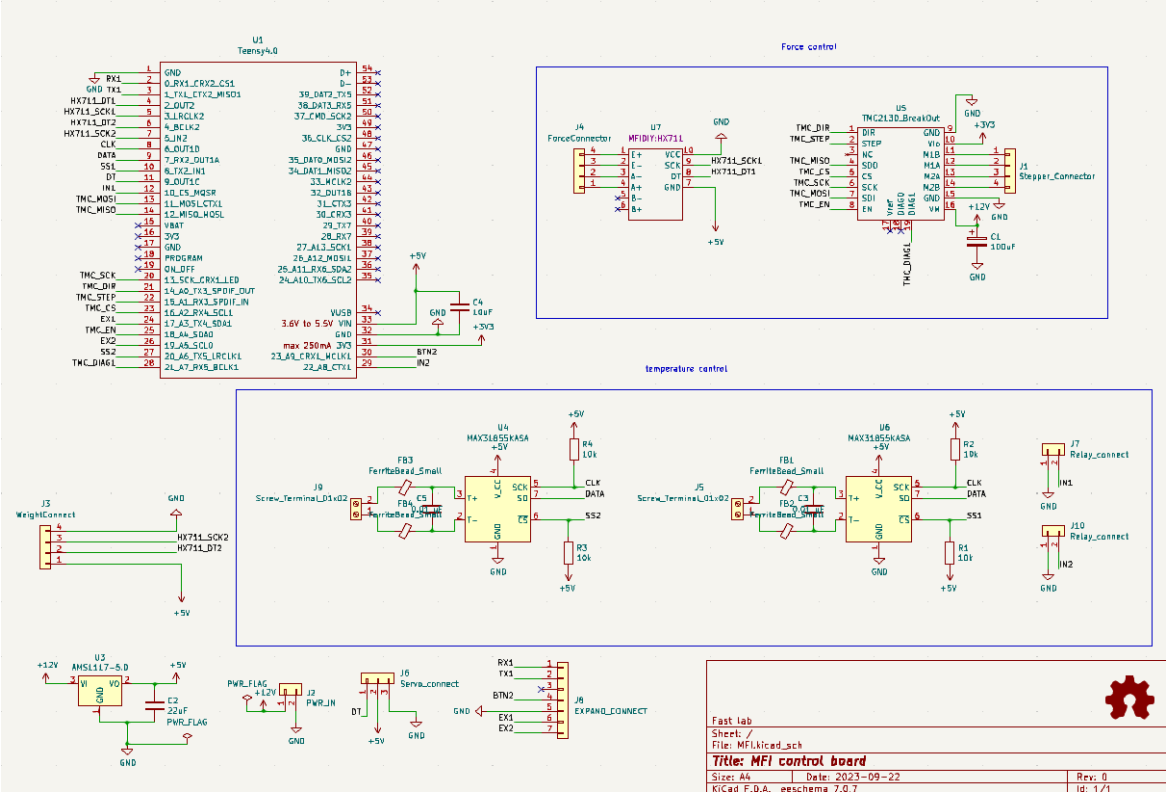

Figure 2: Electronic schematic of the OS MFI device.

2.2.3 Testing and Validation

The operational instructions of the OS MFI device are detailed in Appendix B. To validate the use of the OS MFI, a series of experiments was designed to compare the measurement results of the OS MFI system with a commercial product available on the market. The design of the proposed OS MFI has some differences, such as the diameter

and length of the heating barrel, from the specifications in the standardization documents, such as ISO-1133 [79] and ASTM D1238 [80].

The design of experiments follows the principles of a controlled variable experiment. Except for the difference in testing systems, all other experimental conditions, such as testing parameters and material types, are kept consistent. To compare the developed MFI with its commercial counterpart, an Instron CEAST MF20 machine (Instron, Norwood, MA, US), located at the LRGP laboratory in Nancy, France, was utilized following the ASTM D1238 [80] standard.

Materials were obtained from various sources, including virgin, recycled plastic waste, combinations with compatibilizer, and shredded 3D printing waste from the laboratory. They were dry at 60 °C two days before the test. Virgin PLA pellets were supplied by NatureWorks (Savage, MN, USA) with a specific gravity of 1.24 g/cc. Recycled HDPE/PET blends were obtained from water bottles coming from the French brand Cristaline and processed at the ERPI laboratory in Nancy, France. This material comprised 10 wt% HDPE (cap) and 90 wt% PET (body), hereinafter called rPET90/rHDPE10. The same recycled material was tested with an addition of 10 wt% styrene-ethylene/butylene-styrene block copolymer (SEBS) G-1652 containing approximately 30 wt% polystyrene units (rPET90/rHDPE10/10SEBS), kindly donated by Kraton Polymers (Almere, Netherlands). Additionally, recycled poly(ethylene) terephthalate glycol (PETG) from shredded 3D printing waste at the FAST laboratory was tested. The shredded waste parts were originally fabricated using virgin PETG filaments provided by Polymaker (Shanghai, China).

To ensure the reliability and repeatability of the process, the analysis was performed on three samples of approximately 5g for the commercial and 10g for the developed OS MFI. The materials were tested at temperatures of 190 °C for virgin PLA, 230 °C and 240 °C for recycled PETG, and 255 °C and rPET90/rHDPE10/10SEBS, using a 2.16 kg weight. Measurement procedure can be found in Appendix B in detail.

2.3 Results

Table 1 presents the results obtained from virgin PLA, rPET90/rHDPE10/10SEBS, and recycled PETG using both commercial and OS machines, compared with the data sheets of the virgin materials for PLA and PETG filament, as well as values from the literature on 3D printed PLA[39], [56], [81], [82], PETG[83], [84], [85], HDPE and PET[70], [86]. It can be observed that the MFI of PLA assessed with the commercial device corresponds to 6 g/10min and a relative standard deviation of ~13%, demonstrating both the precision and accuracy of the commercial machine. In contrast, the OS machine exhibited a reduction of ~15% despite a similar relative standard deviation, i.e., ~5%. The results are comparable with the state-of-the-art, which shows significant variations in the MFI values. For instance, Wang et al. obtained MFI of ~4.3 and ~11.1 g/10min at 190 °C and 210 °C[56], whereas Nasir et al. reached ~11 g/10min at 190°C[82]. Tian et al. reported values of ~2 g/10min at 180 °C, which significantly increased at 240 °C[39]. In general, MFI values of 3D printed PLA range between 6 and 10 g/10min[81], confirming the reliability of the results obtained from the commercial and OS MFI devices.

Regarding PETG, the filament datasheet indicated MFI values of 3.9 g/10min and 10.8 g/10min at 220 and 240 °C, respectively. The value obtained with the commercial machine is 9 g/10min at 230 °C with a relative standard deviation of ~6%. This MFI value is within the range of the commercial virgin filament [87], suggesting that the 3D printing and shredding processes do not significantly impact material degradation. Similarly, the MFI obtained with the OS machine fell between the two values from the datasheet, showing a decrease of ~23% compared to the commercial machine. As for PLA, the values are in line with the state-of-the-art, where results of ~10.5 g/10min have been reported at 240 °C [83]. To ensure comparability with the data sheet, tests were conducted at 240°C. The MFI recorded from the commercial machine was 14.3 g/10 min, while similar values were found for the OSMFI, with a value of 13.6 g/10 min. This slight increase in MFI may be attributed to minor degradation of the material during the printing process. On the other hand, significant variability in the results is reported for PETG. For example, Vijayasankar et al. reported MFI of ~20 g/10 min at the same temperature [84]. Kotomin et al. compared the MFI values of PETG from different

temperatures, obtaining ~15 g/10min at 240°C and more than 30 g/10min at 250 °C [85]. For this reason, the values from the measurements with the commercial and OS devices can be considered reliable, confirming the validity of the OS machine.

The HDPE/PET blends derived from the plastic bottle waste stream showed MFI values of 34.5 g/10min without compatibilizer (rPET90/rHDPE10) and 31.1 g/10min with compatibilizer (rPET90/rHDPE10/10SEBS). Compared with the OS device, it can be observed that MFI of rPET90/rHDPE10/10SEBS is ~15% higher. Considering the lack of direct comparison from the state-of-the-art, some considerations can be done by checking the MFI values reported for HDPE and PET. Previous works obtained MFI values ranging between 3.5 and 40g/10min for PET, showing a significant variability given by the pre-heating conditions[86], [88], [89]. HDPE MFI values from the literature also exhibit the same trend [59]. Nevertheless, the results from the commercial and OS MFI devices are comparable, indicating the reliability of the OS machine to test novel material compositions and plastic blends.

Table 1: MFI test parameters and results (mean values and standard deviations) of virgin PLA (vPLA), rPET90/rHDPE10, rPET90/rHDPE10/SEBS10, and recycled PETG (rPETG) obtained with the commercial and OS MFI devices.

Material	**Weight (g)**		**Preheat time (s)**		**Temperature (C°)**	**MFI (g/10min)**		
	Commercial	**OS**	**Commercial**	**OS**		**Data sheet**	**Commercial**	**OS**
vPLA	5	10	300	600	190	6 [90]	6 ± 0.8	5.1 ± 0.25
vPLA	5	10	300	810	190	6	6 ± 0.8	6.0 ± 1.2
rPET90/rHDPE10	5	10	300	600	255	-	34.5 ± 4.3	13.6 ± 2.7

rPET90/rHDPE10/ SEBS10	5	10	300	600	255	-	31.1 ± 4.3	36.9 ± 15
rPETG	5	10	300	600	240	10.8 [87]	14. 3± 1.5	13.6 ± 2.7
rPETG	5	10	300	600	230	-	9 ± 0.6	6.9 ± 0.9
rPETG	5	10	300	600	220	3.9	6.5 ± 0.8	4.2 ± 0.5

First, when dealing with OS MFI data, only the last few(this number depends on sample numbers) sets of data should be accepted. According to Figure 3, there is a clear increasing trend of extrusions' weight through time. However, the results of the commercial product do not show this trend. One factor that can cause this phenomenon is that the temperature inside the die is lower than the desired point at the beginning of measurement. It may be due to insufficient insulation on the bottom of the cap, which can cause heat loss. The difference in materials between the cap and the heat barrel can also lead to differences in heat transfer that can cause this to happen. A preload process may be needed for a more precise result. For example, the first few samples flowing from the die can be discarded as part of the preload process, and the number should be determined through preliminary tests with specific materials. Due to a higher sample mess used in the OS MFI, the whole testing process may take a longer time, which can increase material degradation and affect the results.

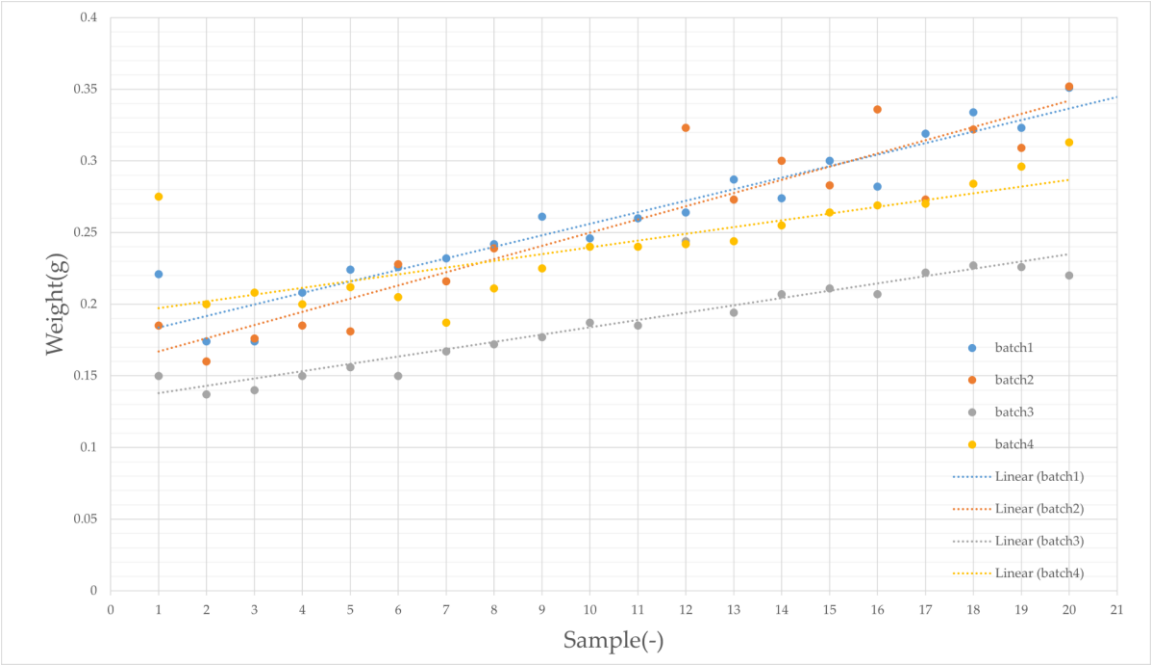

Figure 3 Virgin PLA measurement results.

Multiple experiments were done to verify this phenomenon through OS MFI, as shown in Figure 4. Accordingly, the material is fully heated in ~8 minutes. The results show a clear linear increasing trend with the increase in pre-heating time. Therefore, it is important to keep a constant sample weight throughout the tests. Moreover, according to the standard file ISO 1133, material in flake or powder shapes should undergo a preprocess, i.e., a pressing process with a vacuum pressing tool to evacuate air in samples. This step will reduce the degradation of material caused by oxygen. This fact also explains the severe degradation shown by the rPET90/rHDPE10 measurements.

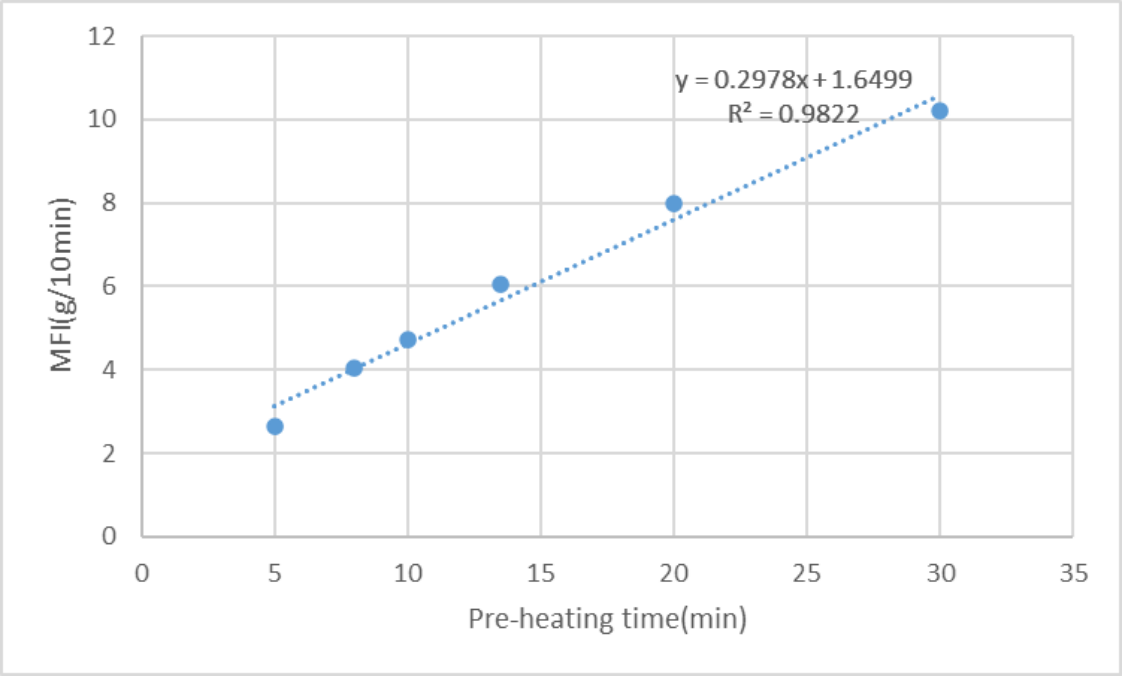

Figure 4. Virgin PLA MFI values changing through different pre-heating times from the tests with the OS MFI device.

Overall, as shown in Figure 5, both systems showed similar measurement precision and were capable of stable operation within a standard deviation of ~5-20%. This indicates that the open-source MFI system is capable of measuring the MFI of different materials with precision comparable to commercial products. Additionally, the study conducted experiments with different materials, either virgin or recycled. Compared to the PLA test data, there is a larger difference between the weight of extrudates made of PETG. This phenomenon could be due to the substantial differences in shape and size of the shredded PETG, e.g., different granulometries and dimensional ratios, leading to the formation of voids during extrusion, thereby affecting the measurement results[79], [91].

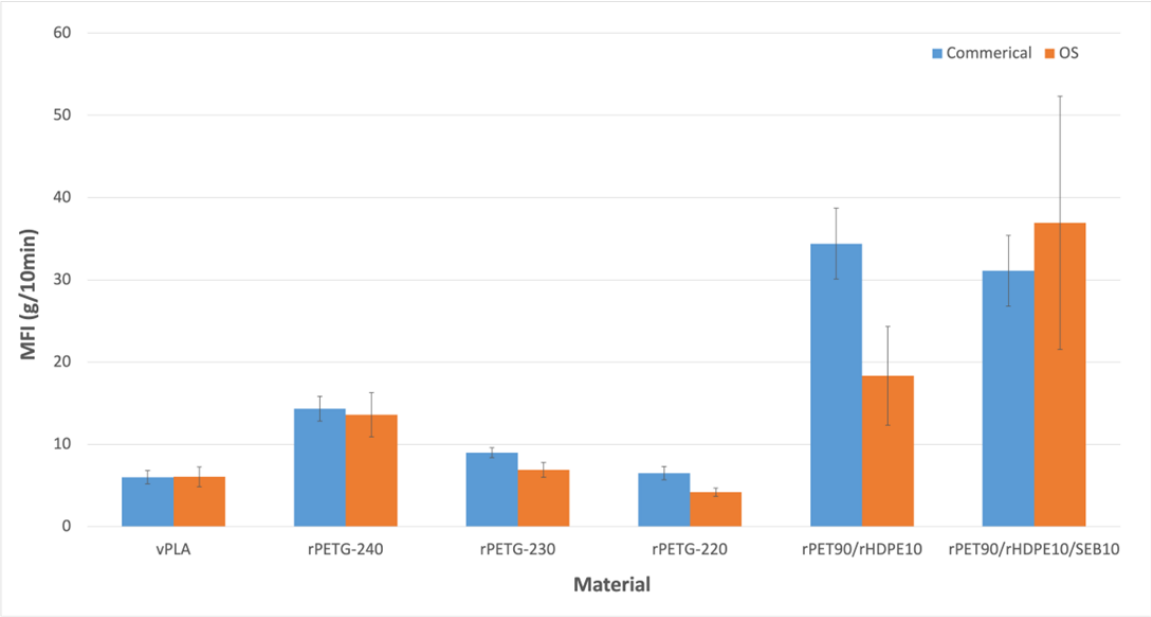

Figure 5. MFI measurement results of virgin PLA (vPLA), recycled PETG (rPETG), rPET90/rHDPE10, and rPET90/rHDPE10/SEBS10 obtained with the commercial equipment (left side bars) and OS MFI devices (right side bars).

2.4 Discussion

The development of the OS MFI offers an accessible and low-cost machine for the rapid assessment of the flowability and printability of recycled thermoplastic materials and blends. To validate the accuracy of the OS machine, a comparison was conducted with a commercial MFI device and the state-of-the-art. From the results, there are differences between results in both the OS MFI system and commercial device compared to the datasheet and the literature. The measurement of the MFI can be significantly affected by different parameters such as temperature, load weight, the diameter of the die, the diameter of the barrel, and their cleanness [50, 63], as well as the heat transfer conditions in the whole device itself. For instance, increasing the testing temperature of 10 °C can lead to a two- or three-fold increase of the MFI values, such as for PETG feedstock [85]. Moreover, the pre-heating conditions can also significantly modify the results, e.g., with differences of one order of magnitude [86]. Despite maintaining equal temperature and load weight, the diameter of the barrel and die might impact the measurements, as well as the properties of the materials used for these components, e.g., different heat capacities

and specific heats [56]. Changes in these factors reasonably explain the differences in the test results between OS and commercial MFI devices. Likewise, in the literature, inconsistencies can be found regarding the MFI test results, even for similar materials. For instance, Singh et al. [55] reported an increase in the MFI of rABS, whereas [72], [73] demonstrated a decrease in the MFI of the same material. Again, these contradictory results highlight the variability in MFI values, which may be influenced by differences in experimental conditions, material processing, measurement techniques, or the measuring equipment used in these studies. Furthermore, according to Rides et al. [64], MFI measurement has larger differences between different laboratories, confirming the variability in the equipment conditions and setup.

Providing all of the code for the OS MFI could help overcome this challenge as now any research lab, community makerspace, or other DRAM facility could use nearly identical systems. Compared to standard commercial MFI devices, the OS MFI developed in this study utilizes a DC motor to apply the load weight, which can impact the measurements, as load weight is a critical parameter. From a user perspective, this feature can simplify the operation and enhance the safety of the measurement process, making it more accessible and repeatable in DRAM contexts. It is important to highlight that MFI is a valuable tool for the rapid assessment of the flowability and potential printability of materials. However, for more detailed and scientifically rigorous results, comprehensive rheological analysis using rheometers should be conducted even when using commercial MFI devices.

Furthermore, MFI can not only be used in DRAM contexts or recycling activities but also laboratory environments [93]. This choice can help make research more affordable and reliable because this characterization can support the fine-tuning of 3D printing parameters with novel material formulations, helping to ensure extrudate consistency and, hence, improving the technical properties of the final parts, e.g., achieving better mechanical properties by reducing voids and defects from extrusion inconsistencies.

There are limitations of the open source MFI device that need future work. Currently cleaning procedures labor intensive. The cap needs to be disassembled to clean it from

the inside, requiring the disconnection of the band heater and thermocouple. Creating or identifying specialized cleaning tools to simplify the cleaning process could reduce the difficulty of cleaning.

Furthermore, the temperature control system could be improved in accuracy as it is showing variations of ~2 °C. Although there are two heating systems, the nichrome wire, and the band heater, temperature difference still exists in the MFI device, for example, the temperature in the hole on the cap could be lower than other parts, for example, it will be 170 degrees when other parts are 190 degrees, which also affects its accuracy. Future experiments could also consider the thread of the cap. Due to the threaded fit of the cap and the pipe (NPT), the cap cannot thread all the way up. This constraint leaves a part of the thread exposed, it can affect the shear force when extruding, potentially influencing the beginning of the measurements. This thread type, however, helps prevent leakage, increasing accuracy and limiting the previous effect.

To have better accuracy, some improvements can also be made to the device. According to previous tests results, which is that when the set temperature is 190 degrees, if the position of the band heater is up, roughly where the bottom of the cap can be exposed, the temperature in the die will be 170 degrees, while if the position of the band heater is down, roughly where the cap can be completely covered, the temperature will be 182 degrees. This test shows that the relative position of the band heater and cap will affect the temperature inside the die, which showed a significant improvement after fixing the position of the band heater and the cap. These results indicate that the stability of the temperature is a key factor in getting a more accurate MFI measurement result. This indicates further accuracy improvements might be med by reinforcing the insulation layer and have a more advanced temperature control system including improved insulation, temperature sensors or advanced temperature control algorithms. The accuracy of the digital scale and its interaction with the cutter system can impact results. In the current OS MFI device, the weight is unevenly distributed on the scale plate, leading to potential measurement errors, improvements of scale and cutter design can enhance accuracy. Better motor control system. Current motor control systems are generally accurate and can introduce some errors in the pressure. Therefore, using more advanced motor control

algorithms [94]can make the pressure more accurate, making the results more accurate as well. Future work could include a Graphical User Interface (GUI) to make the system easier to operate.

Future work should also include further measurements on a variety of other materials, especially recycled PLA. Conducting more tests with additional materials will provide further data, which will help refine the OS MFI's functionality and expand its application across various recycling and manufacturing contexts. Measuring recycled PLA will enable comparisons with existing PLA data, leading to a better analysis and understanding of how the recycling process affects the material. Moreover, further experiments can be conducted, such as measuring materials with different recycling frequencies, to gain a clearer understanding of the recycling lifecycle of PLA materials.

Additionally, exploring the impact of external environmental conditions on MFI experiments is necessary. For humidity-sensitive materials, the presence of moisture can cause material degradation during measurement, thereby affecting the MFI results. Hence, materials need to undergo drying preprocessing. This study did not deeply explore the impact of environmental factors during measurement. Most experiments were conducted in an environment with a temperature of 22°C and a humidity of around 60%. Therefore, further exploration is needed to understand how temperature and humidity in different environments affect experimental results.

2.5 Conclusions

To address the current issues with MFI device, an OS MFI device is developed. Measurements of virgin PLA, recycled PETG and blends of HDPE/PET were carried out using the proposed device. The results show good measurement precision with a ~5-20% standard deviation. Compared to its commercial counterpart, it has a ~5-23% decrease in PLA and PETG measurements, which shows a similar trend. The OS MFI can be a valuable characterization tool for easily sorting different material feedstocks, determining their suitability for FFF/FGF 3D printing, and identifying the optimal 3-D printing temperature. This study demonstrated the feasibility of manufacturing an OS MFI with performance comparable to its commercial counterparts. The validation test reported

similar MFI values for both the commercial and OS MFI devices when using common 3-D printing feedstock, i.e., virgin PLA and recycled PETG, and new polymer blend formulation from plastic waste, such as HDPE/PET blends. Some challenges remain, however, particularly in achieving consistent temperature along the heated barrel and nozzle. Therefore, future machine versions should improve the temperature control system and connection between cap (die) and heat barrel, optimizing the heat transfer in the whole equipment, e.g., improving insulation or changing part of the buy components selected for the current version. To enhance user-friendliness, future work can develop a graphical user interface, guided procedures and accessible tutorials that enables the adjustment of test parameters, such as pre-heating, weight load speed, or automated cutting timings.

The MFI in the market is currently expensive; to make the recycling process easier and more efficient, it is better to have an OS MFI device. A more affordable and accessible version of MFI devices can help enable DRAM to become more widespread.

Chapter 3

3 Distributed Manufacturing of Tourniquet Testing System for Open-Source Tourniquets

Tourniquets are effective for casualty-prevention in emergency situations. The use of centrally-manufactured commercial tourniquets, however, is not always possible due to supply chain disruptions. The open-source hardware model has been applied to overcome these disruptions in humanitarian crises and several low-cost digitally manufacturable open-source tourniquets have been developed. With the low reliability of improvised tourniquets, it is important to ensure that distributed manufacturing of tourniquets is effective and safe. Tourniquets can be tested, but existing tourniquet testers are expensive, bulky, and complex to operate, which limits their accessibility to an even greater extent than tourniquets in extreme settings. This article fulfills a need by providing a small, transportable, open-source additive-manufactured tourniquet tester that enables inexpensive and accurate testing of tourniquets against known clinical parameters. The <$100 tourniquet tester is validated and tested for operating force of tourniquets in the field or in distributed manufacturing facilities. The tourniquet tester has a significant economic and operational advantage compared to proprietary counterparts available on the market. Once calibrated with a blood pressure monitor, the built-in LCD displays the measuring range of the tester as 0 to 200 N, which is enough to test the validation of all tourniquets.

3.1 Hardware in context

A tourniquet is a device that applies pressure to a limb to stop bleeding and prevent shock. Tourniquets are widely used in emergency situations, such as combat injuries, mass casualty events, or accidents [95]. Access to tourniquets and associated training continues to develop as a critical first response to penetrating trauma in the civilian population [96], [97]. In 1999, Walter Reed Army Institute of Research collaborated with Oregon State University to evaluate existing tourniquet systems within U.S. military combat medicine [98]. This research, combined with casualty-prevention data from American military operations, resulted in the creation of the Combat Application

Tourniquet (CAT) and Joint Theater Trauma Systems (JTTS) [99], [100], which would eventually lead to the Committee on Tactical Combat Casualty Care (CoTCCC) [101], and new prehospital treatment protocols from the American College of Surgeons (ACS) and Advanced Trauma Life Support (ATLS) [102]. By the mid-2000s, the successful implementation of tourniquets for hemorrhagic control in combat settings was influencing civilian prehospital treatment protocols worldwide [95], [103]. Casualty-reducing protocols from ATLS, ACS, TCCC, and Stop the Bleed all stress field triage, stabilization, and external hemorrhage control with tourniquets as key factors in pre-hospital survival [104], [105], [106], [107].

The use of commercial tourniquets, however, is not always possible. For example, in 2014, the United Nations Office for the Coordination of Humanitarian Affairs observed significant civilian casualties during a four-week Gaza War [108], [109]. These fatalities resulted from penetrating gunshot wounds and crush injuries from shelling. Dr. Mohammed Al-Attar observed a CAT tourniquet (brought in by a medical colleague) but, due to the Israeli blockade, it was impossible to afford or import CAT-style tourniquets into Gaza [110], [111]. Al-Attar, the Director of Emergency Operations at the General Directorate of Civil Defence initiated hemorrhage control and improvised tourniquet training with Gaza's four ambulance services and the Hayat Center for Emergency & Crisis Management [111], [112], [113]. Although first responders became adept at applying improvised tourniquets, it became apparent that improvised tourniquets had low reliability, were challenging to effectively place over the wound, and required extensive assembly time when compared to hemorrhage speed [111].

Overcoming medical equipment supply chain challenges while maintaining uniformity and thus reliability is often accomplished by utilizing open-source hardware designs [37], [114], [115] coupled with digital manufacturing [116], [117]. In this model, designs are shared with an open source license and then individuals (do-it-yourself: DIY) [118], [119] or companies/organizations working together (do-it-together: DIT) [120], [121], [122] are free to download and replicate them. The opportunity to overcome supply disruptions in humanitarian crises [123], was recently brought into sharp focus during the COVID-19 pandemic [124], [125], [126], [127], [128], [129], [130], [131]. There is hope

that such an approach can be used to solve less acute shortages of medical equipment ranging from tools to help those suffering from chronic respiratory diseases [132] to the needs of surgeons [133]. A large portion of the promise of this approach is the ability to radically reduce costs as enormous economic values are created with replication from electronics [134], scientific tools [135], [136], [137], [138] and even MRI machines [139]. With reduced capital costs, which are generally around 90% [140], and value creation through distributed replication [141] the return on investment for designing new high-value products in the science and medical field is high (hundreds to thousands of percent) [142].

Thus, this open-source 3-D printing approach was used following the success of the Glia stethoscope 3-D printed in Gaza [143]. Al-Attar partnered with Glia's Gaza-based engineers to create a 3-D printed tourniquet that matched the clinical effectiveness of a CAT and published it on GitHub in 2017 [144]. On March 31, 2018, the first four hours of the Great March of Return resulted in 3,500 Palestinian casualties, roughly half of which were gunshot wounds [145], [146]. The Glia Gaza team immediately initiated tourniquet design improvements based on field training and feedback from Gaza EMS, often under live fire, and ramped production from 60-100 units/week to 200 units/week throughout 2018 and 2019 [111], [147], [148]. The tourniquets were effective. Early tourniquet field application, combined with Trauma Stabilization Points managed by the World Health Organization and Gaza EMS, was a critical factor in a 0.03% fatality rate among 5,969 gunshot victims [149]. This high number of casualties requiring tourniquets gave Glia the opportunity to iterate design changes, perform bench tests, and deploy bench-cleared units directly into the field [150].

In March 2022, Glia announced the tourniquet design for open-source emergency use in Ukraine and formed a partnership with Open Source Medical Supplies (OSMS) to coordinate decentralized additive manufacturers [151], [152]. Glia and OSMS quickly saw that additive manufacturers were changing the design to make it easier to print, and departing from clinical efficacy [153]. Additionally, generic CAT clones and independently designed tourniquets flooded the Ukraine market [154]. Dr. Tarek Loubani, Glia Medical Director, visited Ukraine in May 2022 and observed a broad

spectrum of tourniquet unit testing procedures [155]. The wide range of qualities for donated tourniquets, clones, and altered 3-D printed tourniquets has created a severe need for a tourniquet tester. There are no publicly accessible standards for unit testing a tourniquet, either for end-users or tourniquet manufacturers, which has created confusion in validating tourniquet clinical field performance. ASTM has been developing test fixture and tourniquet testing standards since 2016, but these standards are not yet publicly available [156]. Effective tourniquet application requires a combination of end-user training and mechanically effective tourniquet unit performance. The end-user must be confident a tourniquet dependably meets a clinical standard before patient application [157]. Applying a tourniquet incorrectly, can cause complications, such as nerve damage, tissue ischemia, or amputation. Therefore, it is important to ensure that tourniquets are effective and safe before using them on patients.

Tourniquet performance can be validated by a tourniquet tester, which is a device that measures the pressure applied by the tourniquet and the blood flow in the limb [158], [159]. Tourniquet testers can help evaluate the quality of different types of tourniquets, such as pneumatic, elastic, or mechanical systems [160]. They can also help train medical personnel on how to use tourniquets properly and monitor their effects [161], [162]. Unfortunately, existing tourniquet testers are expensive, bulky, or complex to operate (see Table 2). They may also require specialized equipment or calibration procedures that limit their accessibility and usability in low-resource settings [163]. There is a clear need for an open-source additive manufactured unit tester that would allow a manufacturer or end-user to inexpensively and accurately test their device against a known clinical parameter, an important resource for conflict-affected and resource-limited communities.

Table 2. Commercial tourniquet test systems

Product	**Cost**	**Functions**
TrueClot Tourniquet Trainer [164]	USD$725	This device has interior blood flow. When the tourniquet is correctly applied, hemostasis is achieved on

		simulated blood flowing from the wound. Cannot show data.
Tourniquet Task Trainer Arm [165]	USD$490	This device has interior blood flow. When the tourniquet is correctly applied, hemostasis is achieved on simulated blood flowing from the wound. Cannot show data.
Chi Systems' HapMed Tourniquet Trainer [166]	Not available	This device has LEDs and screens, which can demonstrate data and hemostasis indicators.
Sim Limb Bleed Control Tourniquet Trainer [167]	USD$365	This device simulates blood flow from a wound. Cannot show data.
Emergency Tourniquet Trainer – Arm [168]	USD$1529	Simulated upper arm with realistic wounds connected to a pump. When the tourniquet is correctly applied, hemostasis is achieved on simulated blood flowing from the wound.
Humimic Tourniquet Arm Trainer [169]	USD$500	Simulated upper arm with realistic wounds and interior blood flow. When the tourniquet is correctly applied, hemostasis is achieved on simulated blood flowing from the wound. Does not show data.
Humimic Tourniquet & Wound Packing Leg Trainer [170]	USD$632	Simulated upper leg with realistic wounds and interior blood flow. When the tourniquet is correctly applied, hemostasis is achieved on simulated

		blood flowing from the wound. Does not show data.
3B Scientific Hemorrhage Control Arm Trainer P102 [171]	USD $1,975	Simulated upper arm and shoulder with realistic wounds and interior blood flow. When the tourniquet is correctly applied, hemostasis is achieved on simulated blood flowing from the wound. Does not show data.

To fill this need, this article describes an open-source 3-D printed tourniquet tester that is low-cost, portable, and easy to both manufacture and deploy across diverse scenarios. The design and fabrication process of the device using common materials and tools is described. The tourniquet tester is validated for functionality and accuracy by comparing it with a commercial tourniquet tester on different types of tourniquets. A low-cost calibration process is demonstrated, and potential errors are quantified. The advantages and limitations of the device are discussed and future work is outlined.

3.2 Hardware Description

An open-source 3-D printable tourniquet tester is developed. All the custom mechanical components can be fabricated with a low-cost desktop fused filament fabrication-based RepRap-class 3-D printer. The electronic components are all open source and readily available off-the-shelf from a wide variety of vendors. The compact design of the tourniquet tester makes it easy to manufacture and easy to transport. The electronic circuit diagrams are provided to power the testing unit via a USB input. The tourniquet tester is validated and tested on Glia units as well as CAT units for testing the operating force of tourniquets in the field or in distributed manufacturing facilities (e.g., fab labs, makerspaces, 3-D print shops, libraries, schools, or in volunteers' homes). As of this writing, there is no agreement on testing standards from the tourniquet manufacturers, so this open-source 3-D printed tourniquet tester provides a means of democratizing the environments which require tourniquet use. The tourniquet tester has a significant

economic and operational advantage compared to proprietary counterparts available on the market.

- Designed for distributed manufacturing settings and resource-limited communities seeking to validate donated commercial tourniquets validate novel/generic commercial tourniquets and those made with distributed manufacturing consistent with the Glia and other types of open-source tourniquets.
- Low production cost: All the housing components are manufactured by 3-D printing and assembled easily and quickly.
- Portable and durable: The compact design makes the testing unit easy to transport and can be made from the choice of high-durability 3-D printing materials.
- Simple operation: Once the tester is calibrated with a blood pressure cuff, it does not need any extra steps or adjustments. The pressure reading is directly shown on the LCD display. According to the measuring range of the load cell (0-20kg), the measuring range of the tester is 0 to 200 N and 0 to 698.2 mmHg (depending on the calibration factor S), which is enough to test the validation of the tourniquets.

3.3 Operation instructions

Before testing the tourniquet, calibration is required. Due to the nature of the sensor, the calibration consists of two parts,

1. Calibration of the load cell (Force reading)
2. Calibration of the tourniquet tester unit as a whole (Pressure reading)

3.3.1 Calibration of the force measurement.

Initially, the load cell can be calibrated using known weights. Known weights can be placed on the tournbutton-M while the tester is placed flat. This method has limitations on the weight that can be applied. Alternatively, a calibration device may be employed, which consists of a wooden plate, a linear rail, bolts and nuts, and other 3-D printed parts as Figure 9 shows. Once assembled, the tester is placed beneath the 3-D printed platform and connected to a computer. By manipulating the weights on the platform, data can be obtained.

To get the calibration factor of the force measurement, an open-source calibration code [172] is utilized to acquire this factor. To apply this calibration code, first, it needs to be uploaded to the Arduino board through Arduino IDE software. There are instructions to be followed in the code include [173]:

1. Set up the tester and start the sketch without a weight on the tester.

2. Once readings are displayed place the weight on the scale.

3. Press +/- or a/z to adjust the calibration_factor until the output readings match the known weight.

4. Use this calibration_factor on the unit tester sketch.

The example code assumes pounds (lbs). In this project, 100 grams was used as the unit. Unit can be changed in the Serial.print(" lbs"); line to 100g. The parameter that can be obtained could be a positive or negative number, it depends on the way of implementing the load cell. The factor typically ranges between 1500 to 15000. It should be noted that this parameter may differ depending on the environment in which the load cell is installed, thus necessitating recalibration each time the load cell is reinstalled.

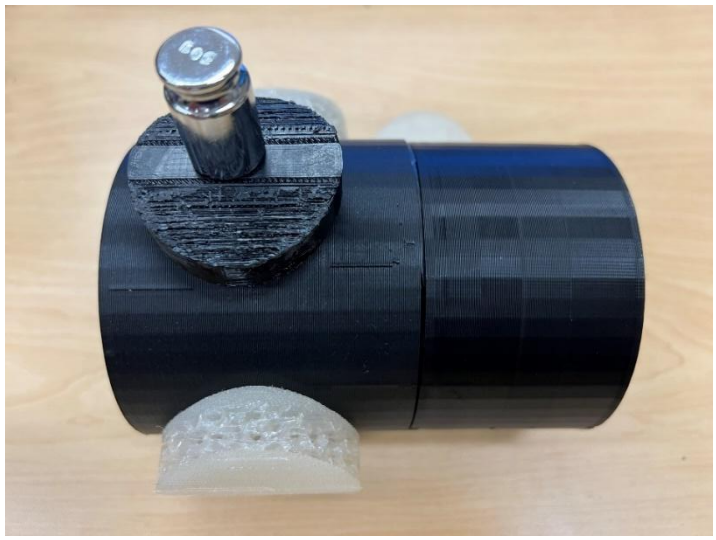

Figure 6. Calibration process with no platform.

3.3.2 Calibrate the pressure parameter.

In most medical and clinical settings, the pressure generated by the tourniquet is recorded in mmHg. However, the sensor used in the unit tester being a load cell, it can only measure the force being applied, not the pressure. Therefore, the force measurement is converted into pressure, following:

$$\boldsymbol{P = \frac{F}{S}\ [Pascal]} \qquad \textbf{Equation 1}$$

where P is pressure (pascal), F is force (N) and S is surface area (m^3). Equation 1 requires an area to convert force into pressure, which in this case is the effective surface area acting on the load cell. Various factors such as the force concentration, width of the tourniquet, the number of turns of the windlass, and the part of the tourniquet that touches the button can also influence the readings. To address this issue and obtain more reliable pressure measurements, the method used to measure occlusion pressure was adopted, which uses a blood pressure cuff as the calibrating unit [160], [163]. These blood pressure cuffs are widely accessible globally. This approach is divided into two parts. First, determining the optimum position of the blood pressure cuff with reference to the load cell/ “tournbutton M” part. Second, determining the effective surface area parameter.

To determine the optimum position of the blood pressure cuff for further testing, a manual pneumatic blood pressure cuff was wrapped around the unit tester, and the tourniquet was applied to the cuff. The pressure generated by the tourniquet was determined by subtracting the original reading from the reading after applying the tourniquet. An infant-sized blood pressure cuff was used to ensure consistency in the measurement position, and five readings were taken at 60 mmHg, 100 mmHg, 140 mmHg, and 180 mmHg, respectively. The cuff was adjusted such that the pneumatic pipe aligns exactly at the center of the tournbutton-M as 0 degrees. The cuff was then rotated by 45 degrees, and the readings were recorded again. This was repeated 8 times from 0 degrees to 315 degrees. Figure 6 shows the readings of pressure applied by the blood pressure cuff and the force recorded by the load cell of the tourniquet tester as the system was rotated (Figure 7). The data in Figure 6 shows similar trends for all the angles of rotation tested. To determine the fixed position of the blood pressure cuff for further testing and validation, the 0-degree angle is chosen, where the cuff is exactly on top of tournbutton M. This was done because the readings showed a linear relationship between the pressure applied by the tourniquet and the force measured by the load cell at the particular position.

Figure 7. Calibration against the blood pressure cuff

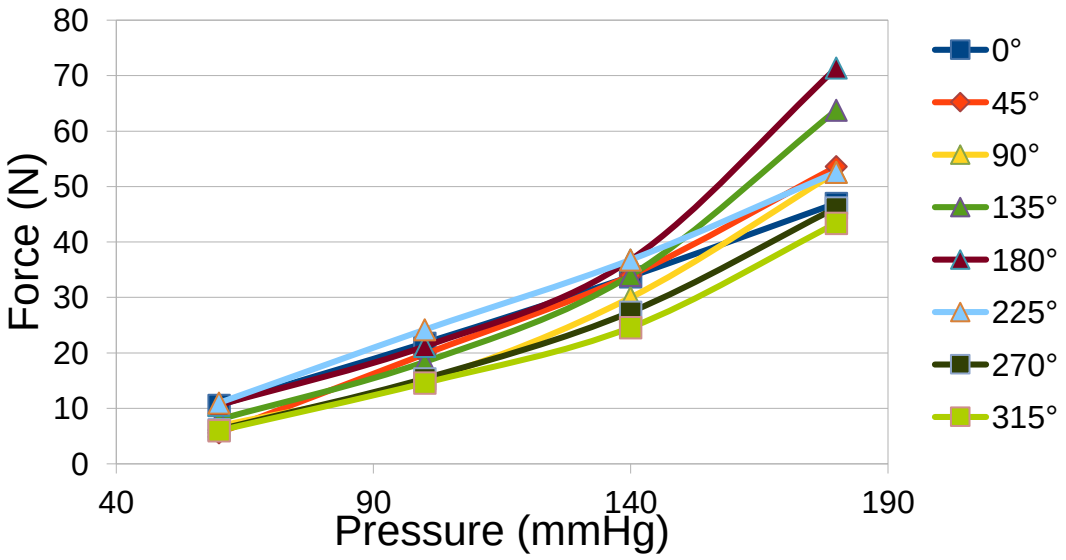

Figure 8. Experiment data of the force measured as a function of the pressure in the various angles of rotation.

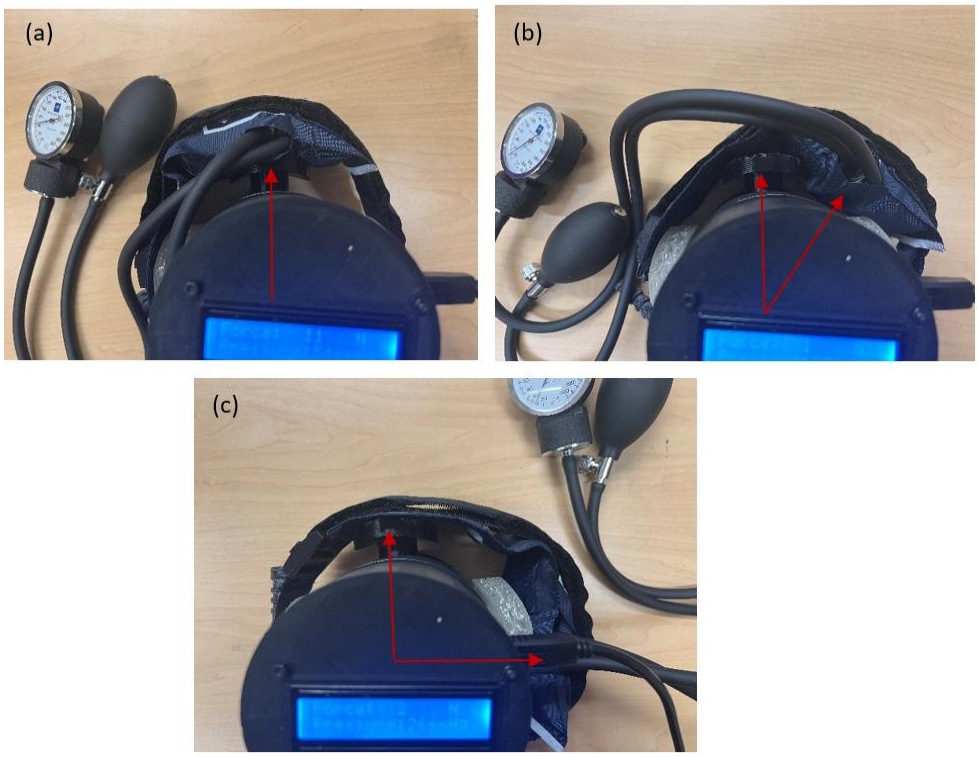

Figure 9. Cuff position at (a) 0°,(b) 45° and (c)90° .

Now, to find out the surface area the procedure is a s follows:

1. Inflate the pneumatic blood pressure cuff to about 20 mmHg. Place the blood pressure cuff around the tester in the 0-degree position.

2. Record the force readings at 10 mmHg increments while increasing the pressure from turning the windlass of the tourniquet.

3. The following equations are used to calculate the value of the surface area, S. First the pressure, P is determined:

$$\boldsymbol{P = c - 20\ [mmHg]} \qquad \textbf{Equation 2}$$

$$\boldsymbol{S = \frac{F}{133.2 * P}\ [m^3]} \qquad \textbf{Equation 3}$$

where c represents the reading on blood pressure cuff in mmHg, F represents the reading of force (N) on the tester. In equation 2, the initially applied pressure of 20 mmHg is

subtracted from the pressure reading. The constant 133.32 is the conversion factor for converting the pressure from mmHg to Pascals.

Measure the force readings at least three times to obtain stable values of force against the applied pressure. Calculate the average of the force measurements and further calculate the surface area parameter S for each of the pressure readings. Finally, the average of all the S values is considered the final calibration factor/surface area parameter.

4. Put S in the equation in the code “unit tester” [172].

Table 3. Calibration data

Blcuff	**P**	**F (Average)**	**Surface Area Parameter**
68	48	13.23	0.00207
80	60	17.47	0.00218
90	70	20.53	0.00220
100	80	22.97	0.00215
110	90	26.27	0.00219
120	100	29.50	0.00221
130	110	33.20	0.00226
140	120	36.70	0.00229
150	130	40.27	0.00232
160	140	44.17	0.00237
170	150	47.60	0.00238

180	160	51.20	0.00240
190	170	55.20	0.00244
200	180	58.33	0.00243
210	190	61.87	0.00244
220	200	65.93	0.00247
230	210	70.60	0.00252
240	220	73.50	0.00251
250	230	77.23	0.00252
		Average	**0.00233**

Once calibration is complete, the tester is ready for measurement. The measurement process is shown in Figure 8 and is as follows:

1. Plug in the power cord and the tester starts up.

2. Insert Tournbutton-M into the hole used for measurement.

3. Wrap the tourniquet around the tester, and make sure that the tourniquet is pressing the Tournbutton-M, and the Tournbutton-M stands vertically on the flat (for the force can distribute evenly).

4. Turn the tourniquet windlass and the corresponding value will appear on LCD.

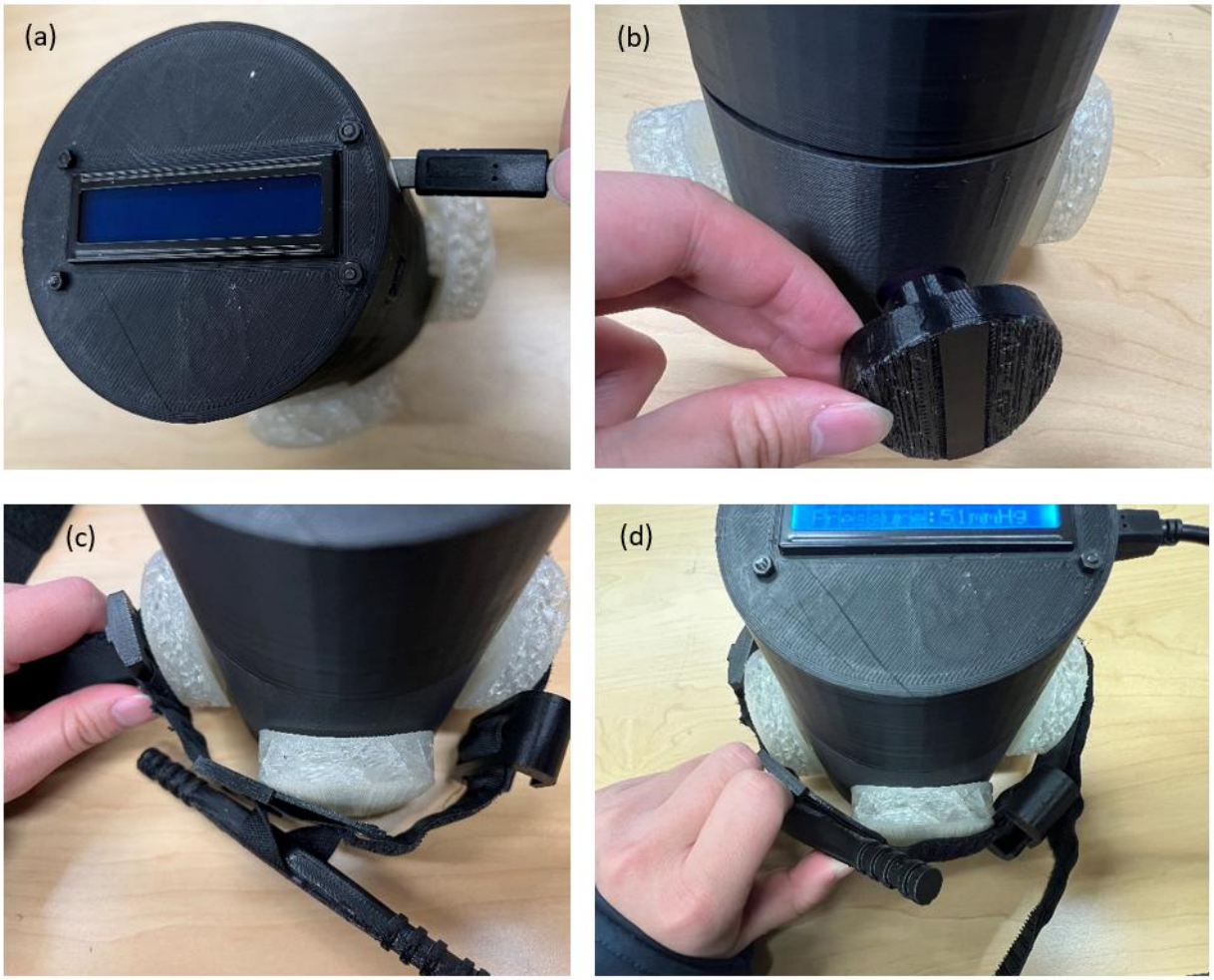

Figure 10. Measurement process (a) Plug in the power cord (b) Insert Tournbutton-M (c) Wrap the tourniquet to the tester (d) Turn the tourniquet windlass.

3.4 Validation

To validate the calibration procedure,

1. Inflate air into the blood pressure cuff to about 20 mmHg.
2. Put the blood pressure cuff in between the tourniquet and the tester.
3. Test the tourniquet on the unit tester. Record the pressure on the tester and blood pressure cuff.
4. Compare the difference between these data.

If the readings do not have a large gap (standard), then it can be concluded that the unit tester is valid.

Figure 9 shows the validation data, where the plot is an average of 5 tests of blood pressure cuff readings vs the calibrated tourniquet tester readings. The results fit within a relatively straight line with the R^2 value of 0.99. The slope of the line is 1.07 to confirm that the BL cuff measurements and the tourniquet measurements correspond to the same value. Thus, it can be confirmed that the tester unit is validated. The same procedure can be used in any distributed manufacturing facility making the testers and then the testers can be deployed to tourniquet manufacturers.

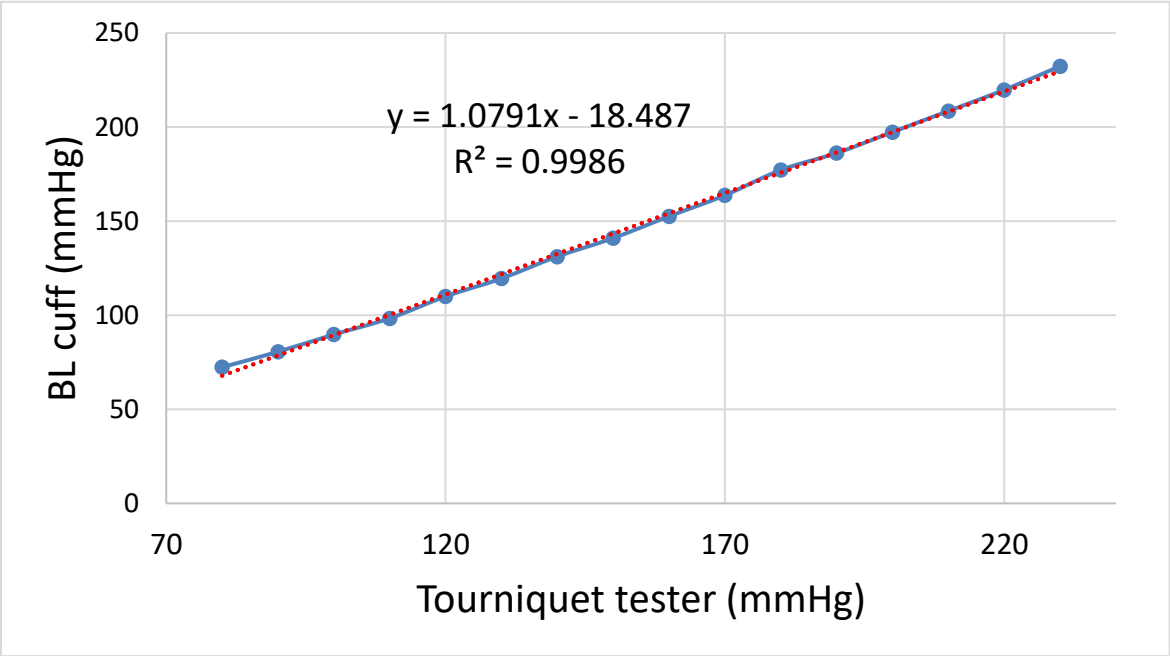

Figure 11. Validation tests, BL cuff vs tourniquet tester readings (p=5).

3.5 Limitations and future works

After testing, the load cell used is stable and has good linear characteristics. The user operation is simple and straightforward, with readings directly on the screen on top of the tester, no additional operation or instrumentation is required. Due to the simple design and principle, the tester is also inexpensive to produce. There are, however, several areas of future work and ways the system can be improved. First, the printing time, the plastic

used, and the cost can all be further reduced by shrinking the size of the assembly. This can in part be done by making a dedicated open-source board for this application or coupling the output of the device to a relatively ubiquitous cell phone for obtaining the readings. Secondly, the snap-fit part can be damaged if it is repeatedly opened and closed roughly. Therefore, it is recommended to reduce the number of disassembles, but also future work can investigate the use of other materials, improving the toughness of the design.

There are some obvious limitations. Due to the housing being fixed, there is a maximum measuring limitation, but it is not the limitation of the tourniquet. It is because the pressure generated by the tourniquet comes from the deformation or compressing of the tourniquet. If the tourniquet cannot deform, then the force applied to the windlass will transfer to the strap itself, but not apply to the cylinder. The TPU parts will help this situation, but the limitation still exists. Another limitation comes from load cell, it has a measurement range, and if the force goes beyond its limit, the data will be inaccurate. It should be pointed out, however, that the value does not (and should not) go above 500 mmHg (approximately 154 N). After this amount of force is applied the patient can be damaged [174]. The tester should be deployed with this value labeled as a warning. Future work can also investigate the potential to make this a stand-alone (zero power) device by incorporating solar photovoltaic cells into the housing design. Other research groups associated with distributed tourniquet manufacturers can test additional types of tourniquets.

Chapter 4

4 Conclusions

This thesis successfully developed an open source MFI and tourniquet tester.

This study has developed the first open-source tourniquet tester and open-source melt flow index system, providing support for the acquisition of tourniquets in regions facing challenging circumstances. The tourniquet tester confirms the effectiveness of tourniquets, while the MFI identifies the 3D printability of recycled materials. Both designs have been validated through empirical testing. The MFI, however, requires further experimentation for calibration. Anyone can access the designs unconditionally, modifying or improving them as needed.

Furthermore, the low cost and high customization potential of open-source and 3D printing offer greater flexibility for various application scenarios. This transition from nothing to something significantly lowers the barriers to entry, allowing more individuals to participate in the project, and drastically reducing usage costs. This provides an alternative method for people in special regions to alleviate or even solve potential shortages.

In terms of sustainable development, the MFI helps in recycling plastic resources. As a lower-cost recycling detector compared to a rheometer, it can attract more people to participate in recycling activities. Lower-cost recycling activities are more likely to engage people, thereby promoting sustainable development.

Regarding the results from the MFI testing, although there are discrepancies from the standard values, methods such as pre-experiments can be utilized to identify these gaps and subsequently establish a calibration formula.

The MFI testing needs more extensive experimental data and will be useful for a wide range of materials. Since properties vary among different materials, a richer dataset would facilitate a more accurate analysis, aiding in the development of a more precise calibration formula.

The functionality of the tourniquet tester to measure tourniquet pressure has also been confirmed. Although this work was successful, the pressure measured by the tourniquet tester may differ from the actual pressure exerted by a tourniquet on the human body. Due to the complexity of human anatomy, it is challenging to ascertain whether the measurements obtained from the tester can be directly correlated with those on a human, and whether a one-to-one physical relationship exists. Thus, experiments involving human subjects are necessary to explore the correlation between the tester readings and their actual effects on the human body.

All experiments conducted with the tourniquet tester were performed using the same type of tourniquet. To determine whether the tester is also effective for other types of tourniquets, further testing is required.

References or Bibliography

[1] Statista Research Department, "Global plastic production 1950-2021," Statista. Accessed: May 08, 2023. [Online]. Available: https://www.statista.com/statistics/282732/global-production-of-plastics-since-1950/

[2] G. Maitlo *et al.*, "Plastic Waste Recycling, Applications, and Future Prospects for a Sustainable Environment," *Sustainability*, vol. 14, no. 18, Art. no. 18, Jan. 2022, doi: 10.3390/su141811637.

[3] A. L. Andrady, Ed., *Plastics and the Environment*, 1st ed. Wiley, 2003. doi: 10.1002/0471721557.

[4] C. J. Moore, "Synthetic polymers in the marine environment: A rapidly increasing, long-term threat," *Environmental Research*, vol. 108, no. 2, pp. 131–139, Oct. 2008, doi: 10.1016/j.envres.2008.07.025.

[5] S. Bejgarn, M. MacLeod, C. Bogdal, and M. Breitholtz, "Toxicity of leachate from weathering plastics: An exploratory screening study with *Nitocra spinipes*," *Chemosphere*, vol. 132, pp. 114–119, Aug. 2015, doi: 10.1016/j.chemosphere.2015.03.010.

[6] L. Bradney *et al.*, "Particulate plastics as a vector for toxic trace-element uptake by aquatic and terrestrial organisms and human health risk," *Environment International*, vol. 131, p. 104937, Oct. 2019, doi: 10.1016/j.envint.2019.104937.

[7] F. M. Lamberti, L. A. Román-Ramírez, and J. Wood, "Recycling of Bioplastics: Routes and Benefits," *J Polym Environ*, vol. 28, no. 10, pp. 2551–2571, Oct. 2020, doi: 10.1007/s10924-020-01795-8.

[8] OECD Global Plastics Outlook Database, "Plastic pollution is growing relentlessly as waste management and recycling fall short, says OECD," OECD. Accessed: May 08, 2023. [Online]. Available: https://www.oecd.org/environment/plastic-pollution-is-growing-relentlessly-as-waste-management-and-recycling-fall-short.htm

[9] S. C. Dertinger *et al.*, "Technical pathways for distributed recycling of polymer composites for distributed manufacturing: Windshield wiper blades," *Resources, Conservation and Recycling*, vol. 157, p. 104810, Jun. 2020, doi: 10.1016/j.resconrec.2020.104810.

[10] S. Zhong and J. M. Pearce, "Tightening the loop on the circular economy: Coupled distributed recycling and manufacturing with recyclebot and RepRap 3-D printing," *Resources, Conservation and Recycling*, vol. 128, pp. 48–58, Jan. 2018, doi: 10.1016/j.resconrec.2017.09.023.

[11] F. A. Cruz Sanchez, H. Boudaoud, M. Camargo, and J. M. Pearce, "Plastic recycling in additive manufacturing: A systematic literature review and opportunities for the circular economy," *Journal of Cleaner Production*, vol. 264, p. 121602, Aug. 2020, doi: 10.1016/j.jclepro.2020.121602.

[12] H. A. Little, N. G. Tanikella, M. J. Reich, M. J. Fiedler, S. L. Snabes, and J. M. Pearce, "Towards Distributed Recycling with Additive Manufacturing of PET Flake Feedstocks," *Materials*, vol. 13, no. 19, p. 4273, Sep. 2020, doi: 10.3390/ma13194273.

[13] M. A. Kreiger, M. L. Mulder, A. G. Glover, and J. M. Pearce, "Life cycle analysis of distributed recycling of post-consumer high density polyethylene for 3-D printing filament," *Journal of Cleaner Production*, vol. 70, pp. 90–96, May 2014, doi: 10.1016/j.jclepro.2014.02.009.

[14] M. Kreiger and J. M. Pearce, "Environmental Life Cycle Analysis of Distributed Three-Dimensional Printing and Conventional Manufacturing of Polymer Products," *ACS Sustainable Chem. Eng.*, vol. 1, no. 12, pp. 1511–1519, Dec. 2013, doi: 10.1021/sc400093k.

[15] J. Gwamuri, B. T. Wittbrodt, N. C. Anzalone, and J. M. Pearce, "Reversing the Trend of Large Scale and Centralization in Manufacturing: The Case of Distributed Manufacturing of Customizable 3-D-Printable Self-Adjustable Glasses," *Challenges in Sustainability*, vol. 2, no. 1, pp. 30–40, Dec. 2014, doi: 10.12924/cis2014.02010030.

[16] E. Petersen and J. Pearce, "Emergence of Home Manufacturing in the Developed World: Return on Investment for Open-Source 3-D Printers," *Technologies*, vol. 5, no. 1, p. 7, Feb. 2017, doi: 10.3390/technologies5010007.

[17] M. Mohammed, D. Wilson, E. Gomez-Kervin, A. Petsiuk, R. Dick, and J. M. Pearce, "Sustainability and feasibility assessment of distributed E-waste recycling using additive manufacturing in a Bi-continental context," *Additive Manufacturing*, vol. 50, p. 102548, Feb. 2022, doi: 10.1016/j.addma.2021.102548.

[18] S. Zhong, P. Rakhe, and J. Pearce, "Energy Payback Time of a Solar Photovoltaic Powered Waste Plastic Recyclebot System," *Recycling*, vol. 2, no. 2, p. 10, Jun. 2017, doi: 10.3390/recycling2020010.

[19] P. Santander, F. A. Cruz Sanchez, H. Boudaoud, and M. Camargo, "Social, political, and technological dimensions of the sustainability evaluation of a recycling network. A literature review," *Cleaner Engineering and Technology*, vol. 6, p. 100397, Feb. 2022, doi: 10.1016/j.clet.2022.100397.

[20] P. Santander, F. A. Cruz Sanchez, H. Boudaoud, and M. Camargo, "Closed loop supply chain network for local and distributed plastic recycling for 3D printing: a MILP-based optimization approach," *Resources, Conservation and Recycling*, vol. 154, p. 104531, Mar. 2020, doi: 10.1016/j.resconrec.2019.104531.

[21] C. Caceres Mendoza, P. Santander, F. Cruz-Sanchez, N. Troussier, M. Camargo, and H. Boudaoud, "Life Cycle Assessment of Distributed Plastic Recycling Via Additive Manufacturing," Sep. 26, 2022, *Rochester, NY*: 4230044. doi: 10.2139/ssrn.4230044.

[22] A. O. Laplume, B. Petersen, and J. M. Pearce, "Global value chains from a 3D printing perspective," *J Int Bus Stud*, vol. 47, no. 5, pp. 595–609, Jun. 2016, doi: 10.1057/jibs.2015.47.

[23] C. Baechler, M. DeVuono, and J. M. Pearce, "Distributed recycling of waste polymer into RepRap feedstock," *Rapid Prototyping Journal*, vol. 19, no. 2, pp. 118–125, Mar. 2013, doi: 10.1108/13552541311302978.

[24] A. L. Woern, J. R. McCaslin, A. M. Pringle, and J. M. Pearce, "RepRapable Recyclebot: Open source 3-D printable extruder for converting plastic to 3-D printing filament," *HardwareX*, vol. 4, p. e00026, Oct. 2018, doi: 10.1016/j.ohx.2018.e00026.

[25] R. Jones *et al.*, "RepRap – the replicating rapid prototyper," *Robotica*, vol. 29, no. 1, pp. 177–191, Jan. 2011, doi: 10.1017/S026357471000069X.

[26] E. Sells, S. Bailard, Z. Smith, A. Bowyer, and V. Olliver, "RepRap: The Replicating Rapid Prototyper: Maximizing Customizability by Breeding the Means of Production," in *Handbook of Research in Mass Customization and Personalization*, World Scientific Publishing Company, 2009, pp. 568–580. doi: 10.1142/9789814280280_0028.

[27] A. Bowyer, "3D Printing and Humanity's First Imperfect Replicator," *3D Printing and Additive Manufacturing*, vol. 1, no. 1, pp. 4–5, Mar. 2014, doi: 10.1089/3dp.2013.0003.

[28] F. Cruz Sanchez, S. Lanza, H. Boudaoud, S. Hoppe, and M. Camargo, "Polymer Recycling and Additive Manufacturing in an Open Source context : Optimization of processes and methods," Aug. 2015.

[29] I. Anderson, "Mechanical Properties of Specimens 3D Printed with Virgin and Recycled Polylactic Acid," *3D Printing and Additive Manufacturing*, vol. 4, no. 2, pp. 110–115, Jun. 2017, doi: 10.1089/3dp.2016.0054.

[30] J. Pakkanen, D. Manfredi, P. Minetola, and L. Iuliano, "About the Use of Recycled or Biodegradable Filaments for Sustainability of 3D Printing," Apr. 2017, pp. 776–785. doi: 10.1007/978-3-319-57078-5_73.

[31] M. I. Mohammed, D. Wilson, E. Gomez-Kervin, C. Vidler, L. Rosson, and J. Long, "The Recycling of E-Waste ABS Plastics by Melt Extrusion and 3D Printing Using Solar Powered Devices as a Transformative Tool for Humanitarian Aid," 2018, Accessed: Mar. 11, 2024. [Online]. Available: https://hdl.handle.net/2152/90080

[32] S. Chong, G.-T. Pan, M. Khalid, T. C.-K. Yang, S.-T. Hung, and C.-M. Huang, "Physical Characterization and Pre-assessment of Recycled High-Density Polyethylene as 3D Printing Material," *Journal of Polymers and the Environment*, vol. 2, no. 25, pp. 136–145, Jul. 2016, doi: 10.1007/s10924-016-0793-4.

[33] M. Pepi, N. Zander, and M. Gillan, "Towards Expeditionary Battlefield Manufacturing Using Recycled, Reclaimed, and Scrap Materials," *JOM*, vol. 70, Jul. 2018, doi: 10.1007/s11837-018-3040-8.

[34] N. Zander, M. Gillan, and R. Lambeth, "Recycled polyethylene terephthalate as a new FFF feedstock material," *Additive Manufacturing*, vol. 21, pp. 174–182, May 2018, doi: 10.1016/j.addma.2018.03.007.

[35] N. Zander, "Recycled Polymer Feedstocks for Material Extrusion Additive Manufacturing," 2019, pp. 37–51. doi: 10.1021/bk-2019-1315.ch003.

[36] K. R. Hart, J. B. Frketic, and J. R. Brown, "Recycling meal-ready-to-eat (MRE) pouches into polymer filament for material extrusion additive manufacturing," *Additive Manufacturing*, vol. 21, pp. 536–543, May 2018, doi: 10.1016/j.addma.2018.04.011.

[37] S. Oberloier, N. G. Whisman, and J. M. Pearce, "Finding Ideal Parameters for Recycled Material Fused Particle Fabrication-Based 3D Printing Using an Open Source Software Implementation of Particle Swarm Optimization," *3D Printing and Additive Manufacturing*, vol. 10, no. 6, pp. 1287–1300, Dec. 2023, doi: 10.1089/3dp.2022.0012.

[38] A. L. Woern and J. M. Pearce, "Distributed Manufacturing of Flexible Products: Technical Feasibility and Economic Viability," *Technologies*, vol. 5, no. 4, Art. no. 4, Dec. 2017, doi: 10.3390/technologies5040071.

[39] X. Tian, T. Liu, Q. Wang, A. Dilmurat, D. Li, and G. Ziegmann, "Recycling and remanufacturing of 3D printed continuous carbon fiber reinforced PLA composites," *Journal of Cleaner Production*, vol. 142, pp. 1609–1618, Jan. 2017, doi: 10.1016/j.jclepro.2016.11.139.

[40] A. Pringle, M. Rudnicki, and J. Pearce, "Wood Furniture Waste-Based Recycled 3-D Printing Filament," *Forest Products Journal*, vol. 68, Nov. 2017, doi: 10.13073/FPJ-D-17-00042.

[41] P. Parandoush and D. Lin, "A review on additive manufacturing of polymer-fiber composites," *Composite Structures*, vol. 182, pp. 36–53, Dec. 2017, doi: 10.1016/j.compstruct.2017.08.088.

[42] B. P. Heller, D. E. Smith, and D. A. Jack, "Planar deposition flow modeling of fiber filled composites in large area additive manufacturing," *Additive Manufacturing*, vol. 25, pp. 227–238, Jan. 2019, doi: 10.1016/j.addma.2018.10.031.

[43] A. Romani, L. Perusin, M. Ciurnelli, and M. Levi, “Characterization of PLA feedstock after multiple recycling processes for large-format material extrusion additive manufacturing,” *Materials Today Sustainability*, vol. 25, p. 100636, Mar. 2024, doi: 10.1016/j.mtsust.2023.100636.

[44] J. M. Justino Netto, H. T. Idogava, L. E. Frezzatto Santos, Z. de C. Silveira, P. Romio, and J. L. Alves, “Screw-assisted 3D printing with granulated materials: a systematic review,” *Int J Adv Manuf Technol*, vol. 115, no. 9, pp. 2711–2727, Aug. 2021, doi: 10.1007/s00170-021-07365-z.

[45] M. J. Reich, A. L. Woern, N. G. Tanikella, and J. M. Pearce, “Mechanical Properties and Applications of Recycled Polycarbonate Particle Material Extrusion-Based Additive Manufacturing,” *Materials*, vol. 12, no. 10, Art. no. 10, Jan. 2019, doi: 10.3390/ma12101642.

[46] A. Romani, M. Levi, and J. M. Pearce, “Recycled polycarbonate and polycarbonate/acrylonitrile butadiene styrene feedstocks for circular economy product applications with fused granular fabrication-based additive manufacturing,” *Sustainable Materials and Technologies*, vol. 38, p. e00730, Dec. 2023, doi: 10.1016/j.susmat.2023.e00730.

[47] C. Suescun Gonzalez, F. A. Cruz Sanchez, H. Boudaoud, C. Nouvel, and J. M. Pearce, “Multi-material distributed recycling via material extrusion: recycled high density polyethylene and poly (ethylene terephthalate) mixture,” *Polymer Engineering & Science*, vol. 64, no. 4, pp. 1555–1570, 2024, doi: 10.1002/pen.26643.

[48] A. Alexandre, F. A. Cruz Sanchez, H. Boudaoud, M. Camargo, and J. M. Pearce, “Mechanical Properties of Direct Waste Printing of Polylactic Acid with Universal Pellets Extruder: Comparison to Fused Filament Fabrication on Open-Source Desktop Three-Dimensional Printers,” *3D Printing and Additive Manufacturing*, vol. 7, no. 5, pp. 237–247, Oct. 2020, doi: 10.1089/3dp.2019.0195.

[49] A. Woern, D. Byard, R. Oakley, M. Fiedler, S. Snabes, and J. Pearce, “Fused Particle Fabrication 3-D Printing: Recycled Materials’ Optimization and Mechanical Properties,” *Materials*, vol. 11, no. 8, p. 1413, Aug. 2018, doi: 10.3390/ma11081413.

[50] S. Whyman, K. M. Arif, and J. Potgieter, “Design and development of an extrusion system for 3D printing biopolymer pellets,” *Int J Adv Manuf Technol*, vol. 96, no. 9, pp. 3417–3428, Jun. 2018, doi: 10.1007/s00170-018-1843-y.

[51] M. Paramatti, A. Romani, G. Pugliese, and M. Levi, “PLA Feedstock Filled with Spent Coffee Grounds for New Product Applications with Large-Format Material Extrusion Additive Manufacturing,” *ACS Omega*, vol. 9, no. 6, pp. 6423–6431, Feb. 2024, doi: 10.1021/acsomega.3c05669.

[52] N. Volpato, D. Kretschek, J. A. Foggiatto, and C. M. Gomez da Silva Cruz, "Experimental analysis of an extrusion system for additive manufacturing based on polymer pellets," *Int J Adv Manuf Technol*, vol. 81, no. 9, pp. 1519–1531, Dec. 2015, doi: 10.1007/s00170-015-7300-2.

[53] D. Byard, A. Woern, R. Oakley, M. Fiedler, S. Snabes, and J. Pearce, "Green fab lab applications of large-area waste polymer-based additive manufacturing," *Additive Manufacturing*, vol. 27, pp. 515–525, May 2019, doi: 10.1016/j.addma.2019.03.006.

[54] W. d'Ambrières, "Plastics recycling worldwide: current overview and desirable changes," *Field Actions Science Reports. The journal of field actions*, no. Special Issue 19, Art. no. Special Issue 19, Mar. 2019.

[55] B. Ruj, V. Pandey, P. Jash, and V. Srivastava, "Sorting of plastic waste for effective recycling," *Int. J. Appl. Sci. Eng. Res.*, vol. 4, Jan. 2015, doi: 10.6088/ijaser.04058.

[56] S. Wang, L. Capoen, D. R. D'hooge, and L. Cardon, "Can the melt flow index be used to predict the success of fused deposition modelling of commercial poly(lactic acid) filaments into 3D printed materials?," *Plastics, Rubber and Composites*, Feb. 2018, Accessed: Jul. 16, 2024. [Online]. Available: https://journals.sagepub.com/doi/full/10.1080/14658011.2017.1397308

[57] M. Spoerk, J. Gonzalez-Gutierrez, J. Sapkota, S. Schuschnigg, and C. Holzer, "Effect of the printing bed temperature on the adhesion of parts produced by fused filament fabrication," *Plastics, Rubber and Composites*, vol. 47, no. 1, pp. 17–24, Feb. 2018, doi: 10.1080/14658011.2017.1399531.

[58] S. Guerreiro, I. João, and L. Pimentel Real, "Evaluation of the influence of testing parameters on the melt flow index of thermoplastics," *Polymer Testing*, vol. 31, pp. 1026–1030, Dec. 2012, doi: 10.1016/j.polymertesting.2012.07.008.

[59] M. Teresa Rodríguez-Hernández, J. L. Angulo-Sánchez, and A. Pérez-Chantaco, "Determination of the molecular characteristics of commercial polyethylenes with different architectures and the relation with the melt flow index," *Journal of Applied Polymer Science*, vol. 104, no. 3, pp. 1572–1578, 2007, doi: 10.1002/app.25625.

[60] A. V. Shenoy and D. R. Saini, "Melt flow index: More than just a quality control rheological parameter. Part I," *Advances in Polymer Technology*, vol. 6, no. 1, pp. 1–58, 1986, doi: 10.1002/adv.1986.060060101.

[61] R. V. Pazhamannil, J. N. V. N., G. P., and A. Edacherian, "Property enhancement approaches of fused filament fabrication technology: A review," *Polymer Engineering & Science*, vol. 62, no. 5, pp. 1356–1376, 2022, doi: 10.1002/pen.25948.

[62] E. E. Ferg and L. L. Bolo, "A correlation between the variable melt flow index and the molecular mass distribution of virgin and recycled polypropylene used in the

manufacturing of battery cases," *Polymer Testing*, vol. 32, no. 8, pp. 1452–1459, Dec. 2013, doi: 10.1016/j.polymertesting.2013.09.009.

[63] B. Singh *et al.*, "Investigations on Melt Flow Rate and Tensile Behaviour of Single, Double and Triple-Sized Copper Reinforced Thermoplastic Composites," *Materials*, vol. 14, no. 13, Art. no. 13, Jan. 2021, doi: 10.3390/ma14133504.

[64] R. Plavec *et al.*, "Influence of Multiple Thermomechanical Processing of 3D Filaments Based on Polylactic Acid and Polyhydroxybutyrate on Their Rheological and Utility Properties," *Polymers*, vol. 14, no. 10, Art. no. 10, Jan. 2022, doi: 10.3390/polym14101947.

[65] N. Sa'ude, K. Kamarudin, M. Ibrahim, and M. H. I. Ibrahim, "Melt Flow Index of Recycle ABS for Fused Deposition Modeling (FDM) Filament," *Applied Mechanics and Materials*, vol. 773–774, pp. 3–7, 2015, doi: 10.4028/www.scientific.net/AMM.773-774.3.

[66] F. Laoutid, S. Lafqir, A. Toncheva, and P. Dubois, "Valorization of Recycled Tire Rubber for 3D Printing of ABS- and TPO-Based Composites," *Materials*, vol. 14, no. 19, Art. no. 19, Jan. 2021, doi: 10.3390/ma14195889.

[67] M. Garwacki, I. Cudnik, D. Dziadowiec, P. Szymczak, and J. Andrzejewski, "The Development of Sustainable Polyethylene Terephthalate Glycol-Based (PETG) Blends for Additive Manufacturing Processing—The Use of Multilayered Foil Waste as the Blend Component," *Materials*, vol. 17, no. 5, Art. no. 5, Jan. 2024, doi: 10.3390/ma17051083.

[68] A. Gupta, M. Misra, and A. K. Mohanty, "Novel sustainable materials from waste plastics: compatibilized blend from discarded bale wrap and plastic bottles," *RSC Adv.*, vol. 11, no. 15, pp. 8594–8605, Feb. 2021, doi: 10.1039/D1RA00254F.

[69] V. Kumar, R. Singh, and I. P. S. Ahuja, "On correlation of rheological, thermal, mechanical and morphological properties of chemical assisted mechanically blended ABS-Graphene composite as tertiary recycling for 3D printing applications," *Advances in Materials and Processing Technologies*, Jul. 2022, Accessed: Jul. 22, 2024. [Online]. Available: https://www.tandfonline.com/doi/abs/10.1080/2374068X.2021.1913324

[70] E. O. Cisneros-López *et al.*, "Recycled poly(lactic acid)–based 3D printed sustainable biocomposites: a comparative study with injection molding," *Materials Today Sustainability*, vol. 7–8, p. 100027, Mar. 2020, doi: 10.1016/j.mtsust.2019.100027.

[71] O. Zabihi *et al.*, "Mechanical upcycling of single-use face mask waste into high-performance composites: An ecofriendly approach with cost-benefit analysis," *Science of The Total Environment*, vol. 919, p. 170469, Apr. 2024, doi: 10.1016/j.scitotenv.2024.170469.

[72] V. Mishra, C. K. Ror, S. Negi, S. Kar, and L. N. Borah, “Development of sustainable 3D printing filaments using recycled/virgin ABS blends: Processing and characterization,” *Polymer Engineering & Science*, vol. 63, no. 7, pp. 1890–1899, 2023, doi: 10.1002/pen.26330.

[73] I. Turku, S. Kasala, and T. Kärki, “Characterization of Polystyrene Wastes as Potential Extruded Feedstock Filament for 3D Printing,” *Recycling*, vol. 3, no. 4, Art. no. 4, Dec. 2018, doi: 10.3390/recycling3040057.

[74] “MXBAOHENG XNR-400B Melt Flow Rate Index Tester MFR Melt Flow Indexer Printing Machine (220V) : Amazon.ca: Tools & Home Improvement.” Accessed: Jul. 17, 2024. [Online]. Available: https://www.amazon.ca/MXBAOHENG-XNR-400B-Indexer-Printing-Machine/dp/B07CMN9SWN?th=1

[75] “Wholesale melt flow index mfi testing machine To Test Electronic Equipment - Alibaba.com.” Accessed: Mar. 15, 2024. [Online]. Available: https://www.alibaba.com/showroom/melt-flow-index-mfi-testing-machine.html

[76] “MELT FLOW INDEXER-tabletop instrument that tests the melt mass.” Accessed: Mar. 15, 2024. [Online]. Available: https://www.mrclab.com/melt-flow-indexer-1

[77] D. Liu and A. Romani, “MFI,” Jun. 2023, Accessed: Jul. 24, 2024. [Online]. Available: https://osf.io/68hbj/

[78] “Teensy® 4.0.” Accessed: Mar. 11, 2024. [Online]. Available: https://www.pjrc.com/store/teensy40.html

[79] 14:00-17:00, “ISO 1133-1:2022,” ISO. Accessed: Jul. 16, 2024. [Online]. Available: https://www.iso.org/standard/83905.html

[80] “compass.” Accessed: Jul. 16, 2024. [Online]. Available: https://compass.astm.org/document/?contentCode=ASTM%7CD1238-10%7Cen-US&proxycl=https%3A%2F%2Fsecure.astm.org&fromLogin=true

[81] M. Y. T. Wu, S. L. Mak, W. F. Tang, C. H. Li, and T. W. Chan, “A Review on Melt Flow Index Characteristics of Polylactide (PLA) for Recycle Use in 3-D Printing,” *Journal of Testing and Evaluation*, vol. 50, no. 4, pp. 2260–2267, 2022, doi: 10.1520/JTE20210314.

[82] M. H. M. Nasir, M. M. Taha, N. Razali, R. A. Ilyas, V. F. Knight, and M. N. F. Norrrahim, “Effect of Chemical Treatment of Sugar Palm Fibre on Rheological and Thermal Properties of the PLA Composites Filament for FDM 3D Printing,” *Materials*, vol. 15, no. 22, Art. no. 22, Jan. 2022, doi: 10.3390/ma15228082.

[83] F. Doronin, A. Rudakova, G. Rytikov, and V. Nazarov, “A novel determination of the melt flow index of composite filaments used in extrusion additive manufacturing,” *Polymer Testing*, vol. 133, p. 108376, Apr. 2024, doi: 10.1016/j.polymertesting.2024.108376.

[84] V. K n, D. Bonthu, M. Doddamani, and F. Pati, “Additive Manufacturing of Short Silk Fiber Reinforced PETG Composites,” *Materials Today Communications*, vol. 33, p. 104772, Dec. 2022, doi: 10.1016/j.mtcomm.2022.104772.

[85] S. V. Kotomin, D. V. Kramarev, I. M. Obidin, and S. V. Polunin, “Influence of 3D Printing Conditions of Polyethylene Terephthalate Glycol on the Mechanical Properties of Products Based on It,” *Polym. Sci. Ser. A*, vol. 64, no. 6, pp. 617–623, Dec. 2022, doi: 10.1134/S0965545X22700365.

[86] R. Singh *et al.*, “On 3D printing of low-cost sensors using recycled PET,” *Sādhanā*, vol. 47, no. 4, p. 260, Nov. 2022, doi: 10.1007/s12046-022-02029-4.

[87] “PolyLite_PETG_TDS_V5.2.pdf.” Accessed: Jul. 24, 2024. [Online]. Available: https://cdn.shopify.com/s/files/1/0548/7299/7945/files/PolyLite_PETG_TDS_V5.2.pdf?v=1640828798

[88] M. Bustos Seibert, G. A. Mazzei Capote, M. Gruber, W. Volk, and T. A. Osswald, “Manufacturing of a PET Filament from Recycled Material for Material Extrusion (MEX),” *Recycling*, vol. 7, no. 5, Art. no. 5, Oct. 2022, doi: 10.3390/recycling7050069.

[89] M. Nofar and H. Oğuz, “Development of PBT/Recycled-PET Blends and the Influence of Using Chain Extender,” *J Polym Environ*, vol. 27, no. 7, pp. 1404–1417, Jul. 2019, doi: 10.1007/s10924-019-01435-w.

[90] “Ingeo Biopolymer 4043D Technical Data Sheet”.

[91] M. Seifali Abbas-Abadi, M. Nekoomanesh Haghighi, H. Yeganeh, and B. Bozorgi, “The effect of melt flow index, melt flow rate, and particle size on the thermal degradation of commercial high density polyethylene powder,” *J Therm Anal Calorim*, vol. 114, no. 3, pp. 1333–1339, Dec. 2013, doi: 10.1007/s10973-013-3133-0.

[92] S. S. Bafna and A.-M. Beall, “A Design of Experiments Study on the Factors Affecting Variability in the Melt Index Measurement”.

[93] A. Shenoy and D. Saini, “Melt flow index: More than just a quality control rheological parameter. Part II,” *Advances in Polymer Technology - ADV POLYM TECHNOL*, vol. 6, pp. 125–145, Jun. 1986, doi: 10.1002/adv.1986.060060201.

[94] S. K. Suman and V. K. Giri, “Speed control of DC motor using optimization techniques based PID Controller,” in *2016 IEEE International Conference on Engineering and Technology (ICETECH)*, Coimbatore, India: IEEE, Mar. 2016, pp. 581–587. doi: 10.1109/ICETECH.2016.7569318.

[95] C. Lee, K. M. Porter, and T. J. Hodgetts, “Tourniquet use in the civilian prehospital setting,” *Emergency Medicine Journal*, vol. 24, no. 8, Art. no. 8, Aug. 2007, doi: 10.1136/emj.2007.046359.

[96] N. Ochs *et al.*, “Hemorrhage-control Tourniquets: How Intuitive are They?,” *Prehospital and Disaster Medicine*, vol. 34, no. s1, pp. s91–s91, May 2019, doi: 10.1017/S1049023X19001894.

[97] M. Lynn, “Use of Tourniquets in Mass Casualty Incidents and ‘Stop the Bleed’ Program,” in *Disasters and Mass Casualty Incidents: The Nuts and Bolts of Preparedness and Response to Protracted and Sudden Onset Emergencies*, M. Lynn, H. Lieberman, L. Lynn, G. D. Pust, K. Stahl, D. D. Yeh, and T. Zakrison, Eds., Cham: Springer International Publishing, 2019, pp. 75–78. doi: 10.1007/978-3-319-97361-6_8.

[98] D. R. Welling, P. L. McKay, T. E. Rasmussen, and N. M. Rich, “A brief history of the tourniquet,” *Journal of Vascular Surgery*, vol. 55, no. 1, pp. 286–290, Jan. 2012, doi: 10.1016/j.jvs.2011.10.085.

[99] A. C. Beekley *et al.*, “Prehospital tourniquet use in Operation Iraqi Freedom: effect on hemorrhage control and outcomes,” *J Trauma*, vol. 64, no. 2 Suppl, Art. no. 2 Suppl, Feb. 2008, doi: 10.1097/TA.0b013e318160937e.

[100] R. S. Kotwal, F. K. Butler, E. P. Edgar, S. A. Shackelford, D. R. Bennett, and J. A. Bailey, “Saving Lives on the Battlefield: A Joint Trauma System Review of Pre-Hospital Trauma Care in Combined Joint Operating Area ? Afghanistan (CJOA-A) Executive Summary,” *J Spec Oper Med*, vol. 13, no. 1, pp. 77–85, 2013.

[101] “Tactical Combat Casualty Care.” Accessed: Mar. 22, 2023. [Online]. Available: https://www.naemt.org/education/naemt-tccc

[102] “CAT Resources – Inventor and Exclusive Manufacturer of the Combat Application Tourniquet®.” Accessed: Mar. 22, 2023. [Online]. Available: https://www.combattourniquet.com/

[103] K. A. Eilertsen, M. Winberg, E. Jeppesen, G. Hval, and T. Wisborg, “Prehospital Tourniquets in Civilians: A Systematic Review,” *Prehospital and Disaster Medicine*, vol. 36, no. 1, pp. 86–94, Feb. 2021, doi: 10.1017/S1049023X20001284.

[104] M. Gilbert and E. Fosse, “Inside Gaza’s Al-Shifa hospital,” *The Lancet*, vol. 373, no. 9659, pp. 200–202, Jan. 2009, doi: 10.1016/S0140-6736(09)60057-X.

[105] E. M. Bulger *et al.*, “An Evidence-based Prehospital Guideline for External Hemorrhage Control: American College of Surgeons Committee on Trauma,” *Prehospital Emergency Care*, vol. 18, no. 2, pp. 163–173, Apr. 2014, doi: 10.3109/10903127.2014.896962.

[106] “Our Story,” Stop The Bleed. Accessed: Mar. 22, 2023. [Online]. Available: https://www.stopthebleed.org/our-story/

[107] "TCCC-Guidelines-update-june-2-2014.pdf." Accessed: Jul. 26, 2024. [Online]. Available: https://www.itstactical.com/wp-content/uploads/2014/07/TCCC-Guidelines-update-june-2-2014.pdf

[108] "Occupied Palestinian Territory: Gaza Emergency Situation Report (as of 20 July 2014, 1500 hrs) - occupied Palestinian territory | ReliefWeb." Accessed: Mar. 22, 2023. [Online]. Available: https://reliefweb.int/report/occupied-palestinian-territory/occupied-palestinian-territory-gaza-emergency-situation-repo-9

[109] "2014 Gaza conflict," UNRWA. Accessed: Mar. 22, 2023. [Online]. Available: https://www.unrwa.org/2014-gaza-conflict

[110] "The Gaza Strip | The humanitarian impact of 15 years of blockade - June 2022 | UNICEF Middle East and North Africa." Accessed: Mar. 22, 2023. [Online]. Available: https://www.unicef.org/mena/documents/gaza-strip-humanitarian-impact-15-years-blockade-june-2022

[111] "M. Al-Attar, personal communication, July 14, 2022."

[112] S. K. Stewart, J. C. Duchesne, and M. A. Khan, "Improvised tourniquets: Obsolete or obligatory?," *Journal of Trauma and Acute Care Surgery*, vol. 78, no. 1, pp. 178–183, Jan. 2015, doi: 10.1097/TA.0000000000000485.

[113] "Islamic University of Gaza :: Faculty of Medicine > Academic Study > Post-Graduation > Hayat Center for Emergency & Crisis Management." Accessed: Mar. 22, 2023. [Online]. Available: https://dnntest.iugaza.edu.ps/medicineen/Academic-Study/Post-Graduation/Hayat-Center-for-Emergency-Crisis-Management

[114] A. Powell, "Democratizing production through open source knowledge: from open software to open hardware," *Media, Culture & Society*, vol. 34, no. 6, pp. 691–708, Sep. 2012, doi: 10.1177/0163443712449497.

[115] A. Gibb, "Building Open Source Hardware: DIY Manufacturing for Hackers and Makers".

[116] A. S. Lowe, "Distributed Manufacturing: Make Things Where You Need Them," *Management for Professionals*, pp. 37–50, 2019.

[117] J. C. Mariscal-Melgar, M. Omer, M. Moritz, P. Hijma, T. Redlich, and J. P. Wulfsberg, "Distributed Manufacturing: A High-Level Node-Based Concept for Open Source Hardware Production," 2022, doi: 10.15488/12171.

[118] A. Tsanni, "African scientists leverage open hardware," *Nature*, vol. 582, no. 7810, pp. 138–138, Jun. 2020, doi: 10.1038/d41586-020-01606-z.

[119] T. Wenzel, "Open hardware: From DIY trend to global transformation in access to laboratory equipment," *PLOS Biology*, vol. 21, no. 1, p. e3001931, Jan. 2023, doi: 10.1371/journal.pbio.3001931.

[120] L. Dupont, F. Kasmi, J. M. Pearce, and R. J. Ortt, """Do-It-Together"": Towards the Factories of the Future," 2021.

[121] S. Mahajan, C.-H. Luo, D.-Y. Wu, and L.-J. Chen, "From Do-It-Yourself (DIY) to Do-It-Together (DIT): Reflections on designing a citizen-driven air quality monitoring framework in Taiwan," *Sustainable Cities and Society*, vol. 66, p. 102628, Mar. 2021, doi: 10.1016/j.scs.2020.102628.

[122] J. M. Pearce, "Strategic Investment in Open Hardware for National Security," *Technologies*, vol. 10, no. 2, Art. no. 2, Apr. 2022, doi: 10.3390/technologies10020053.

[123] L. James, "Opportunities and challenges of distributed manufacturing for humanitarian response," in *2017 IEEE Global Humanitarian Technology Conference (GHTC)*, Oct. 2017, pp. 1–9. doi: 10.1109/GHTC.2017.8239297.

[124] S. Oberloier, N. Gallup, and J. M. Pearce, "Overcoming supply disruptions during pandemics by utilizing found hardware for open source gentle ventilation," *HardwareX*, vol. 11, p. e00255, Apr. 2022, doi: 10.1016/j.ohx.2021.e00255.

[125] A. Vallatos *et al.*, "Adaptive Manufacturing for Healthcare During the COVID-19 Emergency and Beyond," *Front. Med. Technol.*, vol. 3, Aug. 2021, doi: 10.3389/fmedt.2021.702526.

[126] G. Dafermos, "Transforming the productive base of the economy through the open design commons and distributed manufacturing," *Journal of Peer Production*, Jul. 2015, Accessed: Jul. 26, 2024. [Online]. Available: https://www.academia.edu/14030312/Transforming_the_productive_base_of_the_economy_through_the_open_design_commons_and_distributed_manufacturing

[127] A. M. Chagas, J. C. Molloy, L. L. Prieto-Godino, and T. Baden, "Leveraging open hardware to alleviate the burden of COVID-19 on global health systems," *PLOS Biology*, vol. 18, no. 4, p. e3000730, Apr. 2020, doi: 10.1371/journal.pbio.3000730.

[128] J. M. Pearce, "Authors from all over the world share their tech in *HardwareX* to battle COVID-19," *HardwareX*, vol. 9, p. e00190, Apr. 2021, doi: 10.1016/j.ohx.2021.e00190.

[129] J. Stirling and R. Bowman, "The COVID-19 Pandemic Highlights the Need for Open Design Not Just Open Hardware," *The Design Journal*, vol. 24, no. 2, pp. 299–314, Dec. 2020, doi: 10.1080/14606925.2020.1859168.

[130] L. Corsini, V. Dammicco, and J. Moultrie, "Critical Factors for Implementing Open Source Hardware in a Crisis: Lessons Learned from the COVID-19 Pandemic," *Journal of Open Hardware*, vol. 4, no. 1, Art. no. 1, Dec. 2020, doi: 10.5334/joh.24.

[131] J. M. Pearce, “Distributed Manufacturing of Open Source Medical Hardware for Pandemics,” *Journal of Manufacturing and Materials Processing*, vol. 4, no. 2, Art. no. 2, Jun. 2020, doi: 10.3390/jmmp4020049.

[132] R. Farré, D. Gozal, V.-N. Nguyen, J. M. Pearce, and A. T. Dinh-Xuan, “Open-Source Hardware May Address the Shortage in Medical Devices for Patients with Low-Income and Chronic Respiratory Diseases in Low-Resource Countries,” *Journal of Personalized Medicine*, vol. 12, no. 9, Art. no. 9, Sep. 2022, doi: 10.3390/jpm12091498.

[133] J. K. Bow, N. Gallup, S. A. Sadat, and J. M. Pearce, “Open source surgical fracture table for digitally distributed manufacturing,” *PLOS ONE*, vol. 17, no. 7, p. e0270328, Jul. 2022, doi: 10.1371/journal.pone.0270328.

[134] M. Oellermann *et al.*, “Open Hardware in Science: The Benefits of Open Electronics,” *Integrative and Comparative Biology*, vol. 62, no. 4, pp. 1061–1075, Oct. 2022, doi: 10.1093/icb/icac043.

[135] E. Gibney, “‘Open-hardware’ pioneers push for low-cost lab kit,” *Nature*, vol. 531, no. 7593, pp. 147–148, Mar. 2016, doi: 10.1038/531147a.

[136] D. K. Fisher and P. J. Gould, “Open-Source Hardware Is a Low-Cost Alternative for Scientific Instrumentation and Research,” *Modern Instrumentation*, vol. 1, no. 2, Art. no. 2, Apr. 2012, doi: 10.4236/mi.2012.12002.

[137] J. M. Pearce, “Building Research Equipment with Free, Open-Source Hardware,” *Science*, vol. 337, no. 6100, pp. 1303–1304, Sep. 2012, doi: 10.1126/science.1228183.

[138] J. Pearce, *Open-Source Lab: How to Build Your Own Hardware and Reduce Research Costs*. 2014.

[139] M. Moritz, T. Redlich, S. Günyar, L. Winter, and J. P. Wulfsberg, “On the Economic Value of Open Source Hardware – Case Study of an Open Source Magnetic Resonance Imaging Scanner,” *Journal of Open Hardware*, vol. 3, no. 1, Art. no. 1, May 2019, doi: 10.5334/joh.14.

[140] J. M. Pearce, “Economic savings for scientific free and open source technology: A review,” *HardwareX*, vol. 8, p. e00139, Oct. 2020, doi: 10.1016/j.ohx.2020.e00139.

[141] “Quantifying the Value of Open Source Hard-ware Development.” Accessed: Jul. 26, 2024. [Online]. Available: https://www.scirp.org/journal/paperinformation?paperid=53076

[142] J. Pearce, “Return on investment for open source scientific hardware development,” *Science and Public Policy*, vol. 43, Jun. 2015, doi: 10.1093/scipol/scv034.

[143] A. Pavlosky, J. Glauche, S. Chambers, M. Al-Alawi, K. Yanev, and T. Loubani, "Validation of an effective, low cost, Free/open access 3D-printed stethoscope," *PLOS ONE*, vol. 13, no. 3, p. e0193087, Mar. 2018, doi: 10.1371/journal.pone.0193087.

[144] *GliaX/tourniquet*. (Jul. 24, 2024). Glia Free Medical hardware. Accessed: Jul. 26, 2024. [Online]. Available: https://github.com/GliaX/tourniquet

[145] "gaza - great march of return," UNRWA. Accessed: Jul. 26, 2024. [Online]. Available: https://www.unrwa.org/campaign/gaza-great-march-return

[146] P. Issa, "INTERVIEW WITH DR. GHASSAN ABU SITTA: 'There Is No International Community,'" *Journal of Palestine Studies*, vol. 47, no. 4, pp. 46–56, Aug. 2018, doi: 10.1525/jps.2018.47.4.46.

[147] *YouTube. (2018, May 12). Tourniquet training. YouTube. Retrieved February 25, 2023, from https://www.youtube.com/watch?v=kY_iNWeTVz.*

[148] Glia International #EqualCare, *Tourniquet Field Training by Dr. Mohammed Al-Attar*, (May 12, 2018). Accessed: Jul. 26, 2024. [Online Video]. Available: https://www.youtube.com/watch?v=1lbF28hfjmM

[149] C. X. T. Phuong *et al.*, "Evaluation of the World Health Organization standard tourniquet test and a modified tourniquet test in the diagnosis of dengue infection in Viet Nam," *Tropical Medicine & International Health*, vol. 7, no. 2, Art. no. 2, 2002, doi: 10.1046/j.1365-3156.2002.00841.x.

[150] T. Loubani, "3D printed open source tourniquet: Rationale, failure analysis and proposed next steps of the Glia…," Medium. Accessed: Jul. 26, 2024. [Online]. Available: https://trklou.medium.com/3d-printed-open-source-tourniquet-rationale-failure-analysis-and-proposed-next-steps-of-the-glia-97e8441b4c5a

[151] T. Loubani, "Glia's Gaza Tourniquet is ready for emergency use in Ukraine. Make some if you can," Medium. Accessed: Jul. 26, 2024. [Online]. Available: https://trklou.medium.com/glias-gaza-tourniquet-is-ready-for-emergency-use-in-ukraine-make-some-if-you-can-ef5f83260b7c

[152] "Open Source Medical Supplies," Open Source Medical Supplies. Accessed: Jul. 26, 2024. [Online]. Available: https://opensourcemedicalsupplies.org/

[153] T. Loubani, "Reinventing 3D printed tourniquets for Ukraine is a mistake," Medium. Accessed: Jul. 26, 2024. [Online]. Available: https://trklou.medium.com/reinventing-3d-printed-tourniquets-for-ukraine-is-a-mistake-be2937f0ad65

[154] A. Husarska, "Opinion | Ukrainian Engineers, Historians and Housewives Are Keeping Putin on His Toes," *The New York Times*, Jan. 12, 2023. Accessed: Jul. 26,

2024. [Online]. Available: https://www.nytimes.com/2023/01/12/opinion/ukraine-war.html

[155] "Lifehacker: Tarek Loubani on 3D-Printing in Gaza," Logic(s) Magazine. Accessed: Jul. 26, 2024. [Online]. Available: https://logicmag.io/bodies/tarek-loubani-on-3d-printing-in-gaza/

[156] *WK56860 new specification for nonpneumatic limb tourniquets. ASTM International - Standards Worldwide. (2016, December 6). Retrieved February 25, 2023, from https://www.astm.org/workitem-wk56860*.

[157] A. Dennis *et al.*, "Missing expectations: Windlass tourniquet use without formal training yields poor results," *Journal of Trauma and Acute Care Surgery*, vol. 87, no. 5, p. 1096, Nov. 2019, doi: 10.1097/TA.0000000000002431.

[158] J. F. Kragh *et al.*, "Practical use of emergency tourniquets to stop bleeding in major limb trauma," *J Trauma*, vol. 64, no. 2 Suppl, Art. no. 2 Suppl, Feb. 2008, doi: 10.1097/TA.0b013e31816086b1.

[159] J. F. Kragh *et al.*, "Battle casualty survival with emergency tourniquet use to stop limb bleeding," *J Emerg Med*, vol. 41, no. 6, Art. no. 6, Dec. 2011, doi: 10.1016/j.jemermed.2009.07.022.

[160] P. L. Wall *et al.*, "Tourniquet pressures: strap width and tensioning system widths," *J Spec Oper Med*, vol. 14, no. 4, Art. no. 4, 2014, doi: 10.55460/IT3C-9I89.

[161] K. Inaba *et al.*, "Tourniquet use for civilian extremity trauma," *Journal of Trauma and Acute Care Surgery*, vol. 79, no. 2, Art. no. 2, Aug. 2015, doi: 10.1097/TA.0000000000000747.

[162] R. C. Kue *et al.*, "Tourniquet Use in a Civilian Emergency Medical Services Setting: A Descriptive Analysis of the Boston EMS Experience," *Prehospital Emergency Care*, vol. 19, no. 3, Art. no. 3, Jul. 2015, doi: 10.3109/10903127.2014.995842.

[163] P. L. Wall, D. C. Duevel, M. B. Hassan, J. D. Welander, S. M. Sahr, and C. M. Buising, "Tourniquets and Occlusion: The Pressure of Design," *Military Medicine*, vol. 178, no. 5, Art. no. 5, May 2013, doi: 10.7205/MILMED-D-12-00490.

[164] "TrueClot® Tourniquet Trainer," Rescue Essentials. Accessed: Mar. 23, 2023. [Online]. Available: https://www.rescue-essentials.com/trueclot-tourniquet-trainer/

[165] "Tourniquet Task Trainer Arm," TacMed Solutions™. Accessed: Jul. 26, 2024. [Online]. Available: https://tacmedsolutions.com/products/tourniquet-task-trainer-arm

[166] "Home | HapMed Tourniquet Trainer," website. Accessed: Mar. 23, 2023. [Online]. Available: https://www.hapmedtraining.com

[167] "Sim Limb: Tourniquet, Wound Packing, Chest Seal, Suturing Task Trainer," wildmedkits. Accessed: Mar. 23, 2023. [Online]. Available: https://wildmedkits.ca/products/sim-limb-tourniquet-wound-packing-chest-seal-suturing-task-trainer

[168] "Emergency Tourniquet Trainer - Arm," Military Moulage. Accessed: Mar. 23, 2023. [Online]. Available: https://militarymoulage.com/shop/p/emergency-tourniquet-trainer-arm

[169] "HM – Tourniquet Arm Trainer - Humimic Medical." Accessed: Mar. 23, 2023. [Online]. Available: https://humimic.com/product/training-arm/

[170] "HM – Tourniquet & Wound Packing Leg Trainer - Humimic Medical." Accessed: Mar. 23, 2023. [Online]. Available: https://humimic.com/product/hm-wound-management-leg-trainer/

[171] "Simulator to Train Treatment of Critical Bleeding of Upper Extremities." Accessed: Mar. 23, 2023. [Online]. Available: https://www.3bscientific.com/us/hemorrhage-control-arm-trainer-p102-1022652-p102-3b-scientific,p_1455_31844.html?utm_source=google&utm_campaign=gmc_feed&gclid=CjwKCAjwzuqgBhAcEiwAdj5dRnciYq8_Zy6FpnawFfx1JrBZdEd0HdROC_A_xwS6xi1-ZVEZD9EzwxoCgV4QAvD_BwE

[172] J. M. Pearce, D. Liu, and V. Jaqua, "Open source tourniquet tester," Sep. 2022, doi: 10.17605/OSF.IO/DGTW4.

[173] "SparkFun_HX711_Calibration.ino," Feb. 2023, Accessed: Mar. 23, 2023. [Online]. Available: https://osf.io/https://osf.io/ngq2m

[174] J. Ochoa, T. J. Fowler, and R. W. Gilliatt, "Anatomical changes in peripheral nerves compressed by a pneumatic tourniquet.," *J Anat*, vol. 113, no. Pt 3, pp. 433–455, Dec. 1972.

Appendices

Appendix A: List of OS MFI parts.

The bill of materials (BOM) for the make parts is shown in Table 4. The full list with links to commercially available components can be found at https://osf.io/68hbj/. All files are licensed under GNU GPL v3.

Table 4. BOM of the make parts and files for the OS MFI device (hardware).

No.	Design file name	File type	Technology	Material
1	Stand	STL&STEP	FFF 3D printing	PETG
2	Linear support	STL&STEP	FFF 3D printing	PETG
3	Motor mount	STL&STEP	FFF 3D printing	PETG
4	Flange support	STL&STEP	FFF 3D printing	PETG
5	Loadcell fit	STL&STEP	FFF 3D printing	PETG
6	Shaft loadcell coupler	STL&STEP	FFF 3D printing	PETG
7	Cutter connector	STL&STEP	FFF 3D printing	PETG
8	Blade fix	STL&STEP	FFF 3D printing	PETG

9	Extra frame	STL&STEP	FFF 3D printing	PETG
10	Extra frame b	STL&STEP	FFF 3D printing	PETG
11	Foot support	STL&STEP	FFF 3D printing	PETG
12	Housing	STL&STEP	FFF 3D printing	PETG
13	Insulation housing	STL&STEP	FFF 3D printing	PC
14	Cap band	STL&STEP	FFF 3D printing	PC
15	Piston guide	STL&STEP	FFF 3D printing	PETG
16	Piston tip guide	STL&STEP	FFF 3D printing	PETG
17	Scale housing	STL&STEP	FFF 3D printing	PETG
18	Scale plate	STL&STEP	FFF 3D printing	PETG
19	Block	STL&STEP	FFF 3D printing	PETG
20	PCB	zip		//

21	MFI	ino		//

The make parts are listed hereinafter with a short description and a rendering preview.

Part 1 (File 1). Stand: this is the basement of the whole frame, which can hold the two aluminum profiles 90 degrees, making the whole structure vertically (Figure 10).

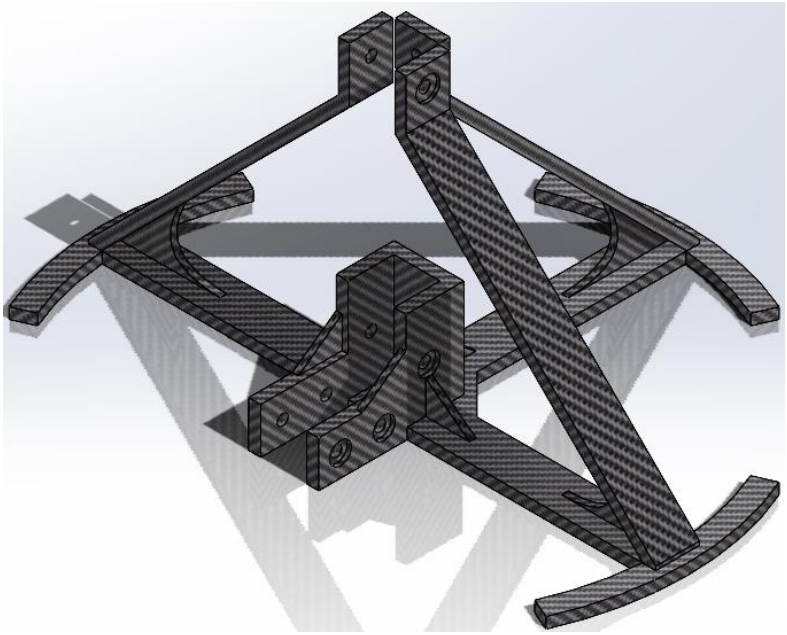

Figure 12 Part 1: Stand.

Part 2 (File 2). Linear support: this part can support the linear rail and the Motor mount part and mount the rail to the aluminum extrusion profile (Figure 11).

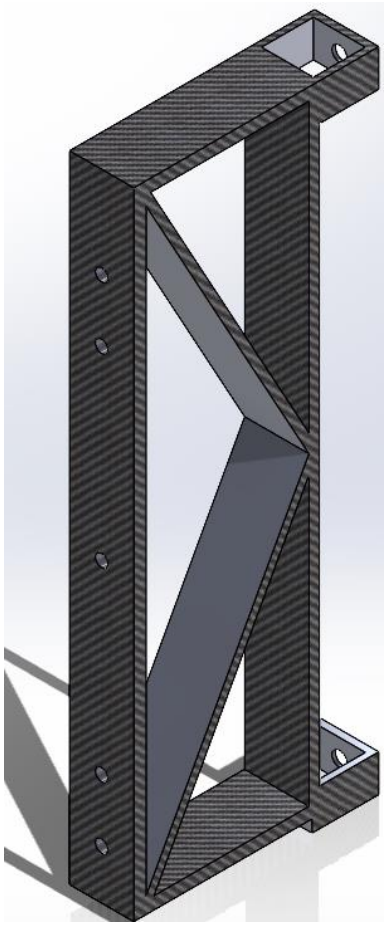

Figure 13. Linear support.

Part 3 (File 3). Motor mount: To support and mount the motor on the aluminum profile (Figure 12).

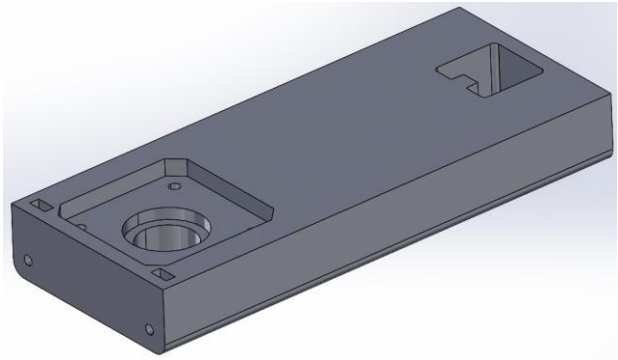

Figure 14. Motor mount.

Part 4 (File 4). Flange support: L-shaped part, with rib to increase strength (Figure 13).

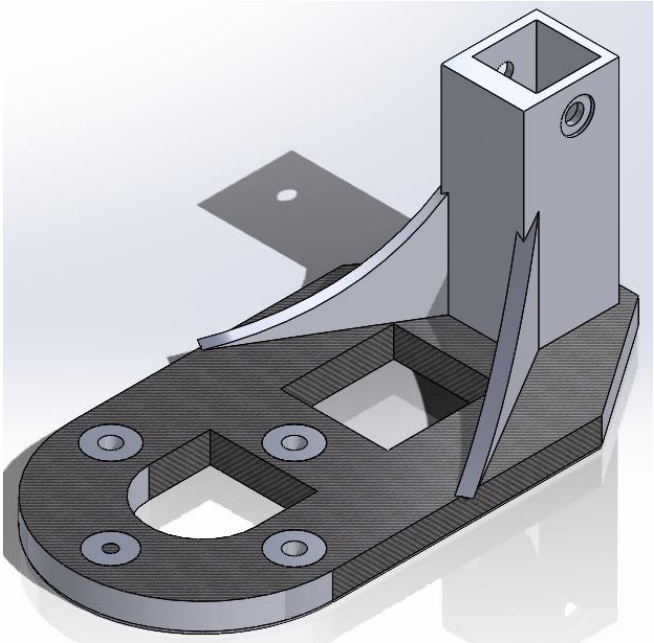

Figure 15. Flange support.

Part 5 (File 5). Loadcell fit: This is used to help connect the shaft coupler and the load cell (Figure 14, left).

Part 6 (File 6). Shaft loadcell coupler: A rectangular part with top and bottom holes. There are four blot holes, which correspond to the slide block of the linear rail. The top part is separate, which can help grip the motor shaft (Figure 14, right).

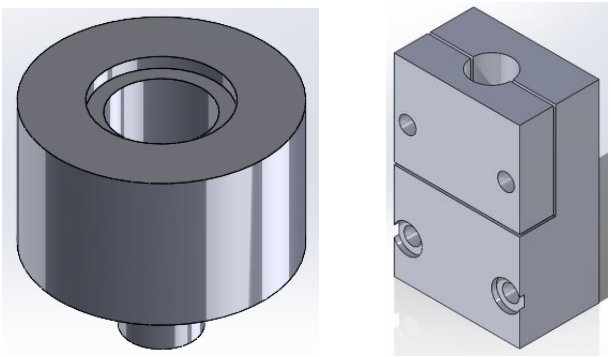

Figure 16. Loadcell fit (left), Shaft loadcell coupler (right).

Part 7 (File 7). Cutter connector: Mount the servo motor on the aluminum extrusion profile (Figure 15, left).

Part 8 (File 8). Blade fix: Attach the blade to the servo motor (Figure 15, right).

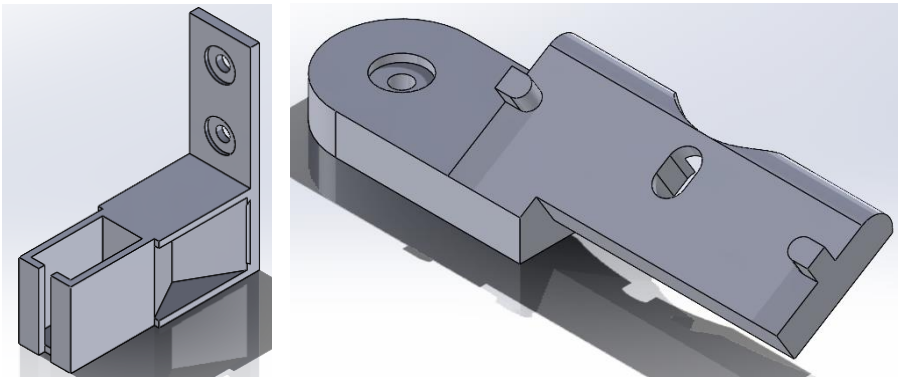

Figure 17. Cutter connector (left), blade fix (right).

Part 9 (File 9). Extra frame: provide extra support for the flange support so that it will not deform when the piston presses down (Figure 16, left).

Part 10 (File 10). Extra frame b: the bottom part of the extra frame (Figure 16, right).

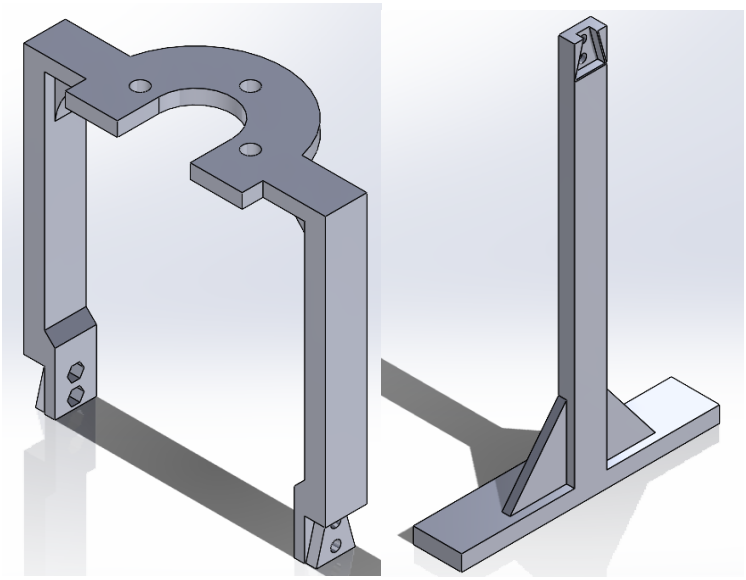

Figure 18. Extra frame (left), extra frame b (right).

Part 11 (File 11). Foot support: this part is the triangle part that goes between two aluminum extrusion profiles, so that they can keep stand vertically (Figure 17, left).

Part 12 (File 12). Housing: The shell of all electronic components (Figure 17, right).

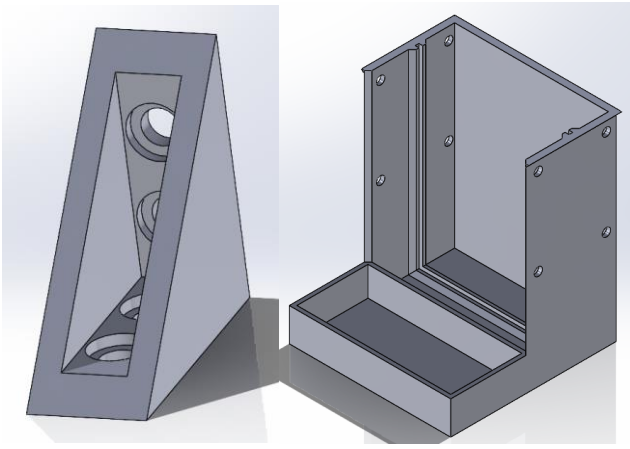

Figure 19. Foot support (left), Housing (right).

Part 13 (File 13). Insulation housing: housing for the insulation layer of the heating pipe, which helps hold insulation in place (Figure 18).

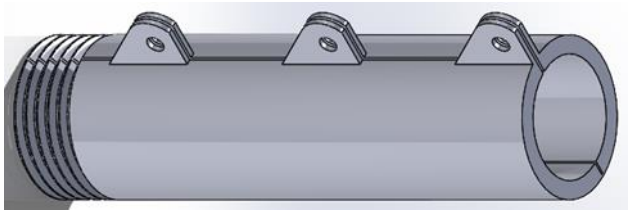

Figure 20. Insulation housing

Part 14 (File 14). Cap band: band-shaped insulation housing for the band heater. The insulation layer is attached to this part so that the insulation can be taken off easily (Figure 19).

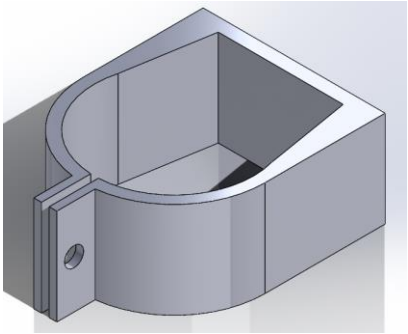

Figure 21. Cap band.

Part 15 (File 15). Piston guide: helps guide the piston insert the pipe. It also works as a fuel when adding materials (Figure 20, left).

Part 16 (File 16). Piston tip guide: A small cap for the piston tip helps keep all the components of the piston tip aligned with the same center point (Figure 20, right).

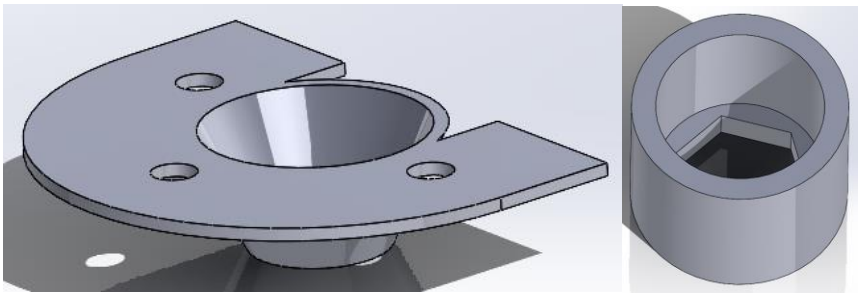

Figure 22. Piston guide (left), piston tip guide (right).

Part 17 (File 17). Scale housing: housing for all the scale components. The scale is apart from the main body of the MFI device to avoid vibration (Figure 21, left).

Part 18 (File 18). Scale plate: a plate that can hold extrusions of the MFI (Figure 21, right).

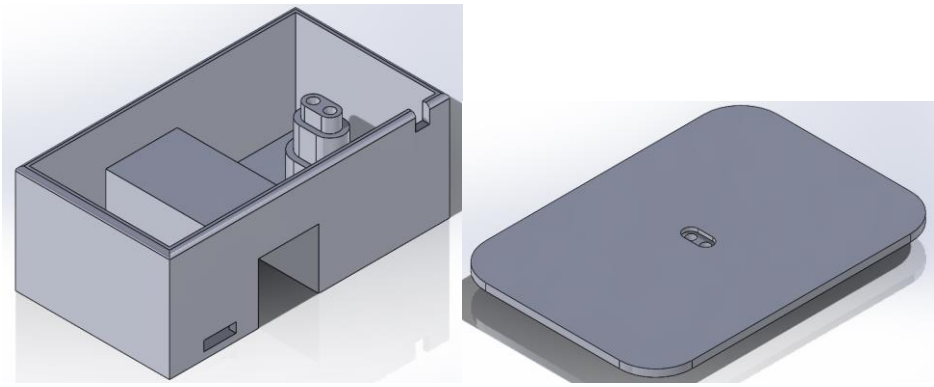

Figure 23. Scale housing (left), scale plate (right).

The BOM for the electronic components is shown in Table 5.

Table 5. BOM of electronic components.

Name	**Model number**	**Quantity**	**Cost per unit**	**Source**
PCB		1	10	JLCPCB
Control board	Teensy board 4.0	1	23.8	Teensy.com
Motor driver	TMC2130	1	10	Amazon
Amplifier	HX711	2	6	Amazon
ADC	MAX31855KASA	1	12.66	Digikey
LDO regulator	AMS1117	1	0.85	Digikey
Force sensor	DYMH-103	1	70.42	AliExpress
Loadcell	100g	1	10.79	Amazon
SMD Resistor	10k	2	0.15	Digikey
Capacitors c1	100 uF	1	0.48	Digikey

Capacitors c2	22 uF	1	0.21	Digikey
Capacitors c3	0.01 uF	1	0.14	Digikey
Capacitors c4	10 uF	1	0.14	Digikey
Ferrite Beads	FERRITE BEAD 120 OHM 0603 1LN	2	0.18	Digikey
Thermocouple	240-080	1	15.8	Digikey
Connecters		8	0.1	Amazon
Motor	Nema 17 Non-captive Linear stepper motor	1	25.84	AliExpress
Servomotor		1	2.9	Amazon
Power supply	110v AC to 12V DC	1	22.88	Amazon
Relay module	12V	1	1.9	Amazon
Wires	Jump wires	10	0.1	Amazon
High temperature-resist wires	Awclub Mica	50mm	0.75/ft	Amazon
High temperature-resist connectors	O Type and U Type	8	0.05	Amazon
Nichrome wire	50’ nichrome 80 wire	1	9.47	Master wire supply

Band heater	12V 40W	1	20	Filastruder

Table 6. BOM of mechanical components.

Name	**Model number**	**Quantity**	**Cost per unit**	**Source**	**Material Type**
Bolts b1	M6-5mm	19	0.1	Amazon	Steel
Bolts b2	M3-20mm	8	0.1	Amazon	Steel
Bolts b3	M6-40mm	3	0.1	Amazon	Steel
Bolts b4	M2-8mm	4	0.1	Amazon	Steel
Bolts b5	M3-15mm	3	0.1	Amazon	Steel
Nuts n1	M6	3	0.24	Amazon	Steel
Nuts n2	M3	3	0.1	Amazon	Steel
Nuts n3	M2	2	0.09	Amazon	Steel
T-nuts t1	M6, 20x20	19	0.2	Amazon	Steel
Serrated Flange Lock Nut	¼ inch	1	0.8	Amazon	Steel
Self-lock nut	¼ inch	1	0.5	Facca Fasteners Limited	Steel
Washers w1	M6	4	0.1	Amazon	Steel
Washer w2	M3	2	0.1	Amazon	Steel
Heat tube	½ inches,	1	20	McMaster-Carr	Steel

cap	½ inches, hex	1	5	McMaster-Carr	Copper
Aluminum profile a1	20x20	75mm	15/1m	McMaster-Carr	Aluminum
Aluminum profile a2	20x20	30mm	15/1m	McMaster-Carr	Aluminum
Linear rail	350mm	2	0.18	Amazon	Steel
Blade	240-080	1	15.8	McMaster-Carr	Steel
Piston rod	¼ inches, 12 inches length	2	1.5	Home Depot	Steel
O-ring	OD5/8	1	0.26	McMaster-Carr	Silicon
Capton tape		1	2.9	Amazon	Mixed
Shaft Coupler	¼ inch	1	3	Amazon	Steel
Insert Nuts	3mm	2	1.9	McMaster-Carr	Steel
Insulation	heat resistance cotton	970 mm^2	0.08/inch^2	McMaster-Carr	Fiberglass

Appendix B: OS MFI build instructions.

1.1. Mechanics

1.1.1. Step 1. Assemble the frame;

Insert t-nut into the slot of the 1-meter aluminum profile, assemble 3D printed part motor mount on the top of the aluminum extrusion profile;

Insert the same aluminum profile into the two holes of linear support;

Push the linear support until it touches the motor support, then secure it to the aluminum extrusion profile with bolts and T-nuts. Attach the linear rail to the linear support with fasteners using the corresponding holes.

Insert the aluminum profile into the 3D printed part Flange support, and fix the position with bolts and t-nuts. The position depends on the length of the linear rail.

Put the 3D printed part of the cutter connector in the right position and fix it with bolts and nuts. The position depends on the length of the heating pipe. It should allow the cutter to cut off the extrusions.

Insert the aluminum extrusion profile into the 3D printed part Stand and fix it with fasteners.

Attach another aluminum extrusion profile to the stand and fix the position with fasteners. Then assemble the 3D printed part foot support and make sure two aluminum extrusion profiles are vertical.

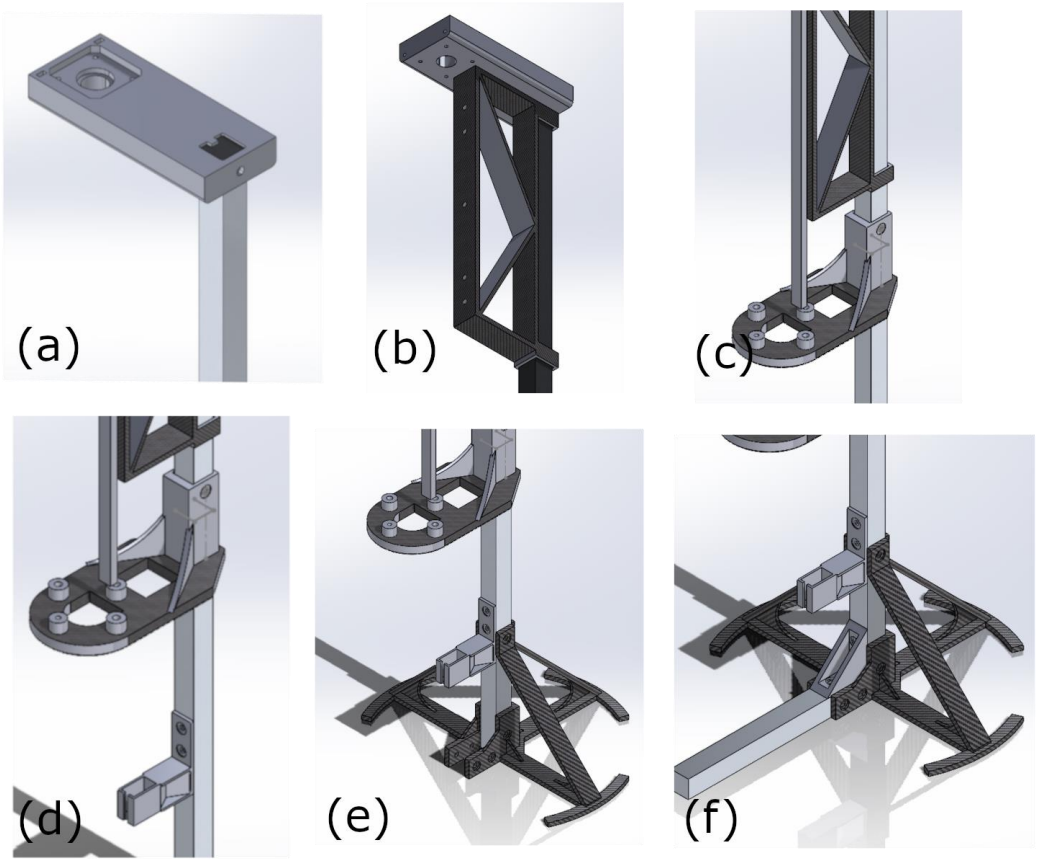

Figure 24. Frame

1.1.2. Step 2. Piston;

Screw the ¼ inch serrated flange lock nut to the ¼-inch threaded rod and stop at 15mm away from the tip.

Put an O-ring on top of the nut, then put a washer on top of it.

Screw another self-lock nut, cover it with a piston guide, and ensure that all pieces have the same center point. Use the 3D printed part Piston tip guide to make sure all the components are centered and not too tight. If the screw is too tight, the O-ring in the middle will deform, which makes it harder to insert into the heating pipe.

Assemble the motor on the 3D printed part Motor Support.

Connect the shaft of the motor to the shaft loadcell coupler.

Screw the Loadcell fit into the Shaft loadcell coupler, then install it on the slide block of the linear rail.

Screw the insert nut into the 3D printed part loadcell fit, connect the loadcell fit and the button loadcell, then screw the button loadcell to the shaft loadcell coupler.

Connect the shaft coupler to loadcell fit.

Connect the piston rod with the shaft coupler.

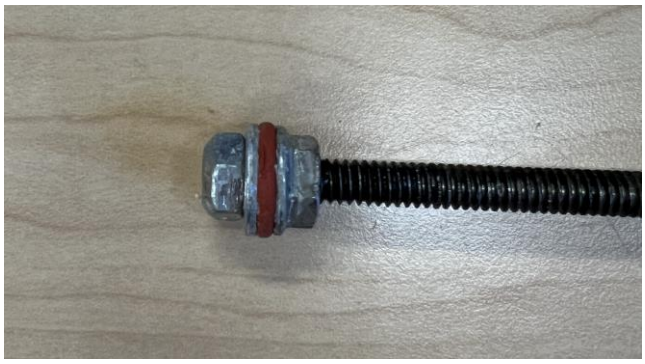

Figure 25. Piston tip.

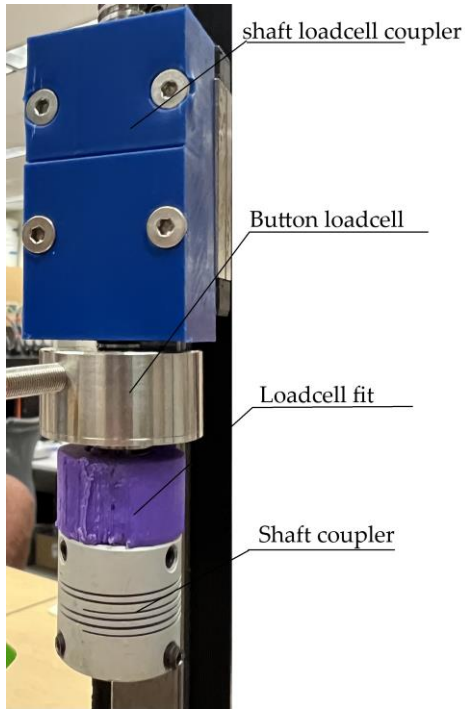

Figure 26. Coupler connection.

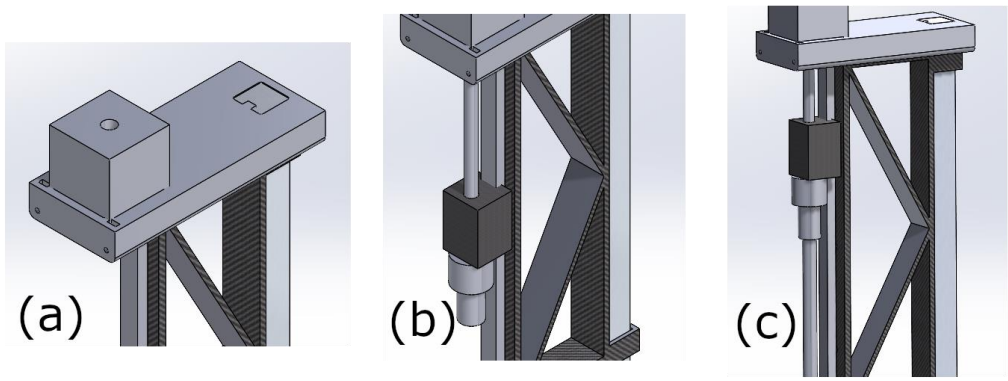

Figure 27. Piston assembling step.

1.1.3. Step 3. Heating pipe;

Cover the whole pipe with high-temperature-resistant tape (Kapton Tape).

Wind Nichrome wire around the iron pipe as required, ensuring the nichrome wire has sufficient resistance to at least meet the maximum current requirements of the relay. The nichrome wires must not touch each other to prevent short-circuiting or excessive heat

generation at the contact points. After winding, wrap high-temperature tape around the outside of the resistance wire to achieve insulation.

Tape the thermocouple to the outside of the resistance wire.

Cover the pipe with heat insulation material, such as fiberglass. Cover the fiberglass layer with Kapton tape so that it can keep on the pipe.

Cover the insulation layer with 3D printed housing (insulation housing).

Drill a 2 mm hole in the center of the cap.

Insert the cap in the band heater.

Tighten the screw on the band heater.

Cover the band heater with a 3D printed insulation cap band.

Screw the cap on one end of the pipe.

Attach the flange and insulation pad to 3D printed part flange support with bolts and nuts. The insulation pad should be between the flange and the flange support.

Fix the extra frame and piston guide with the same bolts and nuts as the last step.

Screw the pipe to the flange.

Adjust the position of the blade. It should touch the bottom of the cap.

Figure 28. Heating pipe.

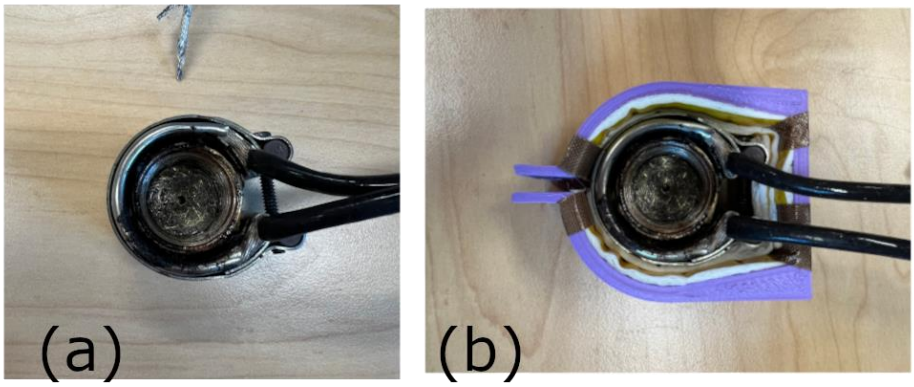

Figure 29. Cap assembly.

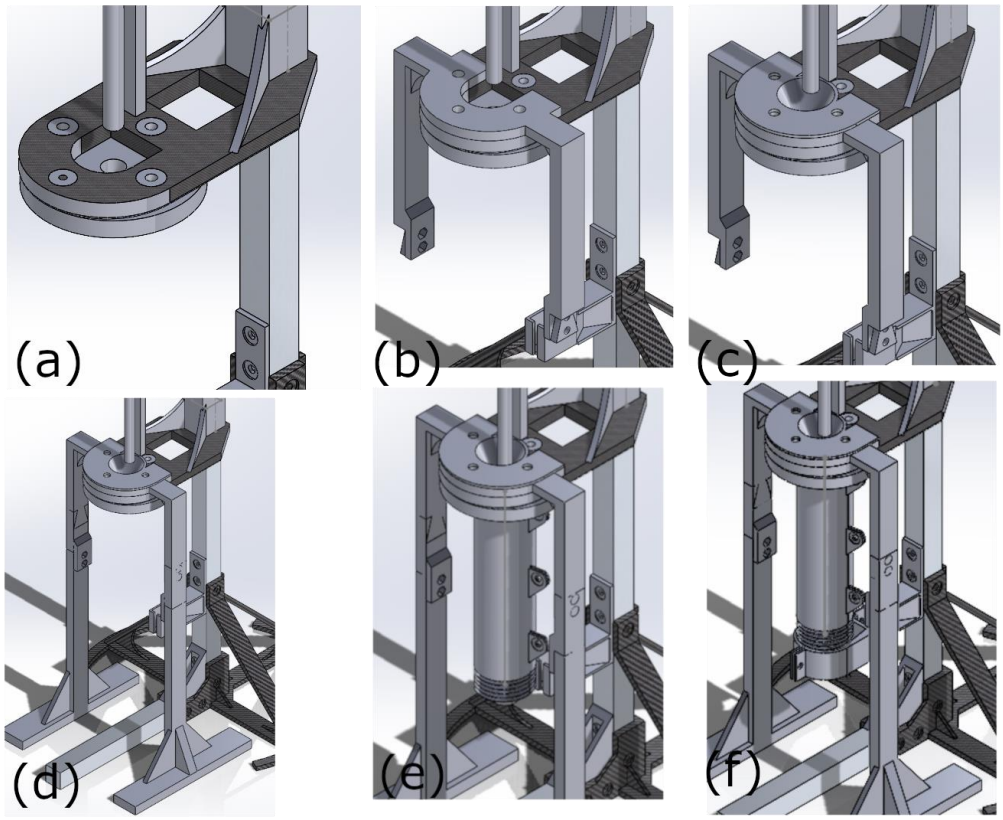

Figure 30. Assembling steps in step 3.

1.1.4 Step 4. Digital scale

Connect wires on the HX711 board.

Assemble the scale platform on the load cell.

Fix the HX711 board on the related slot in the scale housing.

Assemble the load cell on the scale housing.

Pull jump wires out and connect the other end to the main board.

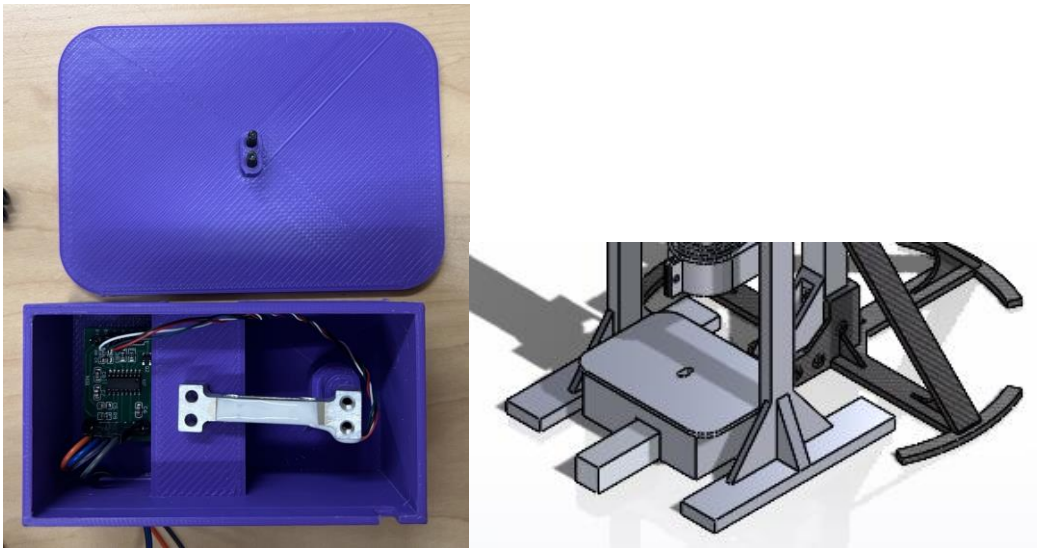

Figure 31. Scale assembly.

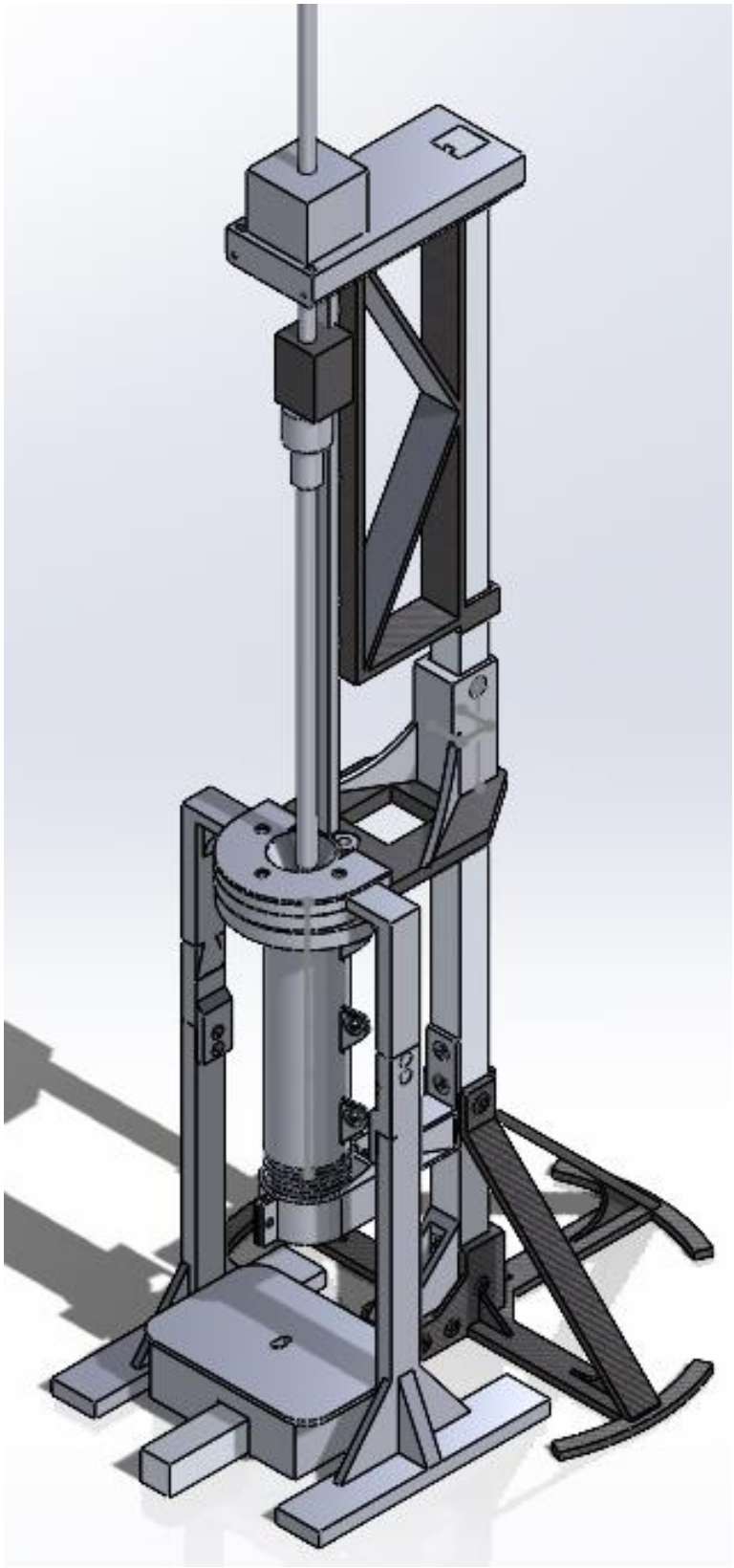

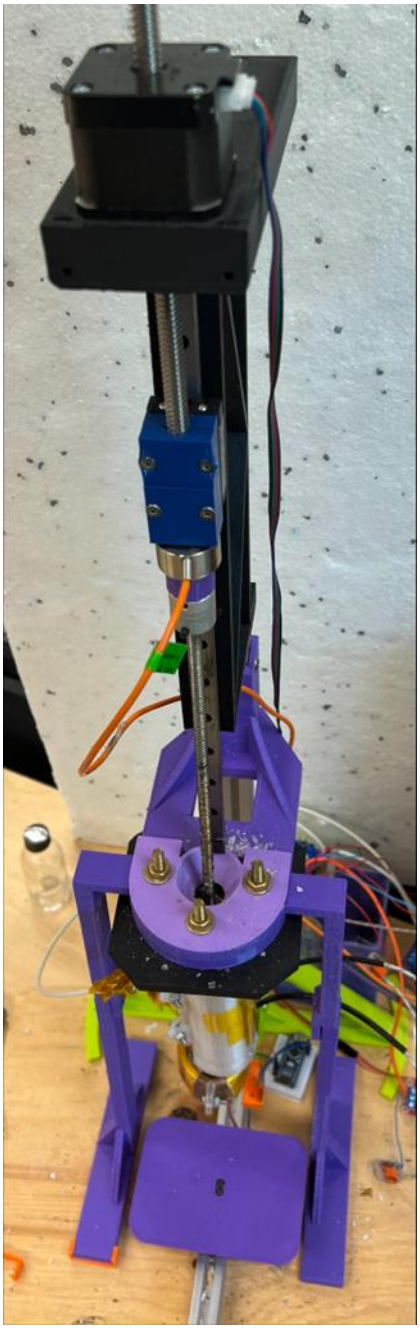

Figure 32. Overall structure

1.2 *Electronic*

Connect a high-temperature resistant connector to one end of the high-temperature resistant wire and connect it to the nichrome wire.

Follow the instructions in the schematic in the Open Science Framework [77].

Operation instructions

Preparation: Humidity-sensitive materials like PETG and PLA should be dried before measurement. Get a specific weight of the material, such as 10 grams, and dry it. The drying process should follow the standard profile.

1. Connect the Teensy board with the laptop.
2. Plugin the power supply.
3. Open the .io file with Arduino IDE and download all the libraries. Setup parameters are needed, and the new firmware is uploaded to the teensy board. More detailed instructions are in the code file.
4. Open the Serial Monitor in Arduino IDE, baud rate 115200. “start” should show up in the Serial monitor.
5. Input start command monitor “a “in Message blank. The temperature will increase, and the piston will start to go down automatically after the heating-up procedure ends.
6. Fill in the samples when the temperature reaches the set point.
7. Bring down the piston using the command “d”. The piston will start to go down automatically after the heating-up procedure ends.
8. Wait for the pressure to get to the set point. Record the readings after the cutter cut-off samples.
9. Clean up the barrel and the cap after the measurement is finished.

Data processing method: get at least 20 data sets, where the first X data sets should be abandoned. This fact is due to the initial temperature instability in the heated barrel and die. Only the last X sets of data should be considered for MFI measurement to achieve accurate results.

Figure 33. Operation instruction step 4.

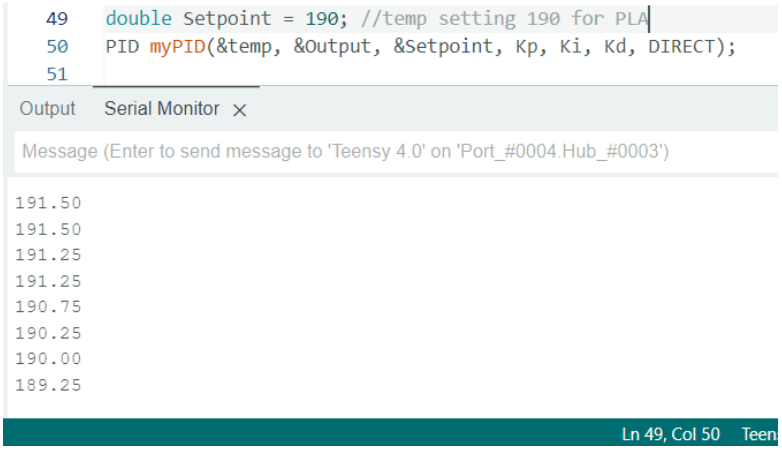

Figure 34. Operation instruction step 5.

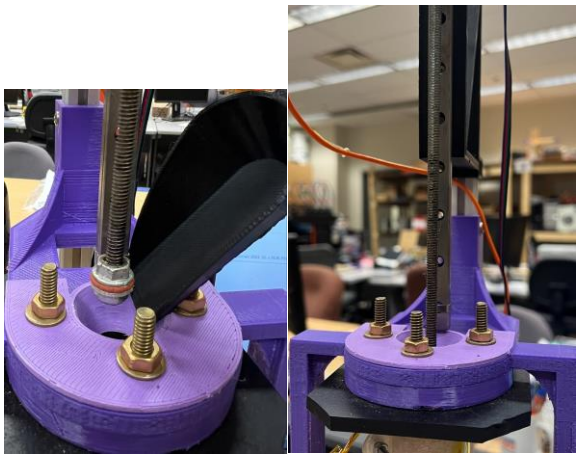

Figure 35. Operation instruction step 6 (left), step 7 (right).

Cleaning instructions

1. Go into cleaning mode by inputting the command in the Arduino IDE serial monitor to keep the temperature.
2. Dissemble the insulation band, unplug the band heater, and unscrew the cap with a clamp or heat-resistant gloves.
3. Plug the band heater back and clean the cap with cleaning tools, such as a copper brush, etc.
4. Pull out the piston and clean the piston tip with cleaning tools.
5. Clean the tube with the piston and cover the piston tip with a cotton rug or robust paper.
6. Screw the cap back after the cleaning process.

Control codes

This is the firmware that should be uploaded to the Teensy 4.0 board. All the experimental factors can be adjusted directly in the code, for example, the setpoint for temperature and the pressure for the weight load. In manual mode, one can adjust the piston position by entering commands in the serial monitor of the Arduino IDE.

```
// librarys

#include <AccelStepper.h>

#include <TMC2130Stepper.h>

#include <Arduino.h>

#include <TMC2130Stepper_REGDEFS.h>

#include <EEPROM.h>

#include <PID_v2.h>

#include <max6675.h>

#include <Servo.h>
```

```
#include "HX711.h"

#include <TimerOne.h>

#include <TimerThree.h>

// define pins and numbers

#define STALL_VALUE 14 // [-64..63]

//TMC2130

#define EN_PIN 18

#define DIR_PIN 14

#define STEP_PIN 15

#define CS_PIN 16

// MAX6675

#define MAXDO   7

#define MAXCLK  6

#define MAXCS1   8

#define MAXCS2   27

#define RELAY_PIN1 10

#define RELAY_PIN2 29

// HX711

#define DOUT1  3

#define CLK1  2
```

```
#define DOUT2  5

#define CLK2  4

//stop button

#define BTN1 20

//limit button

#define BTN2 23

// CLASSES

TMC2130Stepper driver = TMC2130Stepper(EN_PIN, DIR_PIN, STEP_PIN,
CS_PIN);

AccelStepper stepper(AccelStepper::DRIVER, STEP_PIN, DIR_PIN);

Servo myServo;  // create servo object to control a servo

HX711 digiscale; //scale

HX711 Forcesensor;//Force

MAX6675 thermocouple1(MAXCLK, MAXCS1, MAXDO); // thermocouple1

MAX6675 thermocouple2(MAXCLK, MAXCS2, MAXDO); // thermocouple2

IntervalTimer myTimer; // timer for temperature sensor reading

// Setup PID control

double Kp1 = 2, Ki1 = 5, Kd1 = 1;

double temp1, Output1;

double Setpoint1 = 190; //temp setting 190 for PLA,255 for BB
```

```
double Kp2 = 1.1, Ki2 = 2.8, Kd2 = 2.5;

double temp2, Output2;

double Setpoint2 = 195;  // band heater

PID myPID1(&temp1, &Output1, &Setpoint1, Kp1, Ki1, Kd1, DIRECT);

PID myPID2(&temp2, &Output2, &Setpoint2, Kp2, Ki2, Kd2, DIRECT);

// GLOBAL VARIABLES

static bool state = true;

volatile bool limit = false;

int setPressure;

unsigned int sampleCount = 0;

bool FStable = true; // force stable flag, may not be used

int cal_addr = 0;       // Location of calibration values in EEPROM

double current = 600;

double Force = 0;

double DForce = 21.6; // desired force 21.6 for PLA

double pressure; // for ads1232

double weight; // for the scale

bool updateForce = false; // update force flag

bool tempF = false;

bool timerStart = false; // whether the timer has started
```

```
bool timerStart2 = false;

bool Motorsf = false;// motor start flag

bool TF = true; // flag for temperature reach the setpoint

bool FF = false; // flag for reaching desired force

unsigned long startTime; // when the timer started

unsigned long countdownTime = 15 * 1000; // countdown time (15 seconds in
milliseconds)

volatile bool motorEnabled = true;

bool autoMode = false; // Flag for mode

//wait till the material to melt

unsigned long previousMillis = 0; // will store last time an event was triggeredm

const long interval = 10*60000; // heat up and keep temperature for 10 mins

int runCount = 0; // cutter needs to run many times

// numbers for sample weight calculation

double Average;

int n = 10;

int i = 0;

double sum = 0;


void driverSettings()
```

```
{
    driver.begin();                 // Initiate pins and registeries
    driver.push();                  // Reset registers
    driver.rms_current(600);        // Set stepper current
    driver.stealthChop(1);          // Enable extremely quiet stepping
    driver.microsteps(16);
    stepper.setMaxSpeed(2000);
    stepper.setAcceleration(2000);
    stepper.setSpeed(800);
}
void setPins()
{
    pinMode(CS_PIN, OUTPUT);
    pinMode(RELAY_PIN1, OUTPUT);
    pinMode(RELAY_PIN2, OUTPUT);
    pinMode(EN_PIN, OUTPUT);
    digitalWrite(EN_PIN, LOW);
    pinMode(BTN1, INPUT_PULLUP);
}
void Forcechuan(){
```

```
  Forcesensor.begin(DOUT1, CLK1);

  Forcesensor.set_scale(2490); //This value is obtained by using the
SparkFun_HX711_Calibration sketch

  Forcesensor.tare(); //Assuming there is no weight on the scale at start up, reset the
scale to 0

}


void digitalscale(){

  digiscale.begin(DOUT2, CLK2);

  digiscale.set_scale(5947); //This value is obtained by using the
SparkFun_HX711_Calibration sketch

  digiscale.tare(); //Assuming there is no weight on the scale at start up, reset the scale
to 0

}


void setup() {

  Serial.begin(115200);

  while(!Serial);

  Serial.println("Start...");

  // set up motor

  driverSettings();
```

```
  // set up cutter

  myServo.attach(9);

  myServo.write(0);

  // set up for the scale

  digitalscale();

  // set up force sensor

  Forcechuan();

  // Set up the TimerOne interrupt

  Timer1.initialize(500); // Set the timer interval 600 microseconds to output
PWM(was 200)

  //Timer1.attachInterrupt(step);

  myTimer.begin(readtempF, 400000); // temp sensor read every 0.4 seconds

  //set timer 3 to get force readings, not really in use

  //Timer3.initialize(100000000); // Set up timer to expire every 10 senconds

  //Timer3.attachInterrupt(MotorSFlag);

  setPins();

  // PID settings

  myPID1.SetMode(AUTOMATIC);

  myPID2.SetMode(AUTOMATIC);

  delay(500);
```

```
}


void readtempF() {
  tempF = true;
}
void loop() {
  // Stop button
  /*int StopState = digitalRead(BTN1); // read the state of the stop button
  if (StopState == LOW) { // if the button is pressed
    motorEnabled = false; // Stop the motor
    digitalWrite(RELAY_PIN, LOW);
    return; // stop the program
  }*/
  // loop start
  // temperature control
  if (Serial.available()) {
    char command = Serial.read();
    switch (command) {
      case 'u': // Manual up
        manualControl(true);
```

```
    break;
  case 'd': // Manual down
    manualControl(false);
    break;
  case 'a': // Switch to automatic mode
    autoMode = true;
    break;
  case 'm': // Switch to manual mode
    autoMode = false;
    break;
  case 'r': // report motor state
    Serial.println("motorEnabled:");
    Serial.println(motorEnabled);
    Serial.println("state:");
    Serial.println(state);
    break;
  case 's': // report motor state
    motorEnabled = true;
    break;
}
```

```
}
if (autoMode) {
  bool tempFcopy; // don't know why but have to
  noInterrupts();
  tempFcopy = tempF;
  interrupts();
  if (tempFcopy){
    //Serial.print("C = ");
    Serial.println(thermocouple2.readCelsius());
    temp2 = thermocouple2.readCelsius();
    myPID1.Compute();
    if (Output1>25){
      digitalWrite(RELAY_PIN1, HIGH);
    }
    else {
      digitalWrite(RELAY_PIN1, LOW);
    }
    myPID2.Compute();
    if (Output2>25){
      digitalWrite(RELAY_PIN2, HIGH);
```

```
  }
  else {
    digitalWrite(RELAY_PIN2, LOW);
  }
  tempF = false;
  //delay(300);
}
if (temp2 >= Setpoint2 && TF){
  previousMillis = millis();
  timerStart2 = true;
  TF = false;
}
  //Timer3.start(); // start to countdown the 10 seconds
if (timerStart2 && millis() - previousMillis >= interval) {
    Motorsf = true;
    timerStart2 = false;
    Serial.println("motor start");
}


// adjust current & get the force data
```

```
if (Motorsf) {
pressure = Forcesensor.get_units(1);


Force = pressure;// pressure unit 100g, should time 0.1 to get kg
delay(50);
driver.rms_current(current);// adjust the current
Serial.println(Force);
//Serial.println(current);
//updateForce = false; // update the flag


// get the status of the force
// change move direction
//if (MotorSF){
Timer1.attachInterrupt(step);
if (Force<DForce){
        //Timer1.attachInterrupt(step);
        motorEnabled = true; // Start the motor
        driver.shaft_dir(1); // motor down
        Serial.println("motor down");
      }
```

```
else if (Force >= (DForce-1) && Force <= (DForce+1)){
        motorEnabled = false; // Stop the motor
        FF = true;
        Serial.println("motor stop");
        //FStable = false;
} else {
          //Timer1.attachInterrupt(step);
          motorEnabled = true; // Start the motor
          driver.shaft_dir(0); // motor up
        }
}
// cutter


  if (FF&&FStable) {
    startTime = millis(); // start the timer
    timerStart = true; // set the flag for scale and cutter
    FStable = false;
  }
  // after a certain time after reach the desired force, the cutter will work
```

```
    if (timerStart && (millis() - startTime >= countdownTime) && (runCount < 50))
{ //wait 15 seconds

      myServo.write(180); // tell servo to go to position 180

      delay(500);

      myServo.write(0);

      delay(1000);

      // after the cutter, the scale can work



      while (i<n) {

        weight = digiscale.get_units();

        sum = sum + weight;

        i++;

      }

      Average = sum / n;

      Serial.println(Average,3);

      delay(500);

      runCount++; // increase loop time

      //timerStart = false; // reset the flag

      i = 0; // reset the counter

      sum = 0; // reset sum
```

```
        digiscale.tare();  // reset scale reading
        delay(500);
        startTime = millis(); // reset the timer




      }




  }
}
// motor move up and down manually
void manualControl(bool moveUp) {
  Timer1.attachInterrupt(step);
  if (moveUp) {
        motorEnabled = true; // Start the motor
    driver.shaft_dir(0); // motor up
    delay(1000);
    motorEnabled = false; // Start the motor
  } else {
        motorEnabled = true; // Start the motor
```

```
    driver.shaft_dir(1); // motor down

    delay(1000);

    motorEnabled = false; // Start the motor

  }

}

// motor move

void step() {

  if (motorEnabled == false)

    {return;}

  //static bool state = true;

  state =!state; // change the flow direction so the motor turns. can change the speed
by adjust timer intervel

  digitalWrite(STEP_PIN, state);



}
```

Appendix C: OS tourniquet testing system build instructions.

The design files are summarized in Table 7.

Table 7. Tourniquet tester design files.

Design file name	File type	Open source license	Location of the file
Amplifier mounting	STL&STEP	*CERN OHL v2*	https://osf.io/hf4dm
Cap	STL&STEP	*CERN OHL v2*	https://osf.io/dajfv
Flat	STL&STEP	*CERN OHL v2*	https://osf.io/gwbtn
thigh inside cylinder	STL&STEP	*CERN OHL v2*	https://osf.io/vqwc9
Tournbutton – M	STL&STEP	*CERN OHL v2*	https://osf.io/gvmkr
Tournbutton-T	STL&STEP	*CERN OHL v2*	https://osf.io/a6xc8
Unit tester	ino	*GNU General Public License v.3*	https://osf.io/zr79k

The tourniquet tester is cylindrical in shape and has an LCD screen at the top to display the measured values. The housing of the tester is made of hard thermoplastic material, and there are four assembly holes for round buttons made of flexible thermoplastic polyurethane (TPU) material. The tester housing is 3-D printed and can be customized if necessary, which means that different sizes of housings can be made to suit different test conditions.

File 1. Amplifier mounting: This component is part of the amplifier assembling. To hold the amplifier in place, M2.5 bolts and nuts are used to secure the amplifier HX711 to the

Amplifier mounting and then inserted the part into the notches reserved in the cylinder.

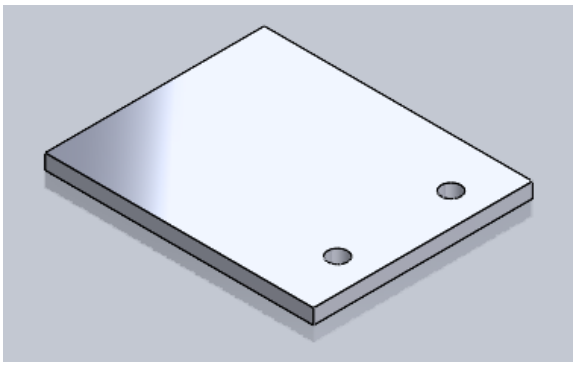

Figure 36. 3-D printed Amplifier.

File 2. Cap: top part of the housing, LCD is mounted on it. There are two holes on the side for the power supply.

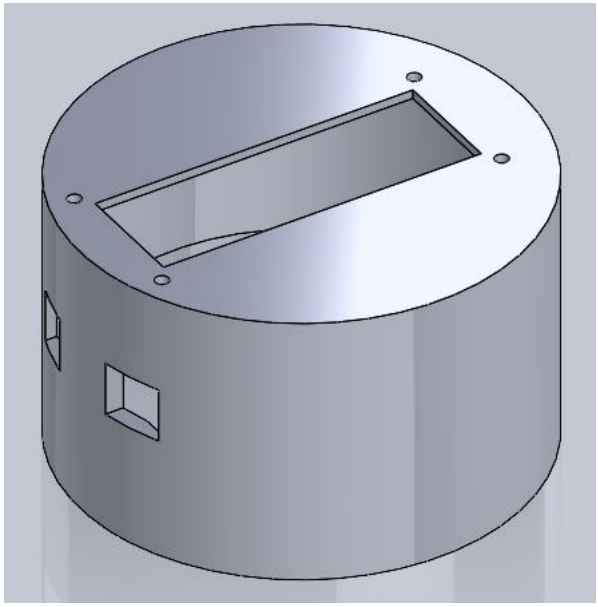

Figure 37. 3-D printed Cap

File 3. Flat: disk-shaped part for the load cell. It is the direct interface with Tournbutton-M.

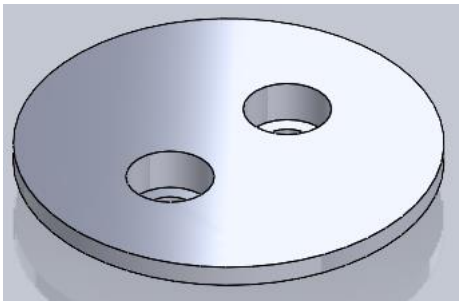

Figure 38. 3-D printed Flat

File 4. Thigh inside cylinder: the main part of the housing. Most electronic parts should be mounted on this part.

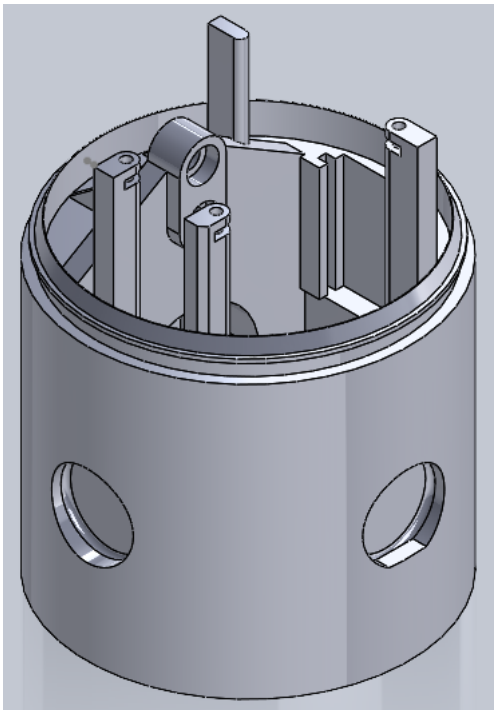

Figure 39. 3-D printed thigh inside cylinder

File 5. Tournbutton-M: the button is made from hard material, for measuring. The cylinder part should be long enough so that it has enough space to be pushed down.

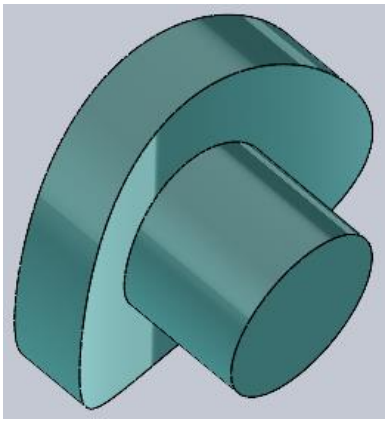

Figure 40. 3-D printed Tournbutton-M

Tournbutton-T: button made of TPU material, mounted on thigh inside the cylinder. It should be thick and flexible enough so that the tourniquet has enough space to generate pressure.

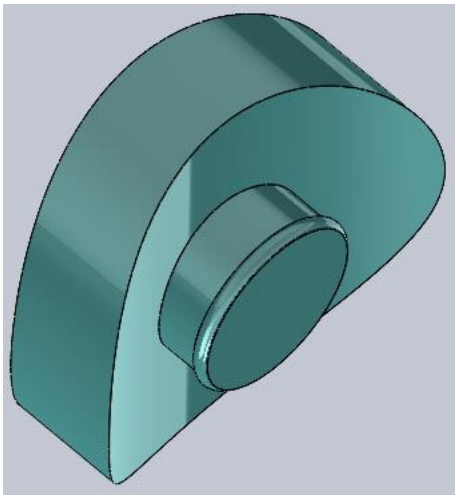

Figure 41. Tournbutton-T

1. **Bill of materials summary**

The full bill of materials can be downloaded from the Open Science Framework [172] containing links to suppliers but is summarized in Table 8. All costs are in Canadian dollars.

Table 8. Bill of materials.

Designator	Component	Number	Cost per/ $CAD	Total cost – $CAD	Source of materials	Material type
1	Thigh inside cylinder	1	0.03/gram	5.1	Amazon	Polymer
2	Cap	1	0.03/gram	1.7	Amazon	Polymer
3	Flat	1	0.03/gram	0.1	Amazon	Polymer
4	Amplifier mounting	1	0.03/gram	0.1	Amazon	Polymer
5	Tournbutton – M	1	0.03/gram	0.3	Amazon	Polymer
6	Tournbutton -T	3	0.03/gram	1.2	Amazon	Polymer
7	20KG-load cell	1	11.5	11.5	Amazon	Aluminum
8	HX711 amplifier	1	4.5	4.5	Amazon	Integrated circuit
9	Arduino Uno	1	47	47	Amazon	Development board
10	16x2 LCD	1	15	15	Amazon	Module

11	Jump wires	8	0.25	2	Amazon	Wire
12	M2.5*5	3	0.1	0.3	Amazon	Metal
13	M2.5*8	2	0.1	0.2	Amazon	Metal
14	M2.5 nuts	5	0.1	0.5	Amazon	Metal
15	M3	2	0.1	0.2	Amazon	Metal
16	M4	2	0.1	0.2	Amazon	Metal
Total				89.9		

2. Build instructions

First, acquire all of the components in the BOM shown in Table 3. For the 3-D printed components detailed in Table7, 3-D print using the setting summarized in Table 9.

Table 9. 3-D printing parameters

Parameters	**Other 3-D printed part**	**Tournbutton-T**
Printer	LulzBot TAZ workhorse	Prusa i3 MK3S+
Slicing software	Cura	PrusaSlicer
Materials	PLA (1.75 mm)	TPU (NinjaFlex 1.75mm)
Nozzle temperature	210 ℃	238 ℃
Printing bed temperature	60 ℃	50 ℃
Wall thickness	2 mm	

Speed	60 mm/s	60 mm/s
Infill	20% (Grid)	10%-15% (Gyroid)
Layer height	0.38 mm	0.2 mm
Support	No	No

1. Assembling the electronic components

Connect the HX711 amplifier to the load cell. For more reliability, solder the wires on the load cell to the amplifier. Then, use the jump wires to connect the LCD and amplifier to the Arduino Uno board as shown in Figure 40. The wiring is further detailed in Table 10.

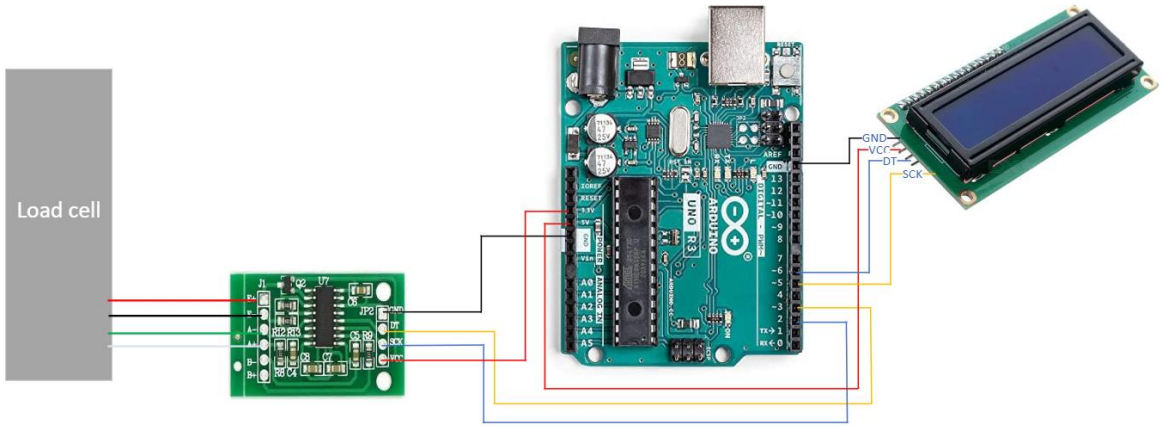

Figure 42. Wire connections.

Table 10. Wire connections.

Load cell to amplifier	**Amplifier to Arduino:**	**LCD to Arduino:**
Red→E+	VCC→ 5V	VCC→ 3.3V

Black→E-	GND→ GND	GND→ GND
Green→A+	CLK→ pin 2	DT→ pin 6
White→A-	DAT→ pin 3	SCK→ pin 5

2. Build the unit tester housing.

Once all the design files are 3-D printed, the assembly process is as follows with the steps shown in Figure 41.

1. Put the flat into the groove inside the cylinder.

2. Insert the load cell into the reserved hole.
3. Use M4 bolts to fix the load cell on the fixing point.
4. Use M3.5 bolts to fix the flat on the load cell.
5. Use M2.5 bolts and nuts to fix the amplifier on the 3-D printed amplifier part, and then insert the part into the reserved notch inside the cylinder.
6. 6. Use M2.5 bolts and nuts to fix the Arduino U no board to the four posts on the cylinder. Only three of them have holes for fixing and one is for support only.
7. Use M2.5 bolts and nuts to fix the LCD on the cap, and then cover the cap, with the holes reserved on the cap aligned with the power and USB slots of the Arduino board.
8. Insert the TPU button into the reserved hole on the cylinder.

The assembly is complete.

Figure 43. Assembly steps of physical components. (a) Put the flat part into the groove, (b) Insert the load cell, (c) Fix the load cell, (d) Fix the flat, (e) Fix the amplifier, (f) Fix the Arduino U no board, (g) Fix the LCD on the cap, and (h) Insert the TPU button.

Because of the use of 3-D printing technology, the design supports changing the size to suit different situations. The cap and the cylinder are connected using a snap fit, which makes installation easy and saves mounting materials such as bolts and nuts.

3. To assemble the calibration platform (optional). See BOM on the OSF [172].

1. Using M3 bolts to mount the linear rail fixing part to the board.
3. Attach the linear rail to the fixing part.
4. Attach the 3-D printed platform to the linear block.

The calibration platform makes the calibration of the tester easy but is not necessary.

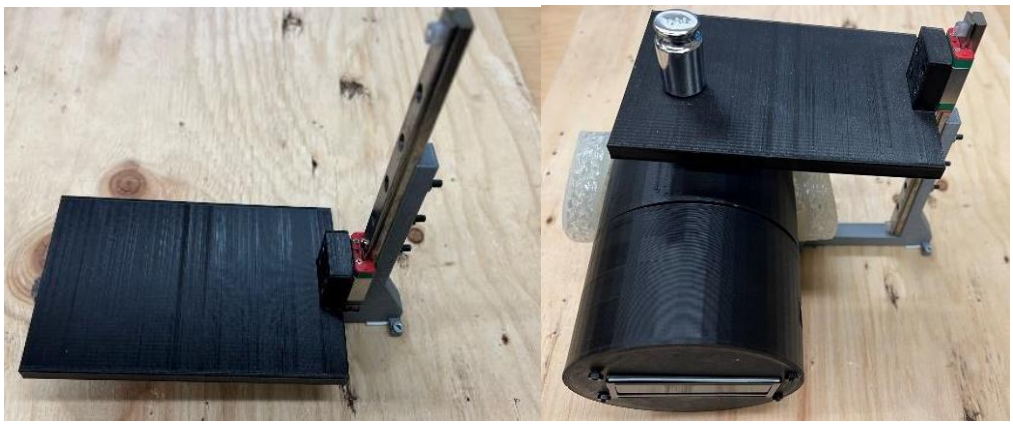

Figure 44. Optional calibration platform shown empty on left and calibrating the tester on the right.

Curriculum Vitae

Name:	Dawei Liu
Post-secondary Education and Degrees:	Tiangong University Tianjin, China 2016-2020 B.E. The University of Western Ontario London, Ontario, Canada 2021-2022 M.Eng.
Related Work Experience	Research Assistant The University of Western Ontario 2022-2024
Publications:	Dawei Liu, Apoorv Kulkarni, Victoria F. Jaqua, Christina A. Cole, Joshua M. Pearce, Distributed manufacturing of an open-source tourniquet testing system, *HardwareX*, 2023, e00442.